Department of Geosciences

Structural assessment and characterisation of the rock slope failure at Skredkallen, Vannøya

Structural analysis using field and desktop methods

Leif Trønnes

Master thesis in GEO-3900 May 2019

Abstract

The University of Tromsø has carried out multiple studies by master students on unstable rock slopes (URS) in Troms County, Northern Norway. This thesis differs from other studies in Troms as Skredkallen is located in Pre-Cambrian rocks as part of West Troms Basement Complex (WTBC). The rocks of the WTBC have been subjected to multiple phases of deformation, and the main structural features from deformation at this field site is from a Paleoproterozoic thrust sheet, 'Skipsfjord Nappe', from Svecofennian deformation.

Skredkallen is an actively deforming URS located on the steep eastern slope of Laukvikfjellet. Previous failure events have occurred in the URS, resulting in rock avalanche deposits of varying size below the slope. What is left is multiple detached terraces and a tall column of rock 'Kaillen', which is still actively deforming. The URS has been identified as moving downslope towards NE by means of satellite InSAR. The location of Skredkallen, as well as a rock slope failure on a mountain ridge further west, align with a thrust boundary. This suggests that there might be a regional pattern between the two instabilities and a possibility of a tectonic boundary forming the rupture surface of the URS. Geophysical data indicates a fault being present close to Skredkallen, and brittle fault structures have played an important role in the origin of the URS. The structural mapping showed four main joint sets; J1(034/82±16.9), J2(205/68±9.0), J3(309/68±10.5) and J4(117/83±15.5). J1 and J4 were the most dominant joint sets, both near-vertical and dipping towards ESE and SW respectively. The foliation (292/14±13.8) dipping towards NNE is oblique to the NE facing slope.

The main failure mechanism is planar sliding along a NE-dipping failure surface, probably contributing to a biplanar compound slide made up by J3 and SF, which together have developed a step-path geometry effectively working as a listric sliding plane. The rock column Kaillen is toppling towards E from the intersection between J1 and J4. The failure on Skredkallen can be considered as a possible DSGSD based on the complexity of geometries made by the surface morphostructures, and from the inferred brittle fault and fracture geometries traced in the bedrock. The two proposed scenarios involve a worst case scenario with a minimum mass of 1.1 Mm^3 sliding down the steep eastern slope of Laukvikfjellet, and the collapse of Kaillen (11,193 m^3). However there are no settlements immediately below the slope, and a failure only poses a threat to an uninhabited cabin and hiking trails and is therefore low risk.

Foreword

This thesis is my final work of my Master of Science (MSc) degree in geology at The University of Tromsø (UiT). Louise Mary Vick (postdoc) and Steffen Bergh (professor) have been my supervisors.

I appreciate the opportunity to study such a spectacular unstable rock slope and I will strongly encourage you to visit Skredkallen.

Thanks to 'Slettnes på Vannøya' facebook group for interesting information about Skredkallen and the area. Special thanks to my co-student and field assistant Martin Mikkelsen who have been very helpful and showed extraordinary working spirit, in spite the fieldwork campaign involved mostly bad weather conditions. Many highs, lows and laughs from the fieldwork will be great future stories and never forgotten.

Tromsø, 15.05.19.

Table of Contents

Abbrevations

DEM   Digital Elevation Model

DSGSD   Deep Seated Gravitational Slope Deformation

GIS   Geographical Information System

InSAR   Interferometric Synthetic Aperture Radar

ka   Thousand years

LOS   Line of sight (InSAR data)

Ma   Million years

NVE   Norwegian Water Resources and Energy Directorate

NGU   Geological Survey of Norway

SLBL   Sloping Local Base Level

UAV   Unmanned Aerial Vehicle

URS   Unstable Rock Slope

VVFC   Vestfjorden Vanna Fault Complex

WTBC   West Troms Basement Complex

1 Introduction

Catastrophic failure of unstable rock slopes is a serious hazard in mountainous Norway posed by both translational sliding of intact rock, and disintegrated rock mass into rock avalanche, rockfall and debris flow activity (Braathen et al., 2004, Bunkholt et al., 2011, Schleier et al., 2015). Landslides from rock slope failure pose a threat to lives, roads, buildings and infrastructure, thus understanding and characterising the deforming rock slopes prior to catastrophic failure is necessary. Such investigations require a complete geological, structural and geomorphological overview of the site, with the goal of understanding the extent, volume and kinematics of a potential failure. Of particular importance is the understanding of the bed rock structure (Stead and Wolter, 2015) and deformation-induced morphostructures (Agliardi et al., 2001).

More than 100 rock slope instabilities have been mapped in Troms County (Oppikofer et al., 2015), and multiple landslide types (Varnes, 1978) and mechanisms are observed. The intention of this project is a complete characterisation of the unstable rock slope at Skredkallen on Vannøya, northern Norway. Multiple studies have been done in the inner Troms region to link rock slope failure/unstable slope deformation with bedrock structure, however these unstable slopes are comprised of Caledonian rocks (Zwaan, 1988) and associated structures. Findings from these studies may not be applicable to the Precambrian West Troms Basement Complex (Bergh et al., 2010) geological environment of Skredkallen. This thesis examines the nature of the basement complex structures within Skredkallen, and the control they have on the unstable rockslope.

1.1 Introduction to unstable rock slopes in Norway

The landscape in Norway is characterised by high topographic relief formed by the carving processes of multiple glaciations. Deep U-shaped valleys are common, especially along the coastline where the valleys become fjords, some of which are several hundreds of kilometres long. These valleys are typically very steep and unstable being ideal for rock deformation. The deformation of unstable rock slopes (URS) can be either uniform over the entire slope or spatially distributed (Hermanns et al., 2013). When the deformation is spatially distributed, the deformation varies between different compartments of the URS, such as blocks, terraces and similar features. URS represent one of the most serious natural hazards in Norway, especially

when terminating into fjords leading to secondary effects such as displacement waves. Compared to rock falls which occur relatively often in Norway, rockslides typically involve large number of casualties. During the last 113 years 174 casualties have occurred due to displacement waves after a rock slope failure (i e. Loen 1905 and 1936, Tafjord 1934; (Blikra et al., 2006)). At the time of writing, NVE (The Norwegian Water Resources and Energy Directorate) are monitoring seven 'high risk' unstable rock slopes in three different Counties; one in Sogn of Fjordane, three in Romsdalen and three in Troms. Compared to snow avalanches, URS failures are very unpredictable and thus of special importance to locate. Systematic mapping by NGU (Geological Survey of Norway) over the last 14 years has detected 300 potential URS in Norway. The distribution of these mapped locations show that URS are highest concentrated close to tectonic lineaments, which can be seen as linear features in the landscape. These lineaments represent a geological structure such as a fault, typically found in connection to fjords.

Historically documented rock avalanches in Troms County (Map 1), show that rock failures are common in areas with steep topographic relief, such as fjords and valleys developed during multiple glacial cycles. These historical events mostly date back to the period shortly after deglaciation (Blikra et al., 2006). Compared with most other regions, the occurrence of active unstable areas in Troms county is high (Oppikofer et al., 2015). The slopes are in various stages of development and based on recurrence intervals the probability for large rock slope failure is relatively low (Blikra et al., 2006).

Previous work in the study area are mostly studies on basement-cover relationships (Opheim and Andresen, 1989, Bergh et al., 2007, Bergh et al., 2010, Rice, 1990, Zwaan, 1995) and geomorphology studies (Corner and Haugane, 1993). The study of (Corner and Haugane, 1993) focused on marine-lacustrine stratigraphy of raised coastal basins and postglacial sea-level change at Lyngen and Vannøya, to reconstruct the relative sea level change during the Holocene and Late Weichselian. Studies on bed rock geology in the area have been conducted to better distinguish the lithology and structures of different ages. This has included U-Pb dating of mafic dikes and meta-sedimentary rocks, and investigations on folds, cleavage, fault and shear zone structures. For example, the Skipsfjord Nappe on Vannøya has long been thought to be of Caledonian age, but is now interpreted by (Bergh et al., 2007, Bergh et al., 2010, Pettersen, 2007) to be of Paleoproterozoic age (from Svecofennian deformation).
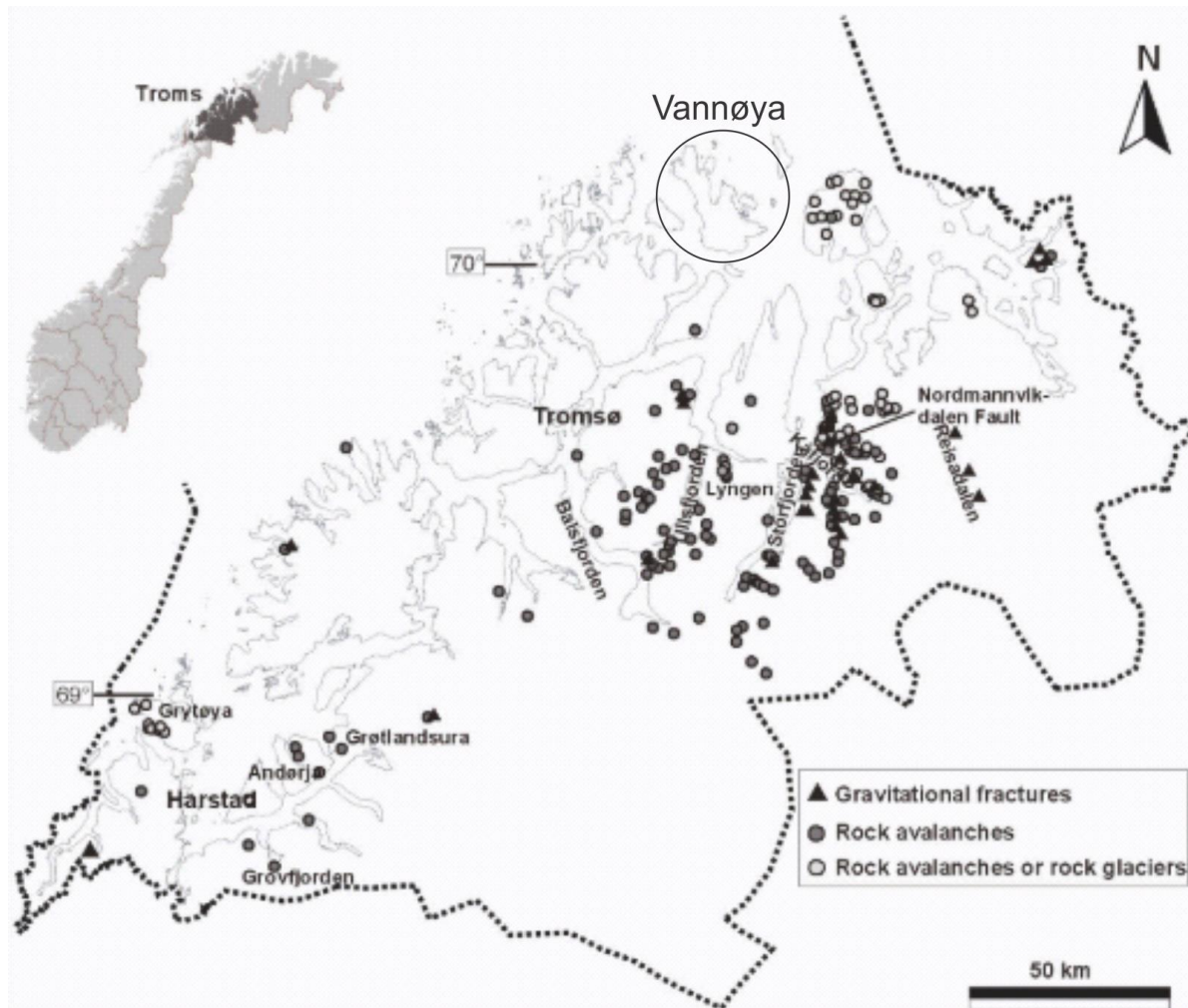
Map 1 - Distribution of rock avalanche events, gravitational fractures and rock glaciers in Troms County. Modified after Blikra et al., (2006).

1.2 Aims of the study

The main aim of this study is to structurally characterise the unstable rock slope at Skredkallen by answering the following questions:

- What are the main failure mechanisms?
- What influences does the regional geological history and inherited bedrock structure play on the failure mechanisms?
- Could the failure be described as a Deep Seated Gravitational Slope Deformation (DSGSD)?
- What are the failure scenarios in terms of extent, volume and runout length?

The datasets used to address these questions include mapping of structural data (joints, foliation etc), geomorphology and morphostructures, photogrammetry data from drone sampling,

elevation data (either from photogrammetry software based on drone imaginery or ArcticDEM obtained from (pgc.umn.edu/data/arcticdem/, 2018).

The following tasks have been undertaken:

- Mapping of the slide's extent, inner structure and geomorphology.
- Mapping bedrock lithology and structures at the site.
- Structural, kinematic and rotational analysis using Dips 7.0.
- Photogrammetry in AgiSoft Photoscan.
- Construct structural data based on semi-automatically structural recognition software (Coltop-3D).
- Volume estimations.
- Potential failure scenarios based on delimiting structures and run-out estimate.

1.3 Available data

- Aerial photos from 2016 (Norgeibilder, 2018).
- InSAR data (insar.ngu.no).
- Bedrock maps (Bergh et al., 2007, Bergh et al., 2010, Opheim and Andresen, 1989).
- Superficial deposits map (NGU, 2018).
- Helicopter-borne magnetic survey of Vanna (NGU, 2012).

1.4 Location, background and geological conditions

The island of Vannøya is located in northern Norway, northwestern part of Troms County (Figure 1A). Vannøya is characterised by an alpine northern- and southern part with several high irregular peaks consisting of basement rocks, such as Vanntinden 1031 m asl. The eastern part of the island is more or less a strandflat with very low relief in the landscape. The central part consisting of two mountain ridges oriented NNW-SSE, is divided by a U-shaped valley Skipsfjorddalen which mouths out into Skipsfjorden. Both mountain ridges are relatively flat situated approximately 500-600 m asl, and could potentially represent a paleosurface. The two mountrain ridges Laukvikfjellet and Kvalkjeften both consist of gentle slopes along their western faces, while the eastern faces are much steeper and some places vertical, on which Skredkallen is located (Figure 1B).
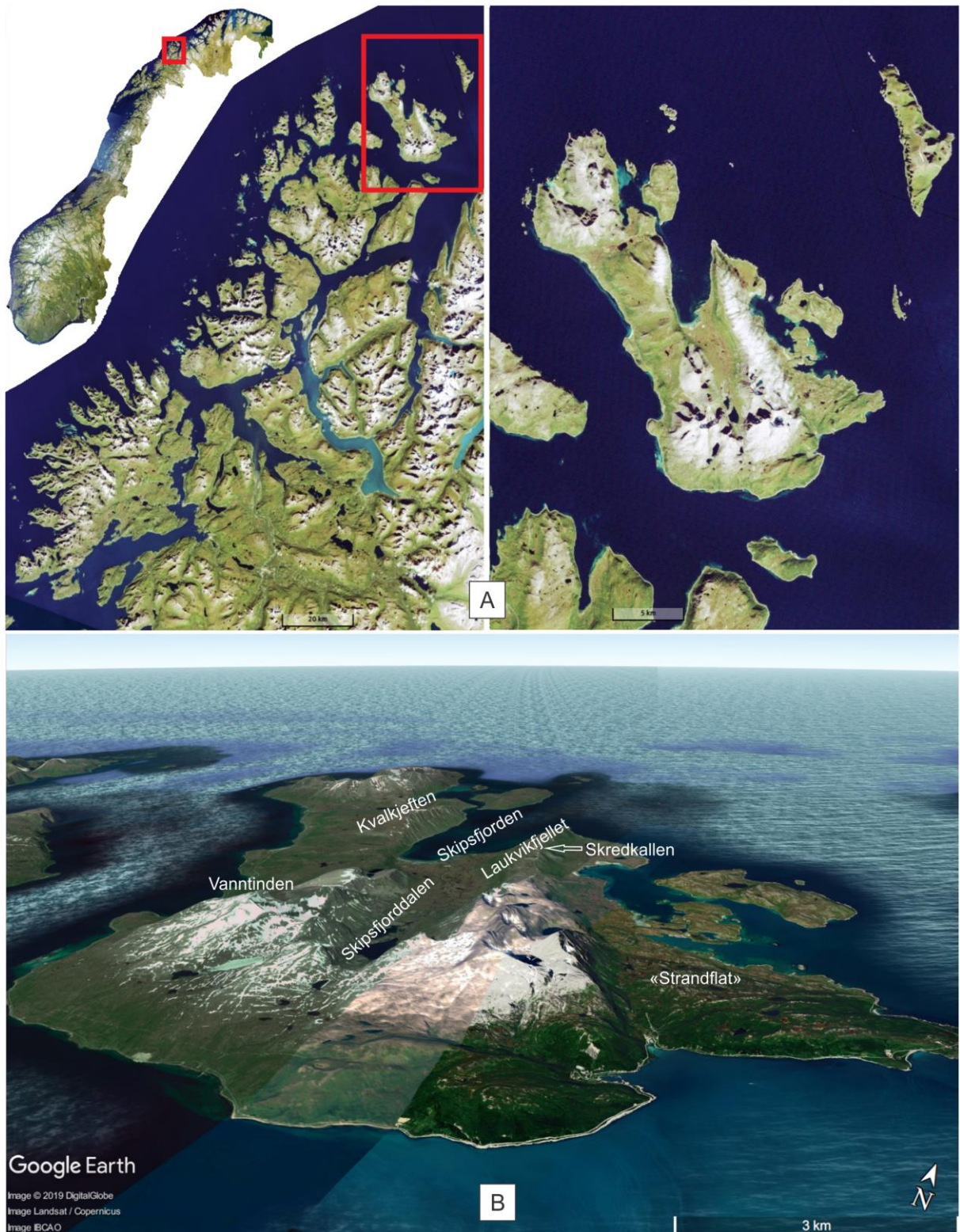
Figure 1 – A: Vannøya location. Obtained from norgeibilder.no. B: Vannøya seen from S. Obtained from Google Earth.

1.4.1 Background for mapping

Skredkallen (482 m asl) is an actively deforming URS located on the east-facing slope of Laukvikfjellet (Figure 2A). It has been identified as moving downslope (towards NE) by means of satellite InSAR (insar.ngu.no). Future events post a threat to hiking trails, an uninhabited cabin and a holiday cabin at the base of the URS. A large portion of the mountain side has collapsed probably sometime after deglaciation, as evidenced by the talus material below the URS. Within the instability there are multiple detached terraces, and a tall column of rock called 'Kaillen' which is still deforming. The main active terrace has subsided c. 20 m. Fresh talus deposits can be found underneath the southeastern section of this terrace, meaning that this slope is actively deforming. The talus material in the lowermost part of the slope, make up a 500 m wide area stretching as far out as 1.3 km from the source area at Skredkallen. This area is locally termed 'Skrea' and consists of blocky avalanche deposits with some vegetation (Figure 2B). Anecdotal evidence, in the form of local legends, tells of historic events linked to avalanche activity and ongoing creeping movement. One legend tells of a man (Søren Andresen, b. 1754) screaming so loudly from the top of Laukvikfjellet that it led to a large rock avalanche event, and the deposit of 'Skrea'. The most recent rock avalanche occured in the 1950s, as reported by local residents, and resulted from the collapse of a tall column of rock called 'Kvinnen'. Multiple local residents ('Slettnes på Vannøya' facebook group, 2018, pers. commun.) have reported that in the past people were able to jump onto the 'Kaillen', the tall column of rock. The grandmother of Signy Karslen, Mathilde (b. 1880), was able to jump this distance as a child. Today the same distance requires a jump of at least 10 m, a generally impassable jumping distance.
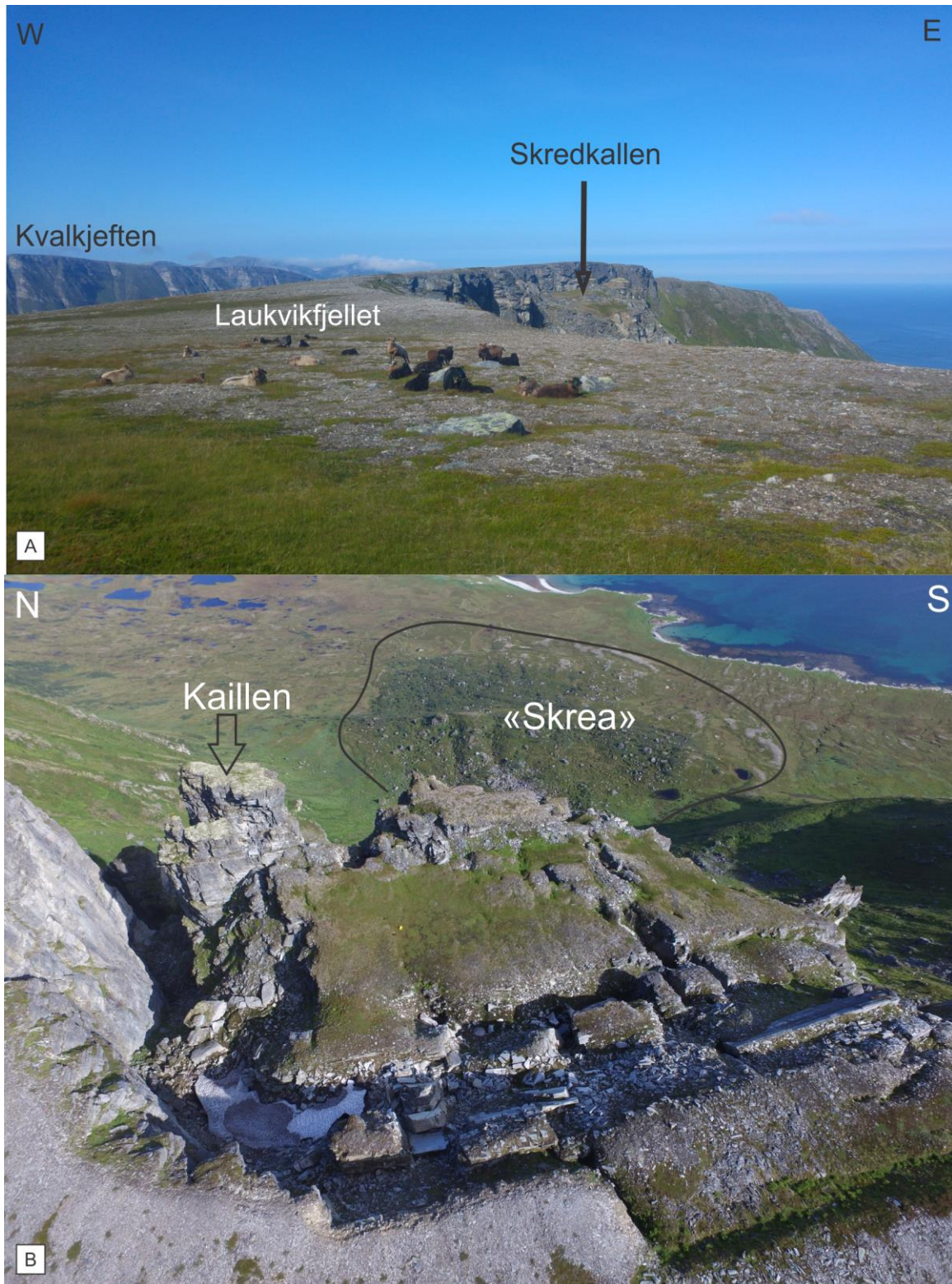
Figure 2 – A: Location of Skredkallen relative to Laukvikfjellet. B: Drone photo. Location of the column Kaillen and Skrea.

1.4.2 Regional geology

Western and coastal regions of Troms comprises Precambrian basement rocks and Caledonian thrust nappes (Andresen and Forslund, 1987). The geology in Norway is dominated by nappes of the Caledonian allochthons and their structures in terms of thrusting, folding and faulting. Precambrian rocks typically outcrops in erosion windows, such as in the coastal areas of Troms (Zwaan, 1995, Bergh et al., 2010).

The island of Vannøya is a part of a basement horst, the West Troms Basement Complex (WTBC), which consists of Neoarchean tonalitic and granitoid gneisses, and Palaeoproterozoic mafic, igneous and volcano-sedimentary cover rocks (Zwaan, 1988). WTBC is a part of the Fennoscandian shield (Map 2), which has been subjected to a long and complex growth history. WTBC has have been subjected to Neoarchean deformation (2.69 – 2.56 Ga), rifting and mafic dyke intrusion (2.4 – 1.98 Ga), volcanic activity and clastic sedimentation (c. 2.85 – 1.97 Ga), arc magmatism and Svecofennian crustal deformation and reworking (1.8 – 1.76 Ga) (Bergh et al., 2010).
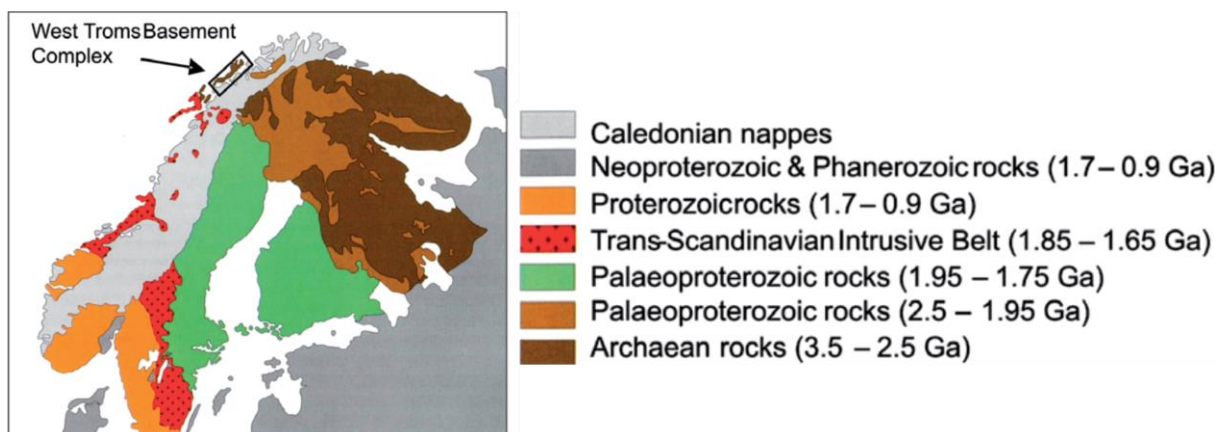
Map 2 - Location of the WTBC. Modified after Nordgulen and Andresen 2008.

The Neoarchean basement gneisses on Vannøya are overlain by a sedimentary unit; Vanna Group meta-sandstones and mudstones (Binns et al., 1981, Johansen, 1987) which underwent Svecofennian (1.8-1.75 Ga) orogenic fold-thrust belt deformation (Bergh et al., 2007). The Skipsfjord nappe, located in the central parts of Vannøya, is thought to be a correlative to the Vanna group (Opheim and Andresen, 1989). This nappe was previously interpreted as a down-faulted Caledonian nappe by the Vannareid Burøysund Fault, but is now considered to be a down-faulted Paleoproterozoic thrust sheet from Svecofennian deformation (Bergh et al., 2007). Of simplified reasons this study differentiates between a 'Lower Nappe' and 'Upper

Nappe' (Map 3), the latter being 'mylonitized tonalite with mafic sheets' as mapped by (Opheim and Andresen, 1989). The majority of structural features in the WTBC can be associated with Svecofennian deformation (Bergh et al., 2010).
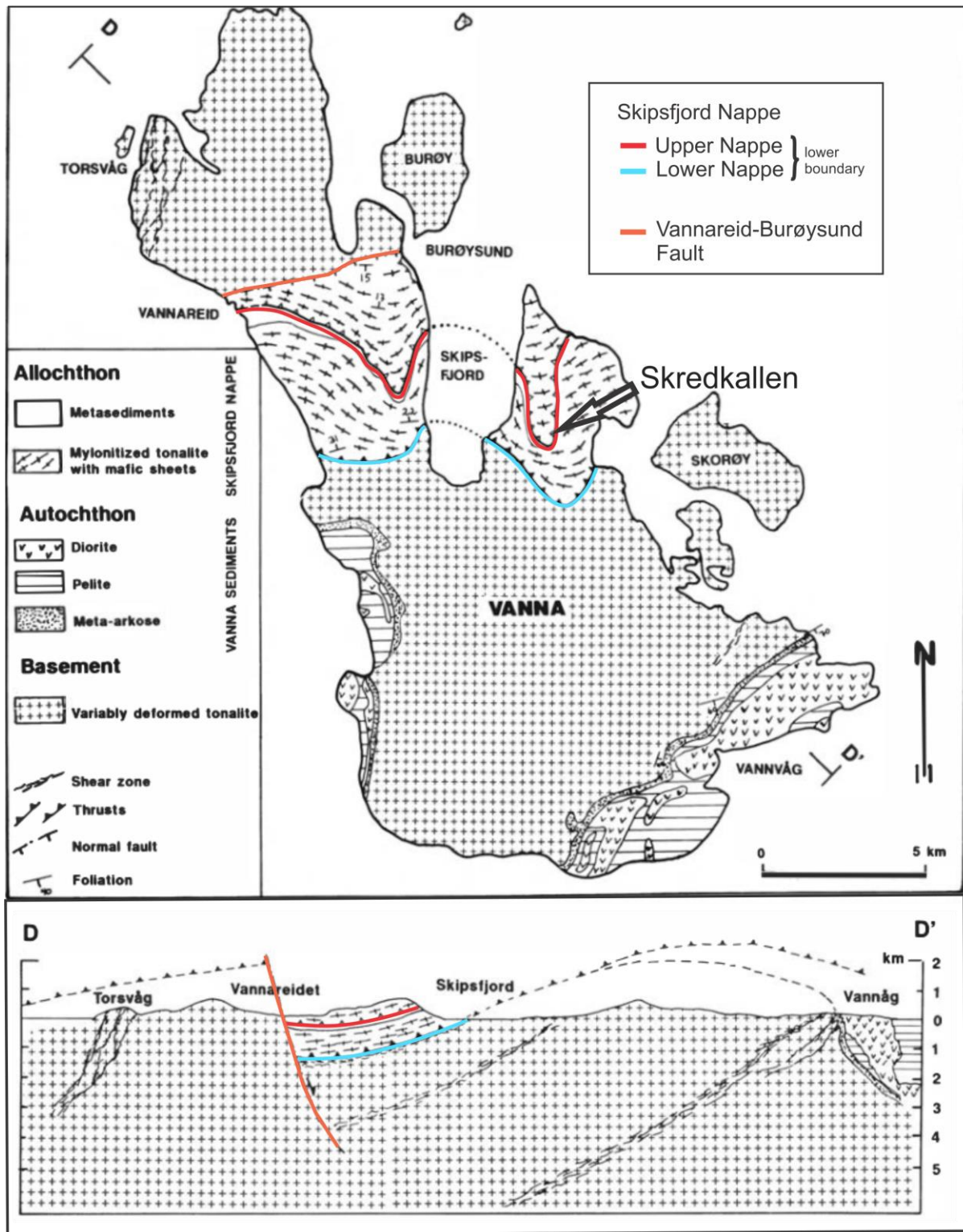
Map 3 - Geological map of Vannøya, modified after Opheim and Andresen (1989). Based on data from Binns et al. (1981), Johansen (1987) and authors work. Profile section showing possible basement cover relationship. Note the Nappe boundaries and the Vannareid Burøysund Fault.

1.4.3 Neoarchean and Svecofennian structures

The long and complex history of the WTBC is presented in a schematic evolution model (Figure 3) by Bergh et al (2010). Three main deformations are presented; D1, D2 and D3.

The northeastern parts of the WTBC (Ringvassøya Greenstone Belt and Skipsfjord Nappe) is thought to be less deformed by D1+D2 deformation than the southwestern parts (Senja Shear Belt) where the latter displays upright macro-folds with steep limbs (Bergh et al., 2010). Sinistral strike-slip reactivation of steep macro-fold limbs creating semi-ductile shear zones can be found in the southwest with decreasing size towards northeast. Less deformation in the northeast and therefore more flat-lying macro-fold hinges lead to the Skipsfjord Nappe being formed by progressive NW-SE directed shortening and subsequent transpression in an orogeny-parallel fold and thrust belt (Bergh et al., 2007).
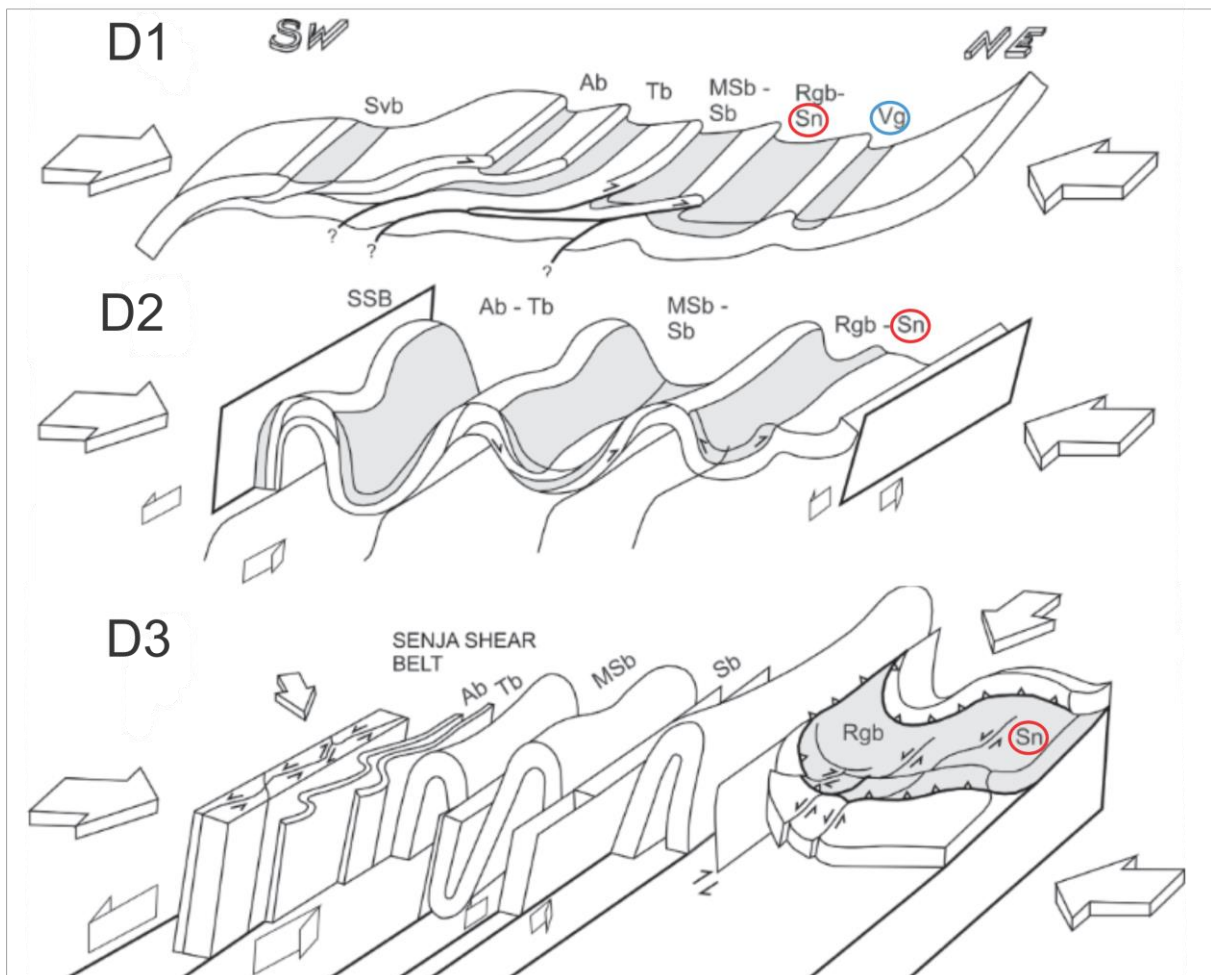

Figure 3 – Modified after Bergh et al (2010). Sn = Skipsfjord Nappe. Vg = Vanna Group. D3: Formation of the Skipsfjord Nappe.

1.4.4 Post-Caledonian structures

The continental margin off Central/Mid Norway was subjected to multiple rift events in the Paleozoic through to Early Cenozoic times as part of the break-up of the North Atlantic Ocean (Doré, 1991, Faleide et al., 1993, Blystad, 1995, Doré and Lundin, 1996, Brekke et al., 2001, Mosar et al., 2002, Faleide et al., 2008). Onshore brittle faults along the West Troms margin are mostly NNE-SSW and ENE-WSW-trending normal faults which are constrained to WTBC. WTBC is flanked in the south by major normal faults (Blystad, 1995, Bergh et al., 2007) and in the north to the SE-dipping Vestfjorden Vanna Fault Complex (VVFC; Figure 4). There is also a subsidiary NW-SE trending fracture system present, best developed in Lofoten.
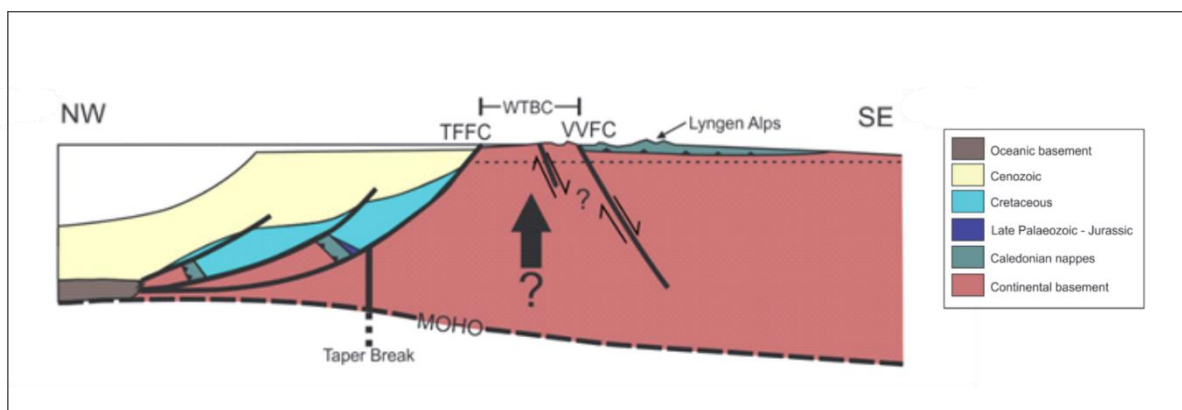
Figure 4 – Modified after Indrevær et al., (2013). Schematic proposed profile of present situation at the Barents Sea margin and WTBC, involving erosion of thin Caledonian nappes, exposing the WTBC. Note the steep SE dipping normal faults of VVFC.

The VVFC in western Troms make a zigzag-shaped pattern which can be traced northwards to Vannøya, outlined bv several smaller-scale fault segments (Andresen and Forslund, 1987, Forslund, 1988, Opheim and Andresen, 1989, Roberts et al., 1997). The fault zones within the VVFC show down to SE normal displacement, up to 3 km based on the offset of Caledonian nappes with known thickness (Forslund, 1988, Opheim and Andresen, 1989, Roberts et al., 1997). Dating results and methods have been interpreted to indicate that faulting in western Troms largely occurred during the Permian to Early Triassic rifting phase.

One of two major fault zones found in the interior parts of WTBC is the Vannareid Burøysund fault (Map 4), striking ENE-WSW and c. 60° dip towards S. This fault zone has downdropped the presumed Paleoproterozoic Skipsfjord Nappe by at least 3 km (Opheim and Andresen, 1989). The fault zone can be seen as a valley trending ENE-WSW in the northern parts of Vannøya and show an at least 20 m wide cataclastic zone of rocks.

The western fault zones of the WTBC are characterised by NE-SW to N-S trending fault segments that commonly show red staining of host-rock granites, with normal to oblique-normal, down towards SE fault movement (Indrevær et al., 2013). Indrevær et al (2013) suggests that the fault zones may link up as en-echelon, right-stepping, fault segments that run parallel to the VVFC. This zone is thought to be a transfer zone that runs NW-SE from the mainland near Nord-Fugløya (Indrevær et al., 2013), just northeast of Vannøya.
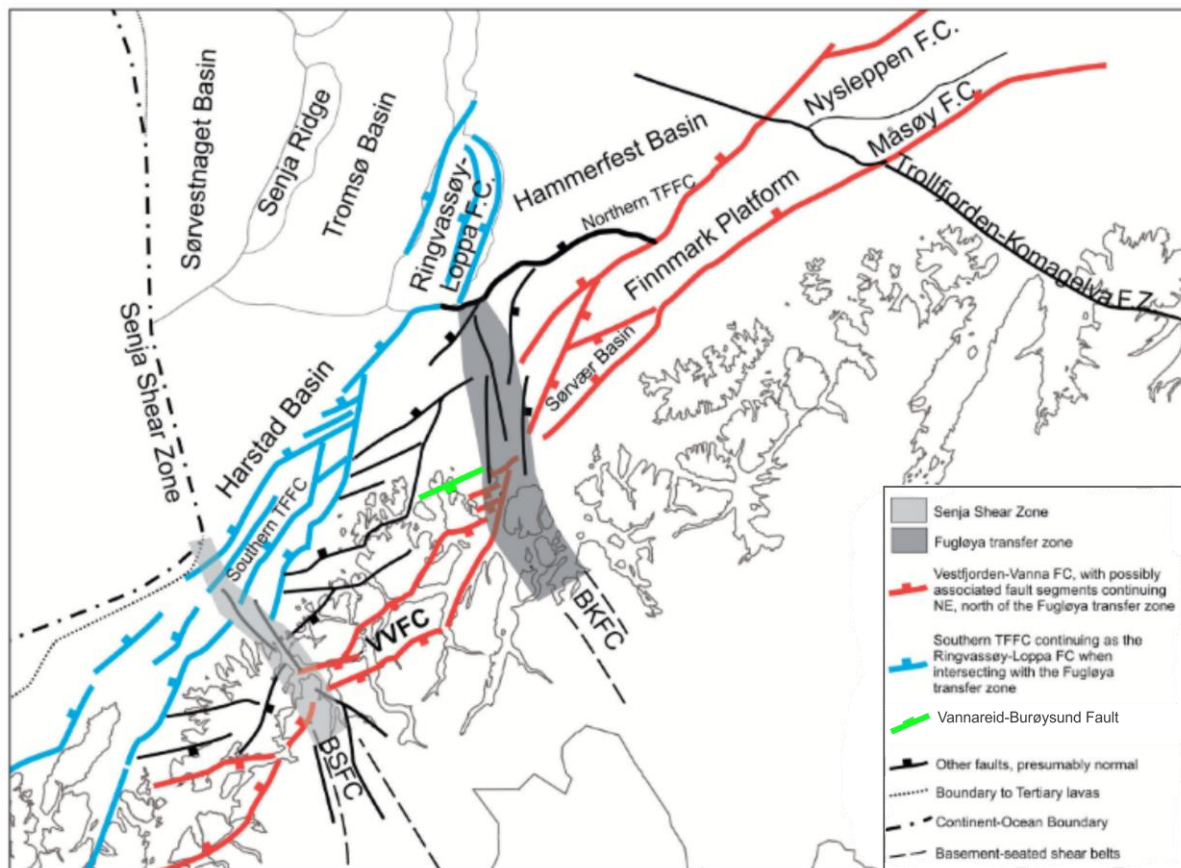
Map 4 - Simplified tectonic map. Modified after Indrevær et al., (2013). NNE-SSW and ENE-WSW-trending fault complexes onshore and offshore. Note the Fugløya transfer zone located just east of Vannøya and the Vannareid Burøysund Fault.

1.4.5 Quaternary geology and geomorphology

Glacial cycles in Scandinavia have been occurring for the last 2-3 Ma whereas the last major deglaciation occurred c. 25 000 years ago (Dahl and Sveian, 2004). Within the Quaternary, frequent and dramatic climatic changes has led to 40 glacial advances at the latitudes of Vannøya (70°N) (Dahl and Sveian, 2004). Despite being just a small fraction of the earth's geological history, the glacial cycles have made a great impact on today's landscape. Slopes

have been heavily eroded, especially along old river valleys, lithological boundaries, fault zones and easily erodible rocks.

The retreat and position in time of the ice-cap in Troms has been interpreted (Stokes et al., 2014) by interpolating ice-front positions based on oxygen isotopes from sediment cores (Rørvik et al., 2013). A transect line from the inner parts of Lyngen fjord out through Fugløysundet, indicates that the last time the ice-front covered the central parts of Vannøya was between 15.5 – 16.1 ka.

The isostatic lift in Troms following glacial retreat varies from c. 80 m in the inner parts of Troms (Lyngen), to c. 20 m in central Vannøya (Marthinussen, 1960). Two raised shorelines can be found along the coastlines in Troms today; The Main Shoreline of Younger Dryas age (12 700 – 11 700 ka) and Tapes-shoreline (8500 ka) (Dahl and Sveian, 2004).

The coastline of Vannøya is characterised by marine deposits up to The Main Shoreline c. 20 m asl. There are hardly any trees on Vannøya and most of the vegetation is made up of either bog or weathered soil. Moraine material is present in valleys such as Skipsfjorddalen in the central parts of the island (Corner and Haugane, 1993). The slopes on Vannøya are predominantly showing landslide processes such as avalanche deposits or solifluction soil. Mountain ridges are covered with weathered rocks from the glacial cycles (Map 5).
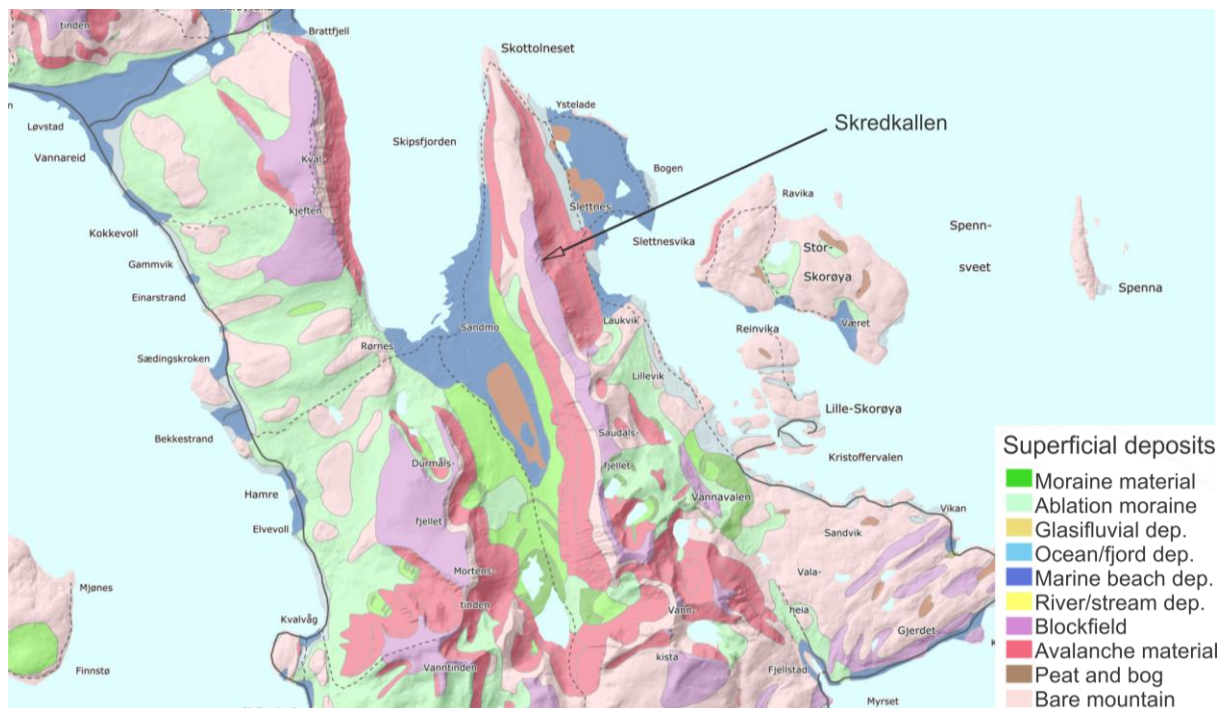
Map 5 - Superficial map modified after ngu.no.

1.4.6 Climate and weather

The climate in Troms is sub-arctic and characterised by long winters and short summers. Troms experiences midnight-sun from mid-May to mid-July and polar-night from late-November to mid-January. The average yearly temperature on Vannøya (Fakken observation station) is c. 4°C. The coldest month is January with average temperature c. -1°C and the warmest July c. 12°C (yr.no). There is great regional differences in terms of precipitation rates and wind. Vannøya is highly exposed to rough weather conditions as it is located on the outer coast of Troms close to the Norwegian Sea.

Since the Norwegian coast is warmed by the North Atlantic Jet Stream, temperatures on latitudes of northern Norway are higher than further inland towards E (i.e. The Siberian Tundra). Thus the lower limit of permafrost is situated relatively high up in the landscape in Troms (800–900 m asl) and a bit lower in the coastal areas (600–700 m asl) (Christiansen et al., 2010) such as on Skredkallen (482 m asl). Measurements the past years show an increase in thickness of the active layer in the permafrost as well as a temperature increase (Christiansen et al., 2010).

Snow can some places be found all year around on Skredkallen, as in the trench along the lateral backscarp.

2 Theory

2.1 Landslides and large rock slope instabilities

Landslides are a gravitational movement downslope of rock, soil or vegetation, both on land and in water (Hermanns, 2016). This thesis focuses on large rock slope instabilities, thus the following chapters describe landslide types including rock material. A rock slope instability has been defined as rock slopes with signs of gravitational deformation which may form the soruces of potential future rock slope failures (Böhme, 2014). Rock slope instabilities vary in size, and therefore complexity (Figure 5).
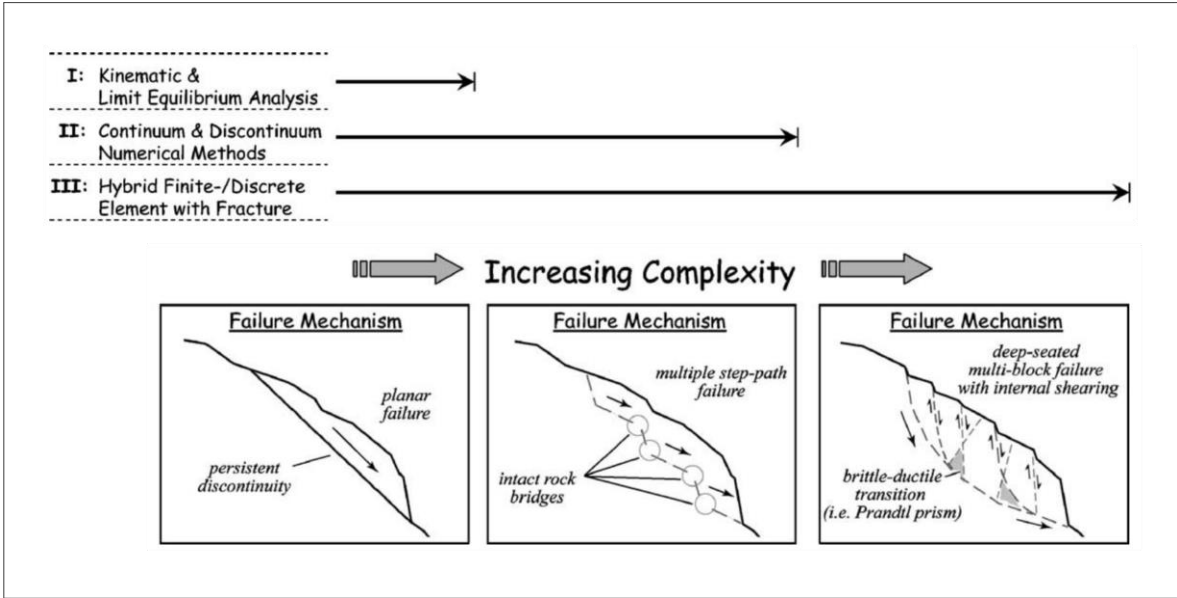
Figure 5 - Flowchart illustrating three levels of landslide analysis and the modes of translational/rotational failure they apply to. Modified after Stead et al., (2006).

2.1.1 Landslide classification and terminology
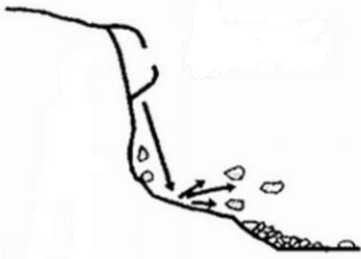
The Varnes classification of landslides (Varnes, 1978) distinguishes different landslide types based on movement type and material involved. Slide-type landslides are specified by relative motion between stable ground and moving ground in which the vectors of relative motion are parallel to the surface of separation or rupture (Varnes, 1978). Hungr et al., (2014) presents an updated version of the Varnes classification, with modifications primarily to accommodate for accepted geological and geotechnical terminology of rock and soil. This classification includes changes related to the six different movement mechanisms (Table 1). A Complex type landslide, as characterised by Varnes (1978) as landslide involving a combination of more than
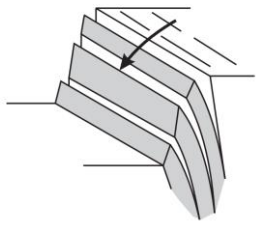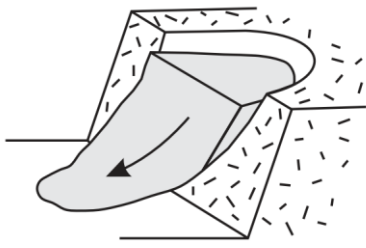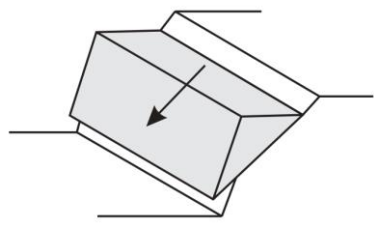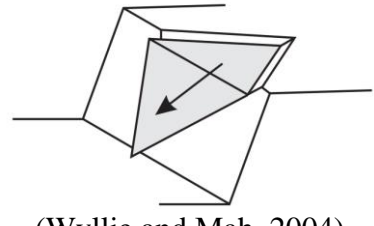
one movement type, is removed in the update by Hungr et al., (2014), and instead 'slope deformation' is added. The definition of slope deformation is markedly similar to that of a Deep Seated Gravitational Slope Deformation (DSGSD; Agliardi et al., (2001)): a deep-seated slow deformation of a valley or hillslope.

Table 1 - Varnes classification system (Varnes, 1978), modified by (Hungr et al., 2014) with movement type (only involving rock material) and failure mechanism.
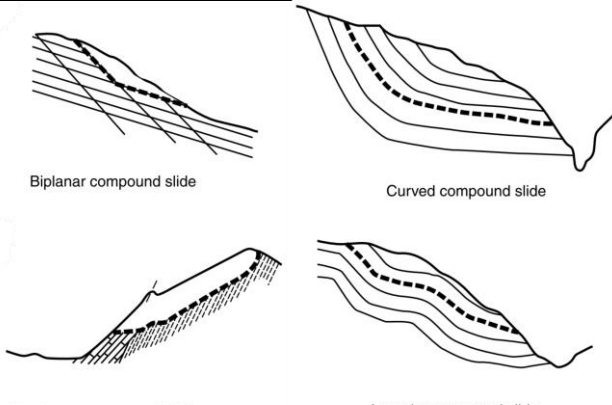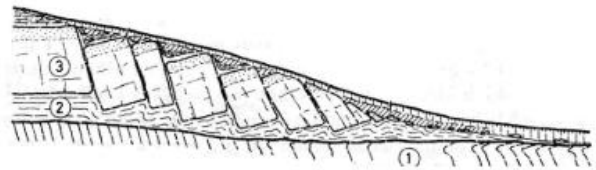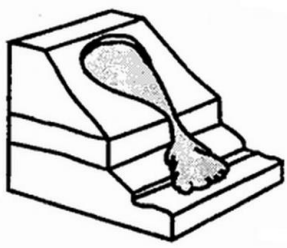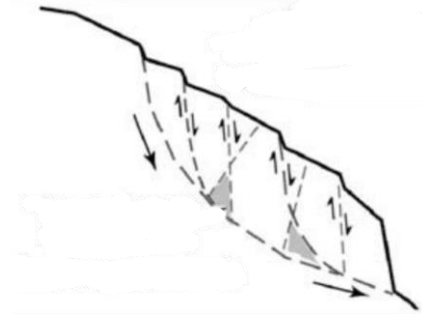
Type of movement	Rock
Fall	Rock fall
Topple	Rock block topple Rock flexural topple
Slide	Rock rotational slide Rock planar slide Rock wedge slide Rock compound slide Rock irregular slide
Spread	Rock slope spread
Flow	Rock creep
Slope deformation	Mountain slope deformation Rock slope deformation

Table 2 - Description of different rock slide types in rock.

Rock fall	
In falls, a mass is detached from a steep slope or cliff, along a surface on which little or no shear displacement takes place, and descends mostly through the air by free fall, leaping, bounding, or rolling.	 (Cruden and Varnes, 1996)

Rock topple Toppling movement consists of the forward rotation of a unit or units about some pivot point, below or low in the unit, under the action of gravity and forces exerted by adjacent units or by fluids in cracks.	(Wyllie and Mah, 2004)
Rock rotational slide Sliding of a weak rockmass on a curved rupture surface, which is generally not structurally-controlled. A common example of a rotational slide is little-deformed slump.	(Wyllie and Mah, 2004)
Rock planar slide / translational slide In translational sliding the mass progresses out or down and out along a more or less planar or gently undulating surface.	(Wyllie and Mah, 2004)
Rock wedge slide Sliding of rock mass on a rupture surface made up by two different planes, forming an intersection oriented downslope.	(Wyllie and Mah, 2004)

Rock compound slide Sliding of rock mass on rupture surface consisting of several planes, or surface of uneven curvature. Motion is only kinematically possible by high internal distortion of the moving mass. Horst-graben features at head and many secondary shear surfaces are common.	 Biplanar compound slide Curved compound slide Toe buttress compund slide Irregular compound slide (Hermanns and Longva, 2012)
Rock slope spread In spreads, the dominant mode of movement is lateral extension accommodated by shear or tensile fractures.	 (Hungr et al., 2014)
Rock creep Flow movements in bedrock include deformations that are distributed among many large or small fractures, generally extremely slow, that could result in folding, bending, bulging, or other manifestations of plastic behaviour.	 (Cruden and Varnes, 1996)
Rock slope deformation Large-scale gravitational deformation of mountain slopes, exhibiting morphostructure such as scarps, benches, cracks, trenches and bulges, and lacking a fully defined rupture surface.	 (Stead et al., 2006)

2.1.2 Controlling factors for large rock slope instabilities

Geological structures play an important role for large rock slope instabilities and catastrophic failures (Hermanns and Strecker, 1999, Agliardi et al., 2001). Structural elements in the instabilities may lead to secondary effects affecting the slope stability (Figure 6), such as ground water inflow in cracks or seismic activity triggering failure plane development. Rock slope instabilities in Norway at high latitudes, may be controlled by additional external factors such as freeze-thaw cycles and precipitation – snowmelt events increasing ground water pressure. Glacial erosion oversteepening rock slopes and/or glacial debuttressing (the process by which support of the rockwalls by glacier ice is removed during deglaciation; (Ballantyne, 2001)) could also be an important conditioning factor for the stability of rock slopes.

With time controlling factors will play a critical role in landslide development. Fatigue of the rock slope, and the gradual accumulation of long term damage will continue until a "critical slope damage threshold" is reached (Eberhardt and Stead, 2013).

Structural Elements

In Situ Stresses
- direction of major stress
- regime (compression/extension)
- interaction with topography

Folds
- hinge orientation
- tightness
- bluntness
- scale

Faults
- orientation
- width
- seismicity
- sense of movement

Discontinuities
- orientation
- persistence (rock bridges)
- roughness
- strength properties
- infill properties

Foliations
- orientation
- type
- deformation history

Slope Stability

Rock Mass Strength
- intact rock
- discontinuities
- damage

Failure Geometry
- landslide block size
- complexity
  - failure surface
  - internal shears
- runout length

Kinematics
- direction of movement
- release surfaces
- mode of failure
  - planar, wedge, toppling, etc.

Hydrogeological Conditions
- conduits/aquitards
- pore pressure distributions

Timing of Failure
- accumulation of damage
- seismic triggers

Figure 6 - The influence of structure on rock slope stability and failure mechanisms. Modified after Stead et al., (2015)

2.1.3 Deep seated gravitational slope deformation (DSGSD)

DSGSD are large scale gravitational slope movements in high relief mountain slopes, displaying geomorphological features (Figure 7) such as doubled ridges, ridge top depressions, scarps and counterscarps, trenches, open tension cracks (Agliardi et al., 2001). DSGSD occurrence is closely related to specific geologic and structural features, such as bedding, foliation, joints, and faults, and to certain topographic situations (Crosta and Zanchi, 2000, Agliardi et al., 2009, Ambrosi and Crosta, 2011). The distribution of this slope movement can be related to glacial debuttressing and the size of a DSGSD is comparable to the slope (Agliardi et al., 2001). Many DSGSD observed by authors in the Alps are characterised by a basal sliding surface, sometimes partially coincident to a pre-existing tectonic surface (Agliardi et al., 2001). Linkage between active faults and the genesis of this phenomenon have been proposed by (Forcella and Orombelli, 1984). Post-glacial isostatic lift have also been mentioned as a factor (Nemcok and Pasek, 1969). In general, DSGSDs are geologically and structurally complex, which make them hard to understand. One example of a DSGSD is located in the Bregaglia Valley in the central Alps, Italy, as seen on Figure 8.
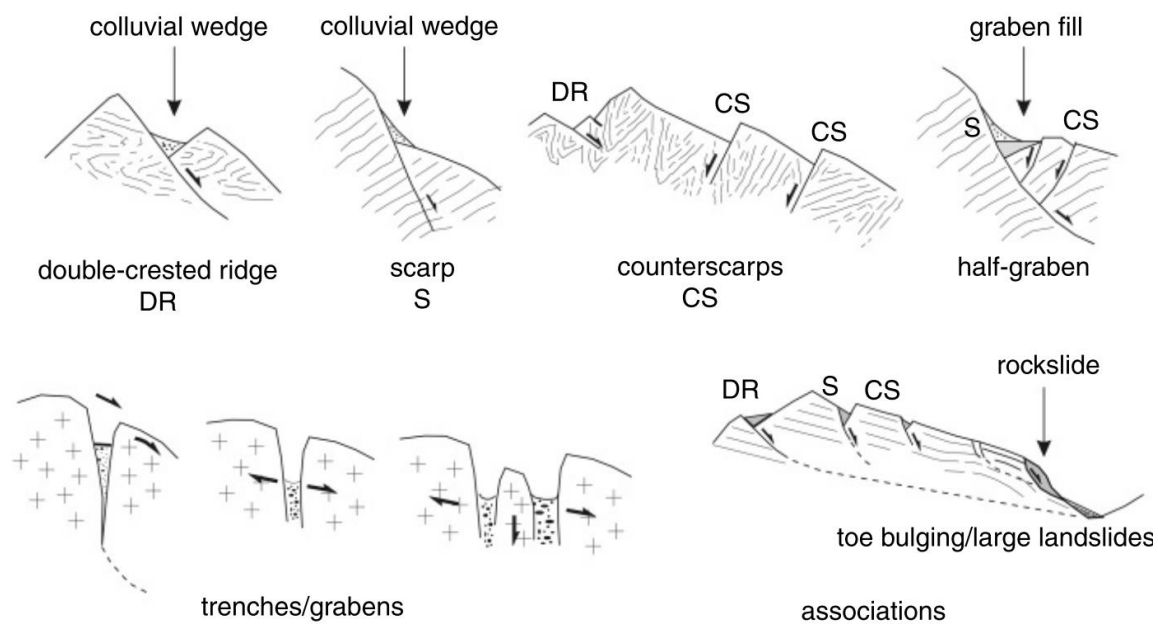
Figure 7 - Morphostructural features diagnostic of DSGSDs phenomena, related kinematic significance, and typical associations. From Clague (2012). Modified after Agliardi et al., (2001).
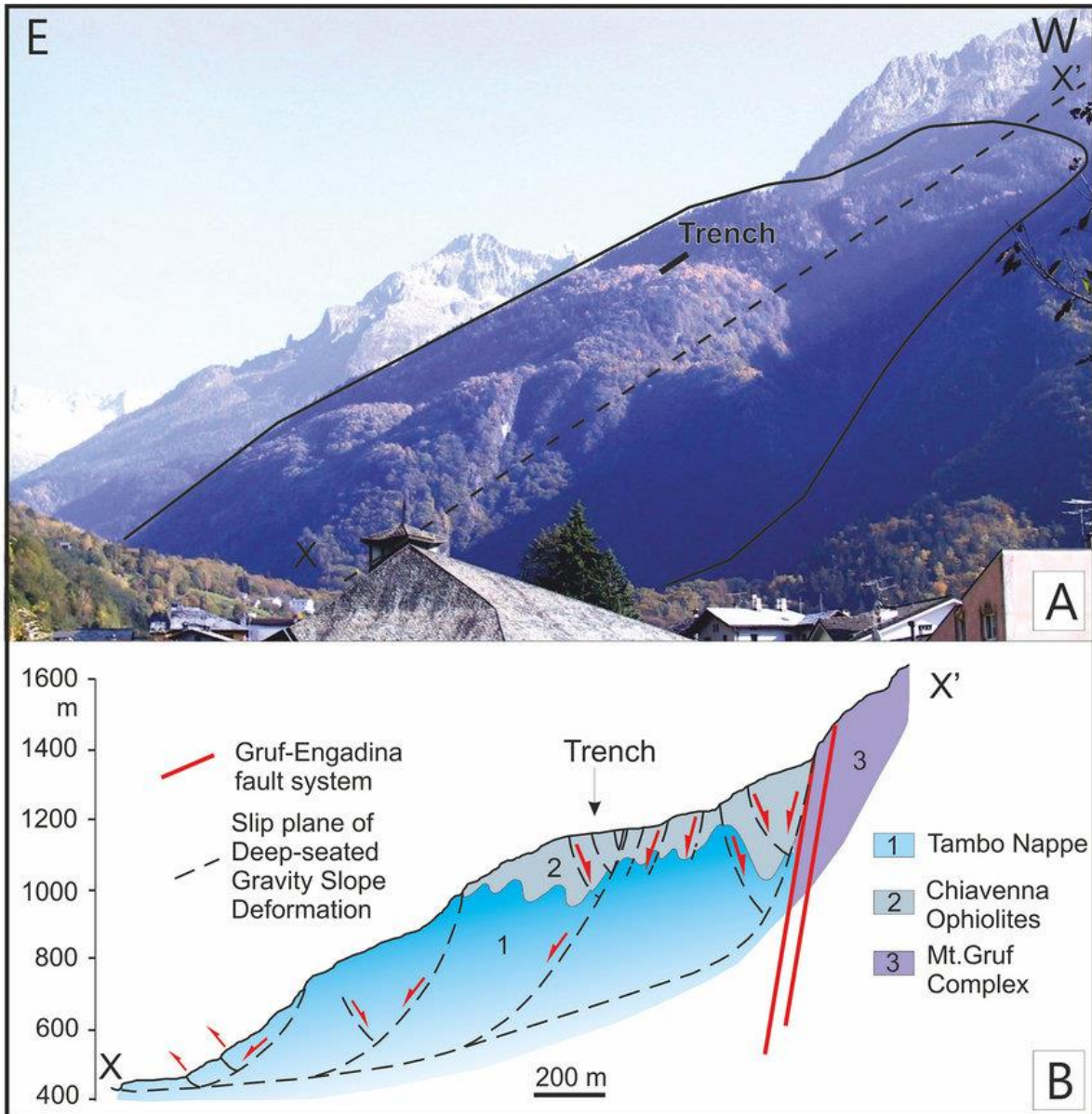
Figure 8 - DSGSD in the central Alps. Figure from Mariotto and Tibaldi (2015).

3 Methods

This chapter presents the methods used in this thesis. As the goal of this thesis predominantly is to understand the geometry of the URS, the study is mostly based on geomorphological/morphostructural mapping and structural measurements to produce maps and structural profiles, as well as rotational- and kinematic analysis. InSAR satellite based data, and drone data for analysis in photogrammetry- and structural recognition software, were used to further compare with the field data.

3.1 Geological mapping

Skredkallen was investigated for two weeks in august 2018 focusing on detailed structural mapping of discontinuities as well as geomorphological- and geological mapping. The structural measurements were obtained by using the FieldMove Clino application (2018) on a LG G4 android phone. The compass was calibrated and controlled for possible inaccuracy by comparing it to conventional compass measurements obtained with a Silva compass. The accuracy can vary a lot depending on phone type and operative system and must be used with caution. The LG G4 did not show any observable deviation from the manual measurements. This made it easier to obtain good measurements especially in areas which were hard to access. Every tenth measurement was obtained with a conventional compass to detect possible inaccuracy in the application.

A total of 436 foliation measurements and 704 joint measurements were obtained during the field campaign, both in the unstable parts of the mountain and in-situ. The field work were mostly confined to the upper part of the URS and along the lateral backscarp. Elsewhere the slopes were too steep or too dangerous to access. The measurements from in-situ rocks were obtained at eleven different localities along the backscarp. At each locality, measurements were typically distributed over a 10 m horizontal distance. The measurements in the unstable parts were obtained on specific blocks, terraces or columns.

If possible, joint measurements were obtained on different aspects at each locality to preserve good representation for further structural analysis, typically on two different aspects. Each locality was given a GPS point using a Garmin Etrex 30x. The most dominant joint sets and foliation were given a description based on spacing, persistence and shape/roughness according to the 'Field description of soil and rock – field sheet' from New Zealand Geotechnical Society (NZGS, 2005).

3.2 Mapping with UAV

A DJI Inspire drone (Unmanned Aerial Vehicle – UAV) was used to map the area from air, with particular focus on the inaccessible parts of the URS. Drone photos were processed into 3D models using photogrammetry software (Agisoft Photoscan), analyzed in semi-automatic structural recognition software (Coltop-3D) and kinematically in Dips 7.0.

A total of 1449 photos and nine videos of the area were obtained with a 12 megapixel Zenmuse Z3 camera mounted on the drone. Two flight missions for photogrammetry were performed; 396 photos (ISO800, low flight speed c. 5 km/h) of the lateral backscarp for structural analysis and 610 photos (ISO400, high flight speed c. 50 km/h) covering the whole area for a complete 3D/DEM model. Both missions were carried out in manual flight mode during light cloud cover and between 2 and 4 pm to avoid noise in the photos from the sun-shade effect. This affected the resolution of the photos because the ISO had to be adjusted up to either 400 or 800 to compensate for the low lighting.

To georeference a 3D model based on UAV photos in photogrammetry software, Ground Control Points (GCP) had to be placed within the photographed area before the flight missions. A total of 24 GCP's were distributed over the entire area at different altitudes. Every GCP location was marked with red spray on easily recognisable objects and given a GPS point with the GPS. A total of seventeen GCPs proved to be visible enough to be used in Agisoft Photoscan.

A Garmin Etrex 30x handheld GPS only provides up to five m horizontal and vertical accuracy, which is not considered adequate for photogrammetry purposes as it can lead to distortion in the model. However, the points were found to be generally within 0.5 m when comparing waypoints and the orthophoto in ArcGIS software. Some GCP's were excluded from the processing as the offset was deemed to be too large, typically in the deeper parts of the trench where the GPS signal was poor.

3.3 Photogrammetry in Agisoft Photoscan

Agisoft Photoscan is a software product that performs photogrammetric processing of digital images and generates 3D spatial data to be used with Geographical Information System (GIS) and other applications. In this study the software was used to make two dense point clouds; one

of the lateral backscarp to perform structural analysis in Coltop-3D, and one of the whole URS to create a high resolution DEM of the area as well as a 3D model for other purposes (Map 6).

Map 6 - Projects in AgiSoft Photoscan

Workflow of both projects:

- Alignment of the photos to orient them spatially by creating a sparse cloud.
- Optimization the point cloud and alignment of the photos to delete points that have a low likelihood of being in the correct place, by using the gradual selection tool.
- Georeferencing of the model by importing the GCP's and place markers in each photo where a GCP was visible.
- Building of a mesh with a face count of 4,535,343 for the backscarp project (with vegetation removed to prevent false structural measurements later), and 841,240 for the overview area.
- Building of a DEM for the overview project.

To meet the computer capacity requirements, the backscarp project had to be divided into chunks to create a complete dense point cloud. Each chunk were made using the batch process

tool, with high quality and aggressive depth filtering. The dense point clouds were then merged into one model using a Python script provided by AgiSoft customer service.

The outputs of the Agisoft processing was a 1.25 cm/pixel resolution dense point cloud of the backscarp, and a 7.51 cm/pixel resolution DEM of the overview area. Survey data, camera calibration and processing parameters for both projects are attached in the appendix.

3.4 Structural analysis

The structural analysis was carried out using Dips 7.0 (Rocscience, 2018) using stereographic projection (lower hemisphere, equal area, fisher distribution). In this study the orientation data is presented in Strike/Dip (right hand rule). The joint and foliation sets were defined by using one standard deviation variability cone.

Structural analysis was performed on two datasets, manual field measurements and structural data from a dense point cloud made in AgiSoft Photoscan (backscarp project) (Figure 9). The structural data from the point cloud were obtained using Coltop-3D software.
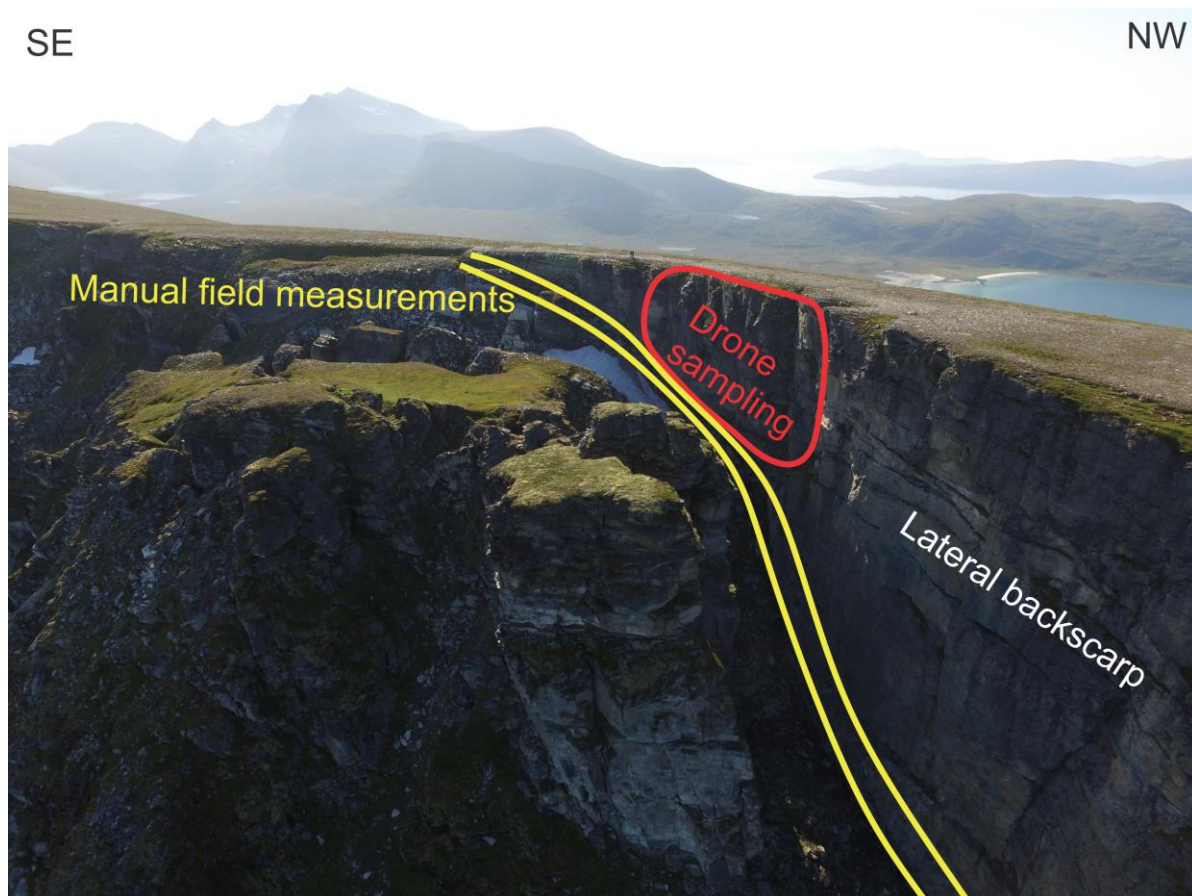
Figure 9 - Drone photo. Location of structural measurements for structural analysis.

3.4.1 Analysis in Coltop-3D

Coltop-3D is a semi-automatic structural recognition software which makes it possible to derive multiple structural measurements from a surface based on a dense point cloud, in this study based on a 3D point cloud made in AgiSoft Photoscan. The program sets different colours to the varying dip angles and dip directions of the surfaces using the HSI wheel (Figure 10).
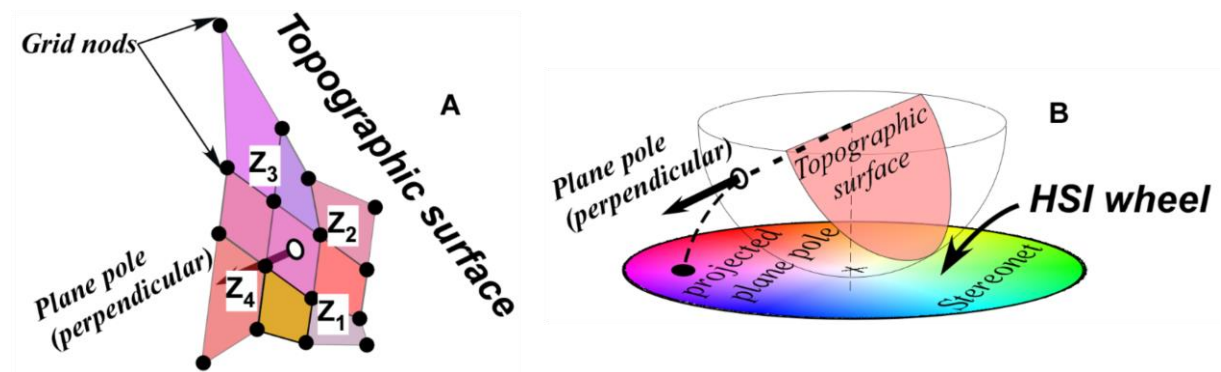
Figure 10 - The dip direction of the square DEM grids are represented by the hue (H) of the wheel from 0 – 360° and the dip of the pole using the saturation (S). The intensity can be changed for representation purposes. Modified after Jaboyedoff et al., (2007).

The dense point cloud from AgiSoft Photoscan contains x-, y-, z- and intensity values and was imported to Coltop-3D with pyramid levels 0.5-1 m, search radius 2 m and minimum/maximum number of points of 6 and 15. After the dense point cloud was imported it was evident which structural planes were repeatedly making up the rock face of the backscarp, based on their display colors. The planes of particular interest were then chosen using the polygon tool. When a polygon was set to a structural plane in the point cloud, it was given a median and mean dip and dip direction. Using the 'direction and dip with tolerance' tool, based on the mean dip and dip direction from the polygon, all planes within a specific tolerance of the mean plane were displayed on the dense point cloud. In this project the tolerance cone was set to be 20°. Five polygons with five different colors were made. Since the dense point cloud contains points in the number of millions and because of computer/software limitations, a selection of 1000 points out of 3,083,632 were imported to Dips 7.0 for structural analysis. The number of points exported from each polygon was based on their percentage of total number of structural data, to best represent the density concentrations in the Dips 7.0 stereonet- for example J1 represented 38.5% of surfaces over the entire model, and therefore 38.5% of the 1000 measurements extracted from Coltop-3D were taken from polygons of J1 planes.

3.4.2 Rotational analysis

The rotational analysis in this thesis was performed in a stereonet by using Dips 7.0 based on foliation measurements. By using the 'rotate data' tool, in situ foliaton planes were rotated to horizontal by X°. The foliation measurements from the unstable area were also rotated by X°. Then the rotation of the plane from the unstable area could be measured by using the 'arrow' tool to obtain trend/plunge. One rotational analysis were performed in this thesis, based on foliation data from the lowermost part of the URS and in-situ measurements.

3.4.3 Kinematic analysis

Kinematic analysis is used to identify possible slope failure modes, such as planar, wedge or toppling failures described in the theory chapter. Structural data is imported and tested for relevant slope dip angle and dip direction. The analysis includes parameters such as lateral limits and friction angles, which depend on the site and the rock properties. Lateral limits define how much oblique to the slope dip direction a failure is feasible, whereas friction angle generally is based on the rock type (Figure 11).

Based on the output results from the kinematic analysis, presented in stereonets (Figure 12), it is possible to see which joint sets that contributes to a feasible failure. If the location of a pole or a great circle lies within or cross-cut red, green or yellow colored fields, the joints they represent contributes to failure. The results in Dips 7.0 also includes tables with percentage on number of critical and total number of feasible failures, which is used to decide which joint sets that contribute the most to failures.

Planar sliding occurs along a joint plane dipping downslope, whereas wedge sliding occurs on a surface made up by two joints, forming an intersection dipping downslope. Additionally, kinematic analysis on flexural toppling and direct toppling was undertaken. Both failure types needs steep discontinuities. Direct toppling occurs in strong rock with orthogonal joints, and flexural toppling occurs in weaker rocks such as in shale (Wyllie and Mah, 2004).

Kinematic analysis on planar- and wedge sliding, and direct toppling was performed in Dips 7.0. The analysis were given a slope dip direction of 72° and a slope dip of 50° based on the DEM from ArcticDEM. The analysis were carried out with lateral tolerance of 30° and friction angle of 20° due to the conservative recommendations for all rock types stated in Hermanns, et al. (2012). The stereonets were edited in CorelDraw to create a better presentation of the results.

In addition the results from each kinematic analysis were described, focusing on which joint sets contributing to the most feasible failures.

Rock class	Friction angle range	Typical rock types
Low friction	20–27°	Schists (high mica content), shale, marl
Medium friction	27–34°	Sandstone, siltstone, chalk, gneiss, slate
High friction	34–40°	Basalt, granite, limestone, conglomerate

Figure 11 - From Wyllie and Mah 2004.
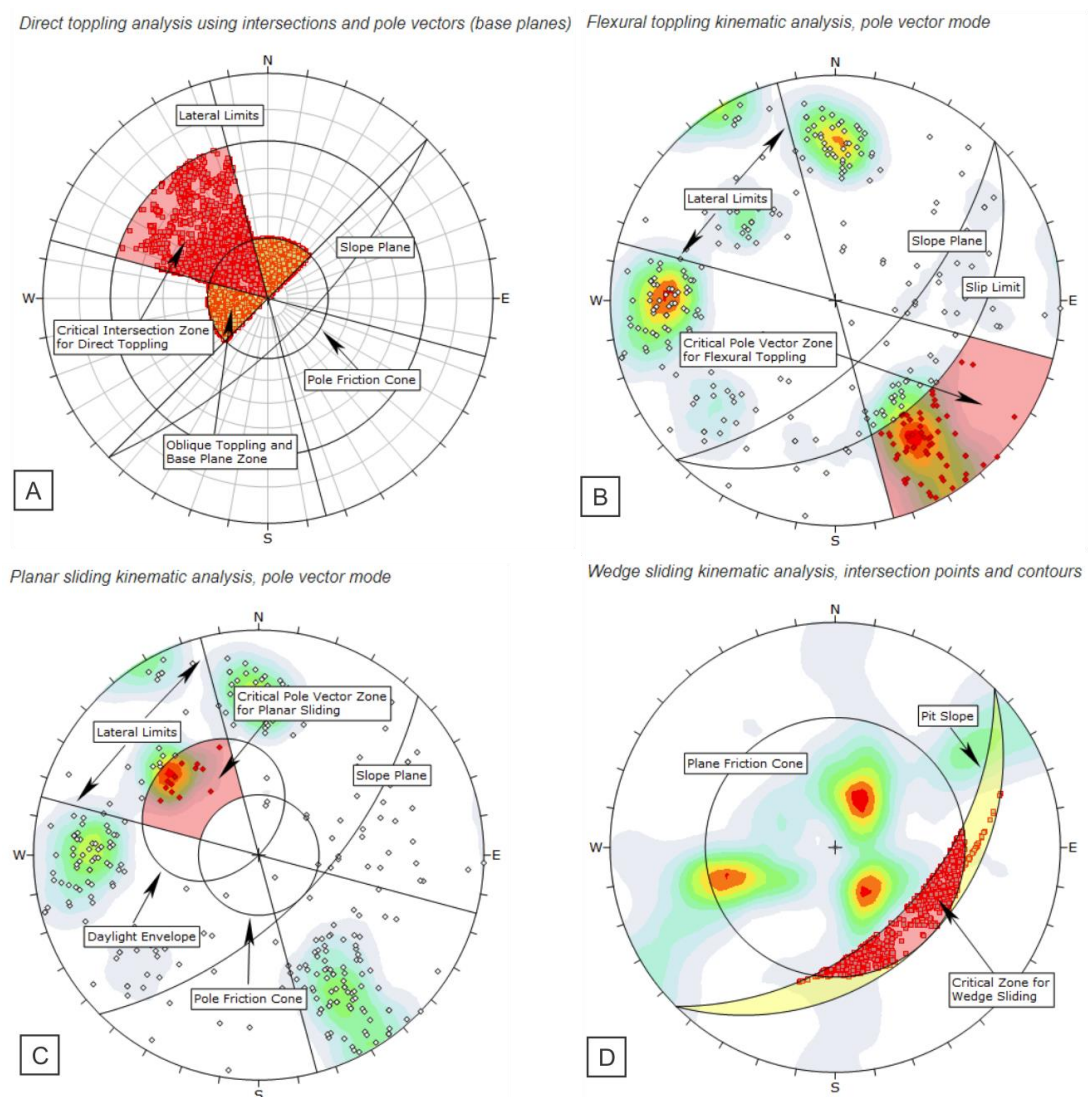
Figure 12 - Kinematic analysis on A: direct toppling, B: flexural toppling, C: planar sliding and D: wedge sliding. Figures modified after Rocscience (2018).

3.5 Volume calculations using AgiSoft Photoscan

Volume calculations were performed by following the tutorial on 'Volume Measurements with AgiSoft Photoscan Pro 1.1' (agisoft.com). AgiSoft Photoscan calculates the volume from a mesh which is built on the basis of a point cloud. The points outside the area of interest were cropped out before generating the mesh. In this way two areas were highlighted for volume calculations: the overall unstable area and the unstable column. Both 3D models were enclosed for volume calculation using 'Close holes' command. This tool closes an open mesh/3D surface to form a convex hull. The volume is then calculated based on the geometry of the hull.

3.6 InSAR data

Interferometric synthetic aperture radar (InSAR) is data used to measure relative displacement between two images. The data can be captured using both ground-based and satellite-based radar. The interferometry derived from satellite is measured as a phase shift between stacked images within the line of sight (LOS) of the satellite for a specified area. Satellite SAR instruments LOS depends on the azimuth-, track- and incidence angle of the equipment.

Satellite-based InSAR from Sentinel-1 and Sentinel-2 imagery was acquired from InSAR Norge (insar.ngu.no). The satellite has a repeat cycle of c. one week, and two ascending and descending tracks have been used as the polar location of Troms, which means that satellite's paths overlap. The datasets cover the summer months between July 2016 and September 2018, making it a valuable tool for monitoring of current day movement rates. For this study the ascending lines are used, as they have a LOS down towards ENE (Trend/plunge: Ascending 1-076/37. Ascending 2-078/41), which aligns with the expected movement vector of Skredkallen.

The data are presented in InSAR Norge in point format. The steep nature of the ridgeline at Skredkallen means that it is generally in the satellite shadow, and therefore there are limited data points in the unstable area (c. 50 points).

The InSAR data was collected by using the 'Compute Average' tool. Two polygons were made, one for each area of interest: rock column Kaillen and on the central part of the URS. The average displacement rate for each polygon were obtained from both Ascending 1 and Ascending 2 datasets.

4   Results

This chapter presents the results of this thesis, beginning with the main findings from the fieldwork campaign, followed by analysis using desktop methods. The datasets presented are:

- Regional lineaments
- Geophysical data
- Lithology
- Geological structures (foliation and joint sets)
- Structural analysis from Coltop-3D
- Geomorphological map of the area
- Morphostructures
- Rotational analysis
- Kinematic analysis
- Volume estimations and run-out estimate
- InSAR data

4.1   Regional lineaments

Lineaments best seen on a regional scale, can be found on the mountain ridges on Laukvikfjellet and Kvalkjeften, displaying a wide range of orientations and geometries (Figure 13A). The lineaments on the western face of Laukvikfjellet are displayed in (Figure 13B). In particular two sets of lineaments are repeating: NE-SW (orange) or E-W (blue). These can be found in areas were the relatively flat mountain ridges of Laukvikfjellet and Kvalkjeften show great changes in surface topography, either in steep slopes such as northwest of Skredkallen, along streams or even small canyons located south on Laukvikfjellet. In addition there are two sets oriented NNW-SSE (green) and E-W (light blue) which both display a distinctive curved geometry. These can be recognized either as depressions along streams or small steps in the surface topography.
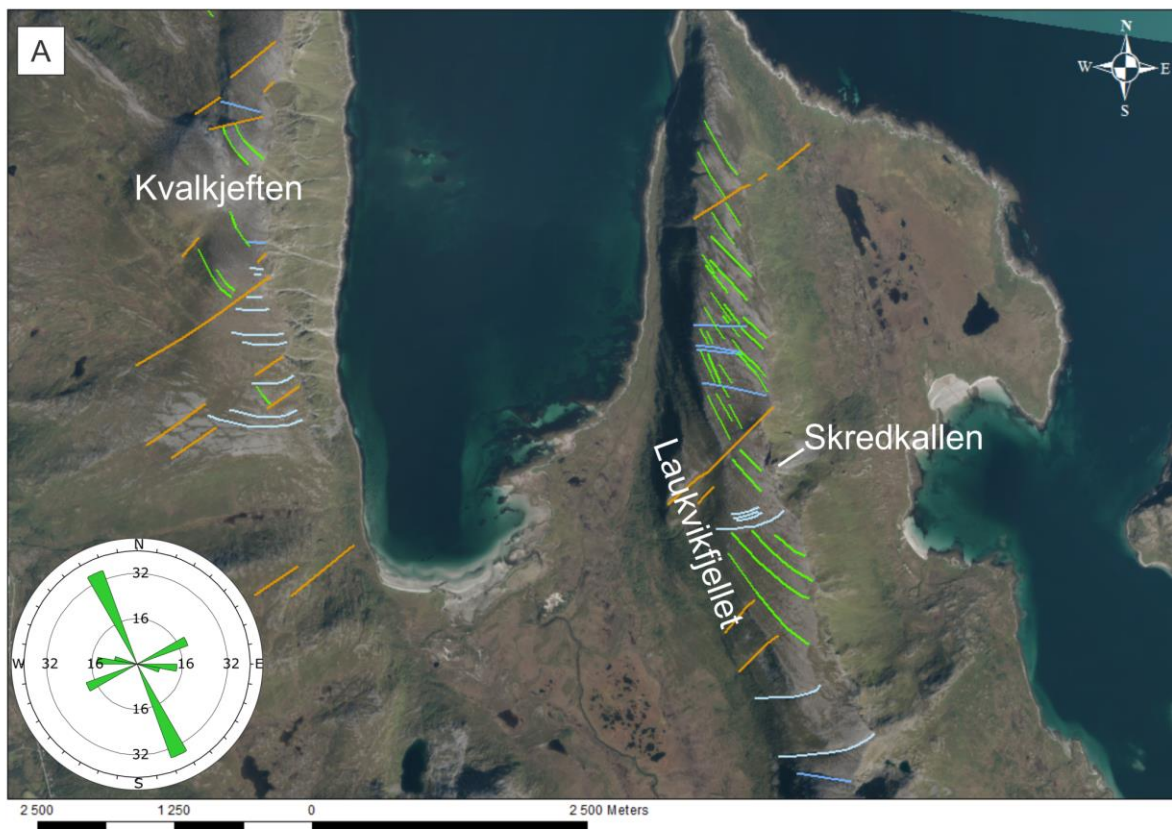
Figure 13 – A: Lineaments on Laukvikfjellet and Kvalkjeften. B: Drone photo. Lineaments on the western face of Laukvikfjellet. Note the change in surface topography just NW of Skredkallen.

4.2 Geophysical data

The tilt derivative map of helicopter-borne magnetic data based on magnetic anomalies provided by (NGU) is presented in Map 7. Based on magnetic anomaly data, first and second vertical derivative maps are commonly used to sharpen the edges of magnetic anomalies and enhance shallow features (Telford et al., 1990). This data can be used to better understand regional geological structures. Magnetically dislocations of structures is a basic tool for determination of steep faults and fault zones (Henkel, 1991).

Two dominant lineaments are interpreted from the data, one striking ENE-WSW through Skredkallen and one parallel major lineament 7.5 km further NW representing the Vannareid Burøysund Fault.
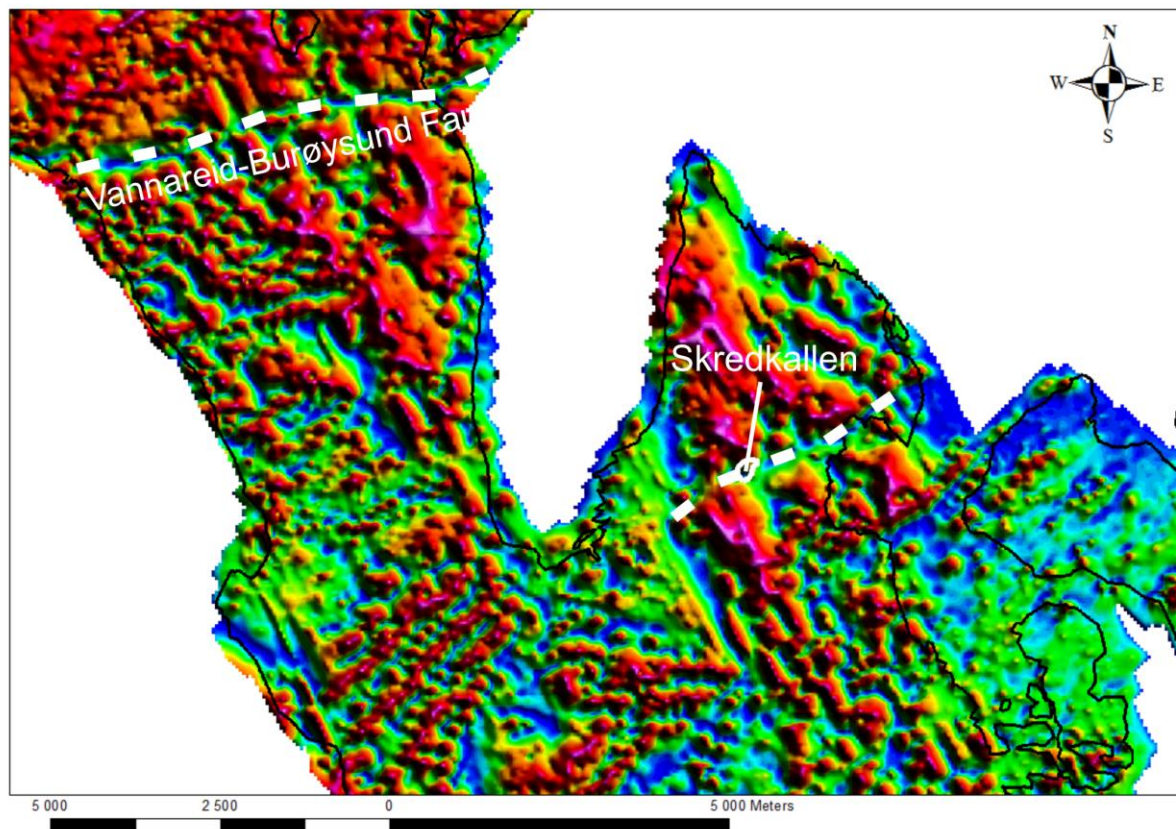
Map 7 - Tilt derivative from magnetic anomalies. Skredkallen location and lineaments are displayed. Data from NGU (2012).

4.3 Lithology

The lithology of Skredkallen is predominantly consisting of tonalitic gneisses with mylonitic foliation cross-cut by numerous mafic sills (Bergh et al., 2007). The tonalitic gneisses are very homogenous and show little variations both in color and texture, although variations in plagioclase and quartz content can vary locally. The rocks are very strong and require numerous hammer strikes to break apart. The mafic sills are parallel to an older generation of foliation, which in some places are crosscut by zones that display a phyllitic to mylonitic structure in a grey/brownish matrix. These zones are parallel to the later-stage dominant foliation, dipping gently towards NNE and can be up to 0.5 m thick, but on average c. 10 cm (Figure 14). These zones are often located in the upper part of the mafic sills. In some places these zones are heavily weathered (Figure 15), and could easily be broken by a hammer strike. It is likely these zones represent 'internal shear zones' related to thrusting of the Skipsfjord Nappe.
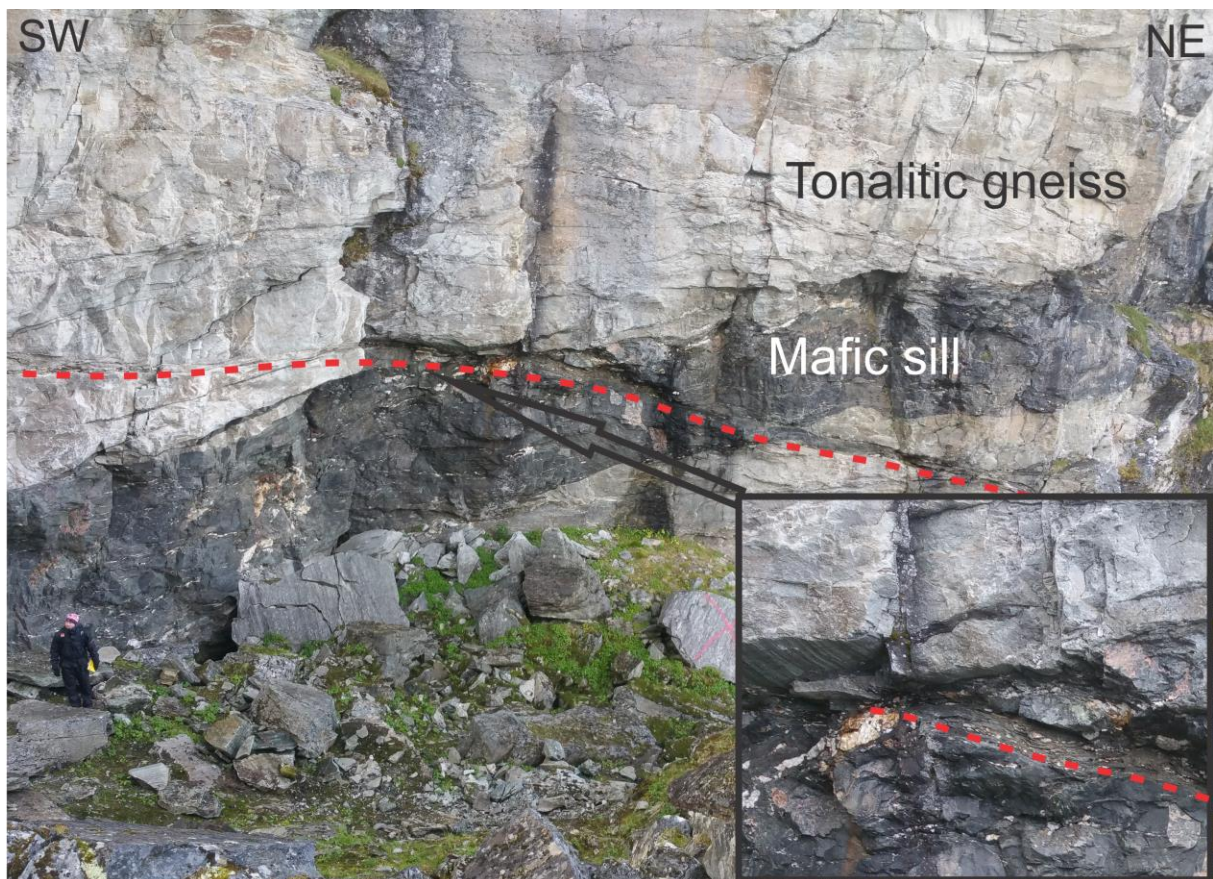
Figure 14 - Station 7. From the lateral backscarp on Skredkallen. Mafic sill in tonalitic gneiss. Red stippled line displaying the lower boundary of an 'internal shear zone'.

Figure 15 – Station 10. 'Internal shear zone'. Phyllitic (upper) and mylonitic (lower) separated by the red stippled line. Note the symmetric sigmoid porphyroblast indicating pure sense of shear.

4.4 Geological structures

This chapter describes the geological structures (Table 3) based on field observations which have been analysed in Dips 7.0. Other features within the geological structures, such as folds, stretching lineations and slickenlines/slickenslides, are also included. All structural measurements and observations from the field were collected from field stations indexed on Map 8.

Table 3 - Geological structures.

Geological structure	Strike/dip
Foliation (SF)	292/14±13.8
J1	034/82±16.9
J2	205/68±9.0
J3	309/68±10.5
J4	117/83±15.5
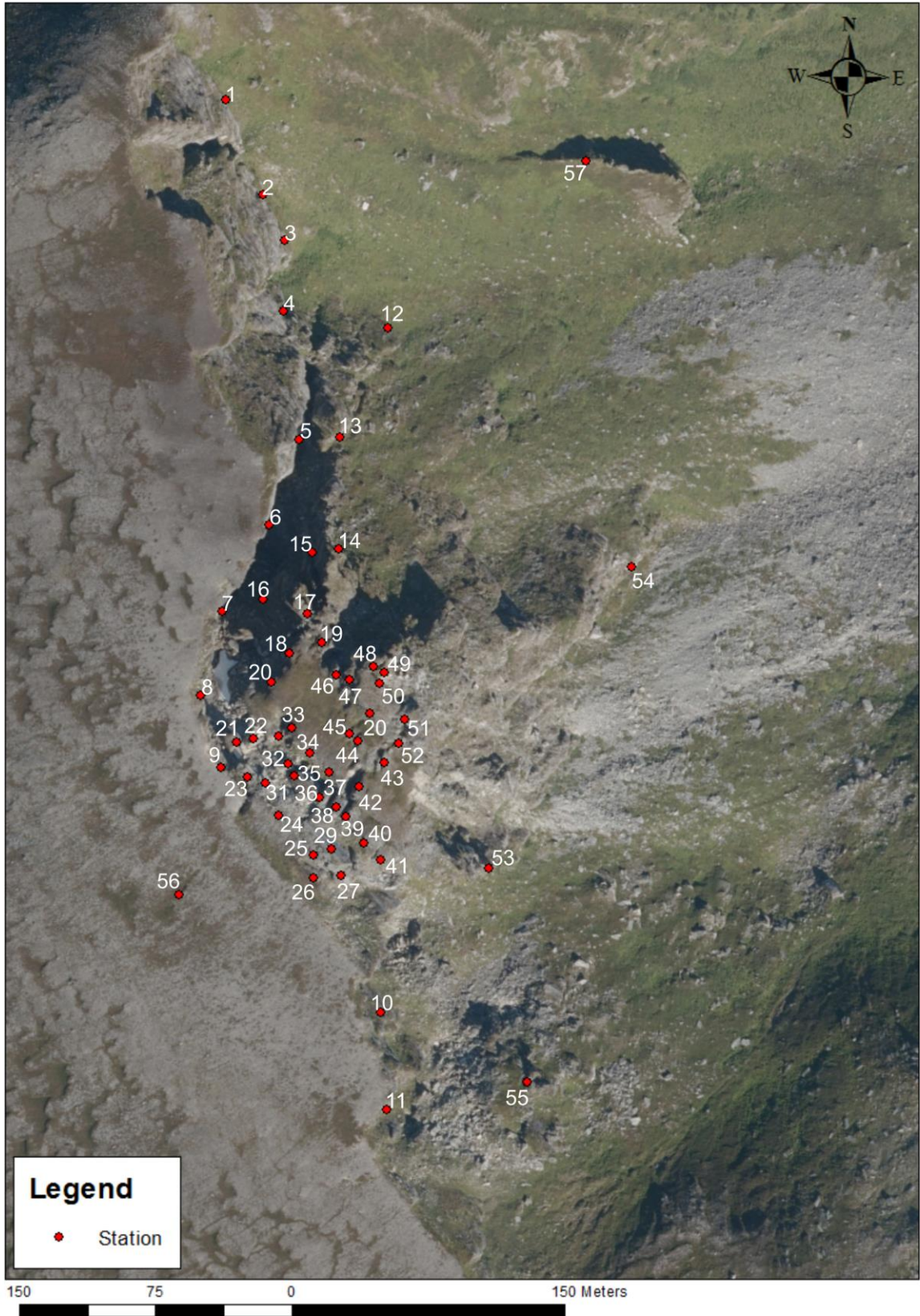
Map 8 - 57 field localities

4.4.1 Foliation (SF)

The foliation along the backscarp is dipping gently towards NNE (292/14±13.8), with dip angle variations up to 13°. The foliation is thickly layered, well developed and displays mica-rich surfaces. Slickenslided surfaces with sense of shear trending NW-SE can be found along the foliation. Stretching lineations (ductile structure) visible from the intersection between joint sets and foliation or cleavage and foliation dipping gently towards NW, are very abundant. The foliation in and around Skredkallen appeared planar, or unfolded. Two km south of Skredkallen, on top of Laukvikfjellet, there was a 0.5 m wide fold with a gently NW-dipping axial plane (Trend/plunge - 304/34). A folded foliation was also observed along the backscarp (Figure 16, station 2), dipping steeply towards SE and terminating against a planar bedrock structure with very low roughness, probably a small scale inherited fault (Figure 16). However, these observations are outside the defined instability area. The main parts of the URS show a foliation orientation which is very similar to the foliation mapped in the backscarp, but slightly tilted in varying directions. Smaller parts of blocks are generally tilted either towards NE or SW, as seen by the foliation which often strikes NW-SE (Map 9).

Figure 16 – Station 2. Right: foliation folded steeply towards SE. Left – planar foliation. Orange stippled line: bedrock structure/small fault. Inset: smooth stained surface of the 'fault'.
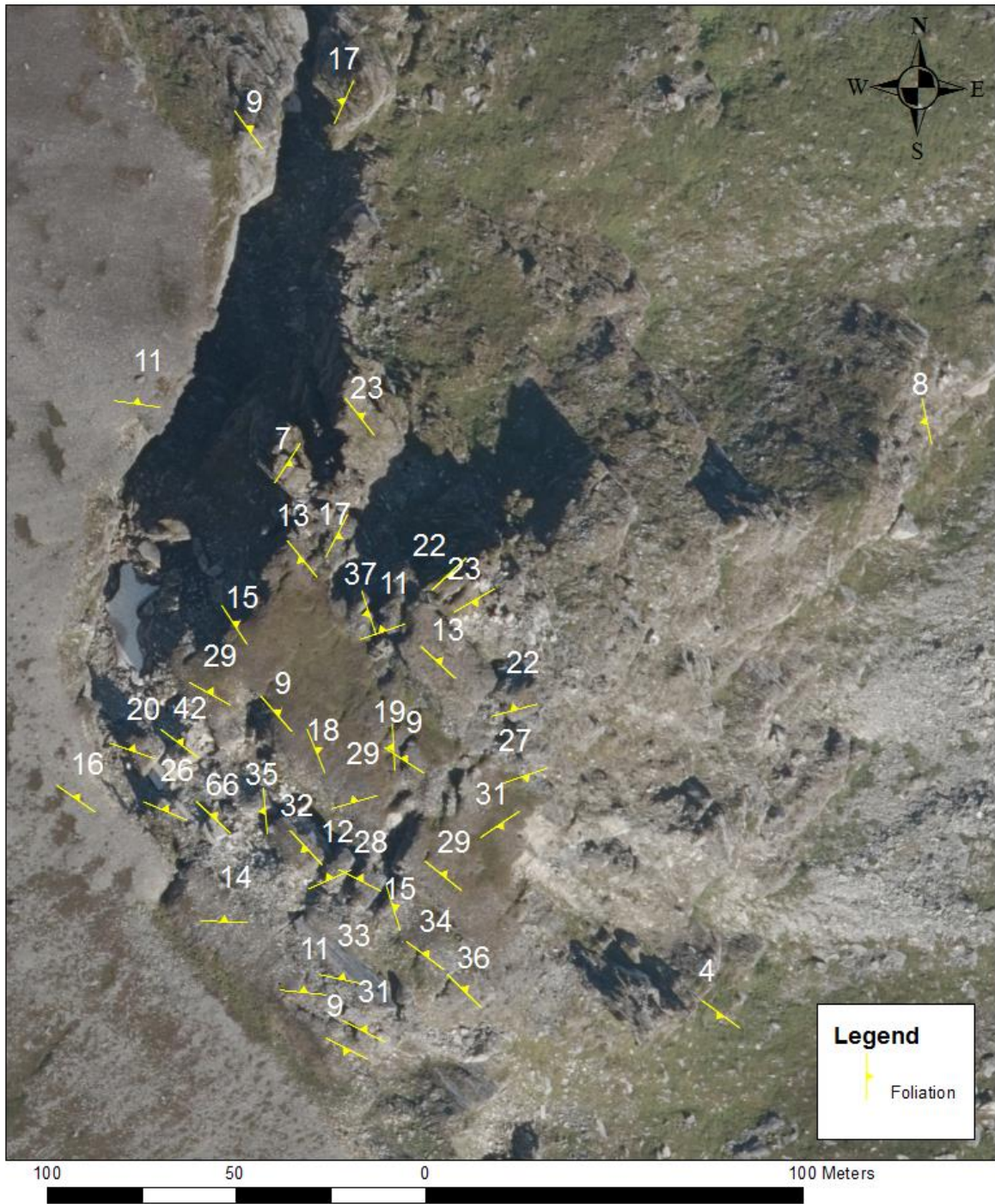
Map 9 - Foliation measurements. Note that the foliation usually strikes either NW-SE.

4.4.2 Joint sets

The joint sets were defined on the basis of field observations and measurements along the backscarp using Dips 7.0 with 1σ standard deviation variability cone (Figure 17). Most measurements were obtained along the lateral backscarp because it was the most accessible. Structural measurements obtained from photogrammetry will be presented later.

Four joint sets and foliation were identified in Dips (Table 4). The most dominant joint set on Skredkallen is Joint set 1 (J1) striking NNE-SSW and dipping steeply towards ESE. Joint set 2 (J2), striking NNE-SSW and dipping moderately towards NNW, were observed only occasionally. Joint set 3 (J3) striking NW-SE and dipping moderately towards NE, was difficult to measure in the field, although many observations of its occurrence were made. J3 would likely show a much greater pole concentration if the main backscarp striking NW-SE was more exposed. Most measurements were taken from outcrop slopes which were oriented so that J3 and foliation (SF) did not daylight. Joint set 4 (J4) striking NW-SE and dipping steeply towards SW, is the second most prominent joint set on Skredkallen.

There are great variations within all joint sets in terms of strike/dip, and there is a possibility that more than four joint sets are present, most likely a near-vertical joint set striking N-S and dipping towards E, as seen from the cluster concentrations (Figure 17). This joint set might be a subsidiary set to J1. However as the sets were difficult to differentiate from each other, four sets that were clearly observed in the field were chosen. Joint set characteristics (spacing, persistence, shape and roughness) were mainly obtained from station 11 (Figure 18) south of the unstable area.
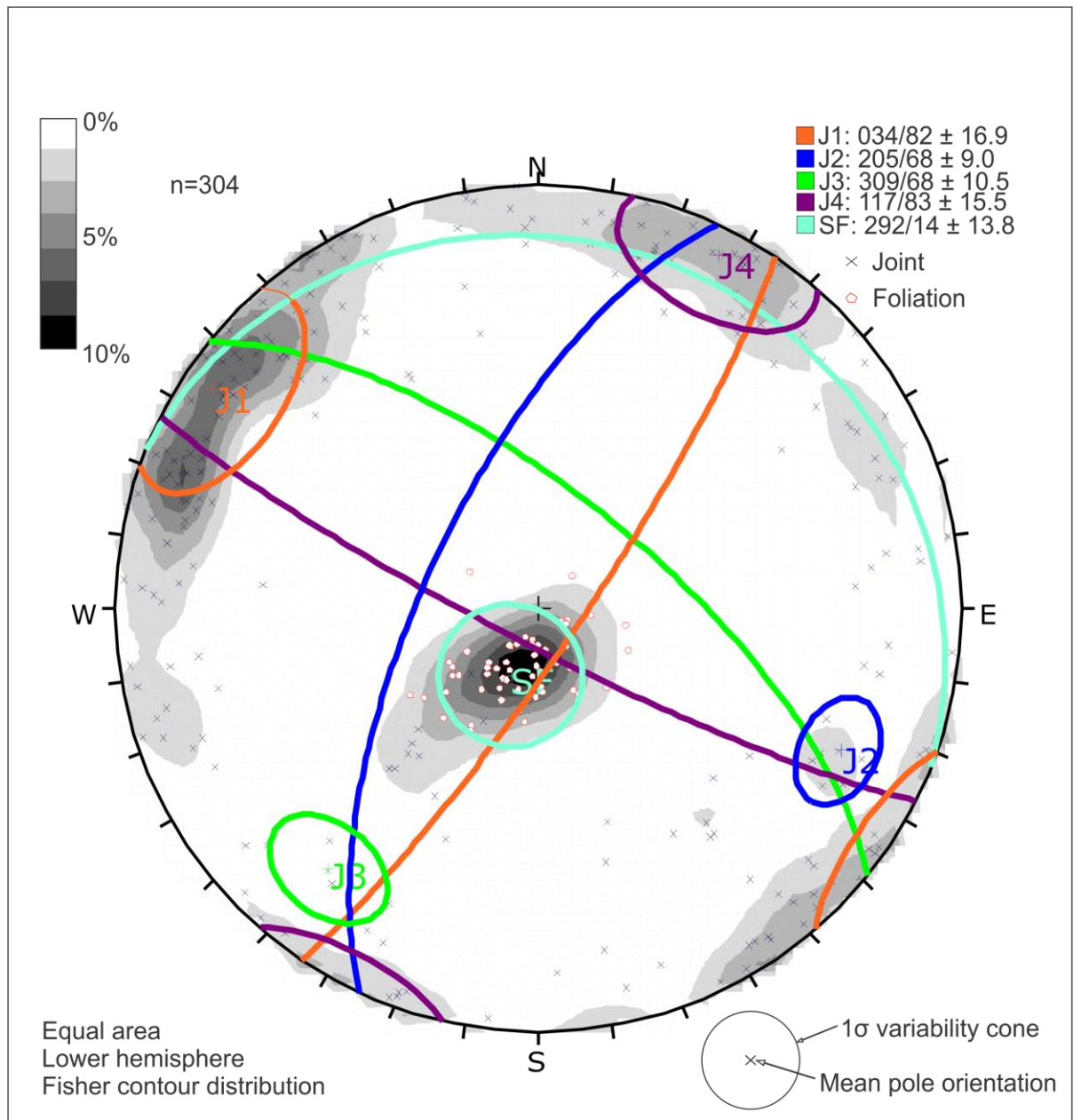
Figure 17 - Stereographic analysis from Dips 7.0.

Table 4: Joint sets and foliation, and their properties. Note that spacing and persistence have been obtained from different slope aspects, as indicated (NZGS, 2005).

Joint set	Spacing		Persistence		Shape	Roug -hness	Comment
	NE/SW	SE/NW	NE/SW	SE/NW			
J1 034/82 ± 16.9	-	0.5 – 2 m	-	10 – 25 m	Planar. Occasionally listric.	Smooth to very smooth	Often orange coating or more seldom pink staining.
J2 205/68 ± 9.0	-	0.2 - 1 m	-	0.5 – 1 m.	Planar	Smooth	Often orange coating
J3 309/68 ± 10.5	0.2 – 0.5 m	-	Mostly 0.1 - 0.5 m. Max. 25 m	-	Both planar and undulating.	Rough	Slope parallel
J4 117/83 ± 15.5	0.5 - 1 m	-	0.5 – 20 m.	-	Planar	Rough	-
SF 292/14 ± 13.8	0.05 – 0.5 m	-	0.1 – 2 m	-	Planar.	Rough	Some places hard to differ from J3

Figure 18 - Station 11. Joint set presentation. In-situ rocks 0.5 km south of Skredkallen. ESE facing aspect. Note the great variations within joint set 1 in terms of strike. NB: upwards perspective creates distortion so that J3 and J4 appear similar when in fact they are conjugate.

4.4.2.1 Joint set 1

J1 (034/82±16.9) joints are very well distributed along the whole backscarp with high persistence and smooth to very smooth planar planes, and in some places become listric with depth. Some planes display slickenslided surfaces with slickenlines indicating pure-dip slip down towards SSE (Figure 20A-B). The joints displaying a listric geometry are consistent in terms of strike orientation, disguisable from the general J1 set as they strike further to the east (up to 056 °; Figure 20D). Similar structures were observed to control parts of the unstable area (Figure 20E).

4.4.2.2 Joint set 2

J2 (205/68±9.0) dipping towards NNW, was much less observed as seen from the low cluster concentration in the structural analysis. The set could be observed as being part of a conjugate set, either as small fissures or planes displaying orange coating (Figure 19C).

Figure 19 - A + B: Slickenlines (station 6). C: Conjugate set with orange coating (station 1). D and E: Joints with listric geometry (station 8).

4.4.2.3 Joint set 3

J3 (309/68±10.5) dipping towards NE being slope parallel, has low persistence and frequency. J3 some places displays a very distinctive undulating geometry as it tends to refract along foliation (Figure 20A). This geometry can be seen both in small- and large scale on similar slope aspect along the whole backscarp; step-path failure on small scale and steep undulating walls on large scale.

4.4.2.4 Joint set 4

J4 (117/83±15.5) dipping towards SW some places show calcite slickenlines indicating dextral strike-slip movement (Figure 19B). This joint set appears both as fissures with low persistence (Figure 20C) and highly persistent near-vertical walls along the backscarp.
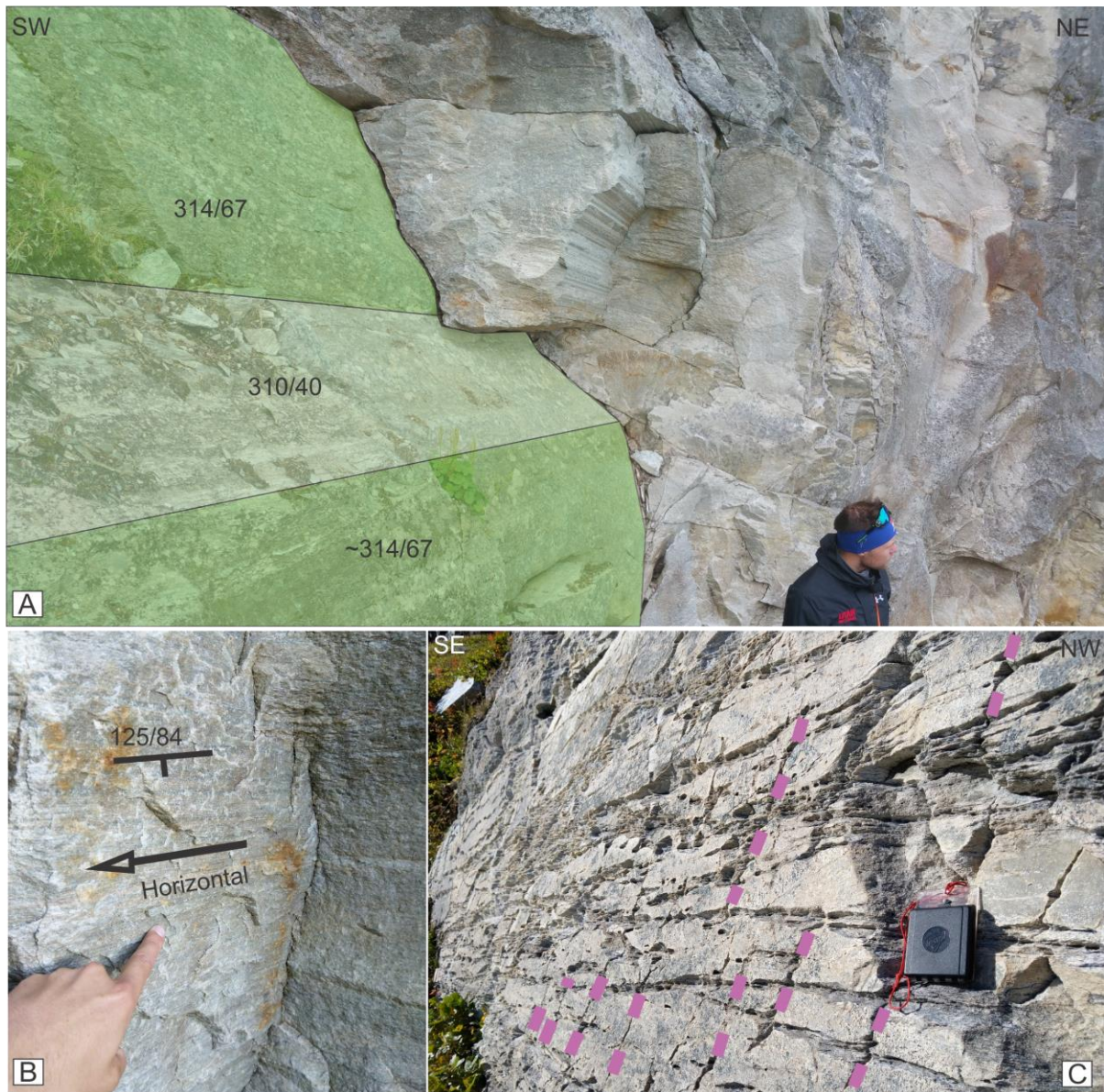
Figure 20 - A: J3 undulating geometry (station 9). B: Slickenlines along J4 (station 10). C: J4 as fissures (station 53).

4.5 Structural analysis from Coltop-3D

The structural data from Coltop-3D are presented in Table 5 and visually with the point cloud in Figure 21. The structural analysis on the dataset in Dips 7.0 (Figure 22) aligns well with field measurements (comparison in Table 6). The strikes of the sets are very similar; however the dip of two sets is measured to be shallower in the point cloud.

The most dominant joint set found in the field, J1 is also the most frequently sampled in the point cloud. J2 was also dominant in the point cloud, and J3 and 4 were much less frequent. Foliation was sampled the least.

The point cloud visualisation from Coltop-3D (Figure 21), presents well how J3 and 4 interact with stretching lineations, where the intersection between J3 (green) and J4 (purple) is shown as alternating color bands.

Table 5 – Structural data from Coltop-3D. Joint set distribution verifying the dominance of NE-SW striking discontinuities.

Joint set	Mean strike/dip in Coltop-3D	Number of structural planes from the point cloud	% of total number of structural data
J1	037/71	3,629,337	38.5 %
J2	149/52	3,470,634	36.9 %
J3	314/51	772,660	8.2 %
J4	201/71	960,333	10.2 %
SF	283/21	583,237	6.2 %
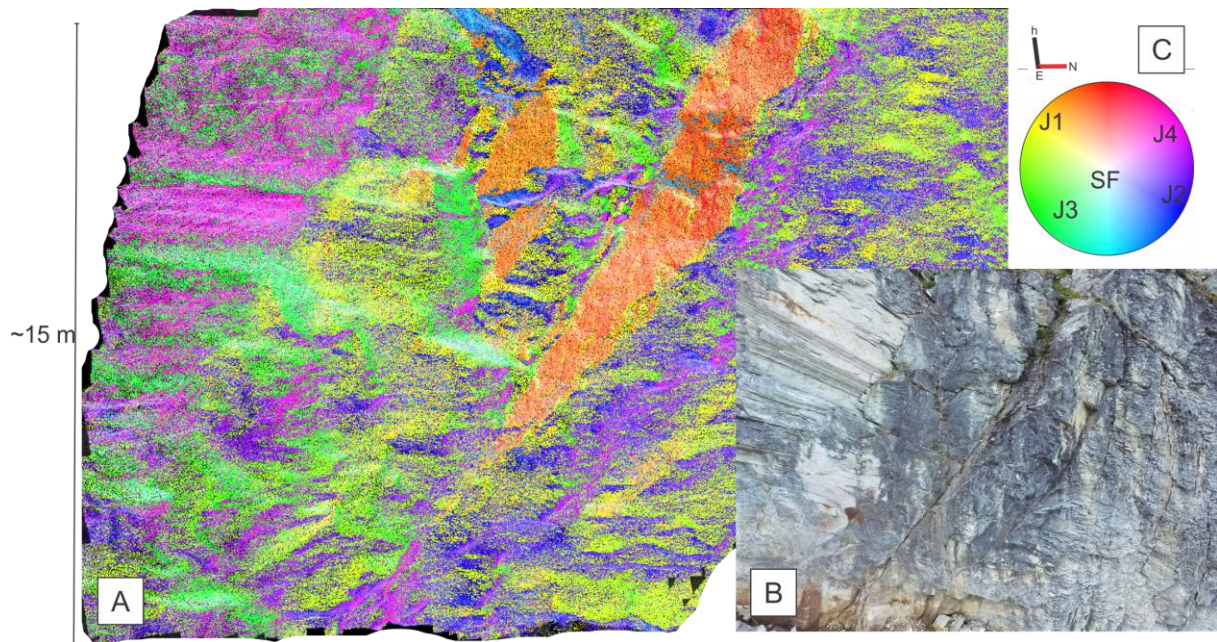
Figure 21 – The two listric joints presented in Figure 19D are in the center of A and B. A: Coltop-3D presentation B: Photo from the same perspective. C: HSI wheel.
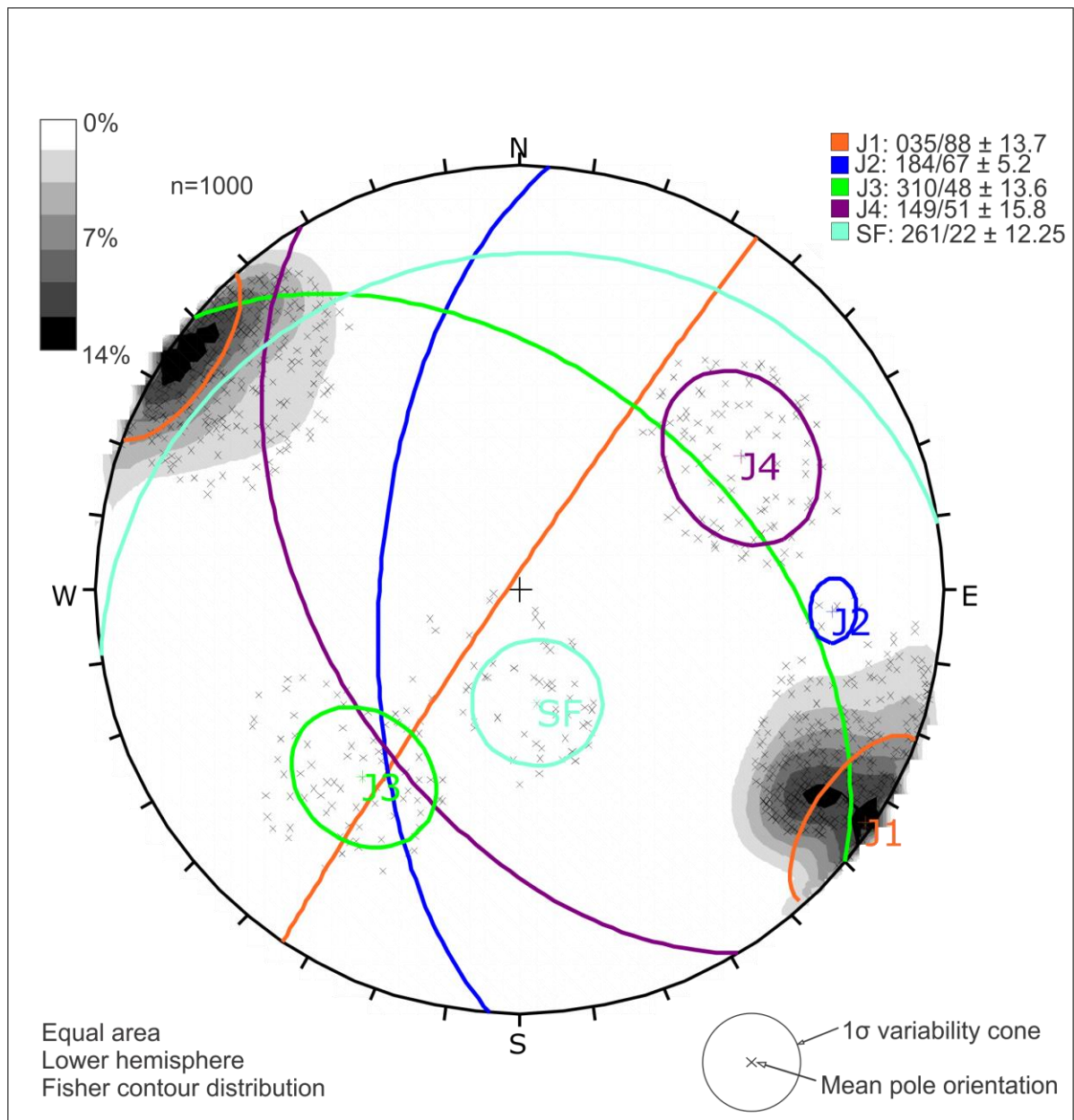
Figure 22 - Joint sets based on structural data from Coltop-3D.

Table 6 – Comparison of joint sets from the field measurements and point cloud, both defined with 1σ standard deviation variability cones.

Joint set	J1	J2	J3	J4	SF
Field measurements	034/82±16.9	205/68±9.0	309/68±10.5	117/83±15.5	292/14±13.8
Point Cloud	035/88±13.7	184/67±5.2	310/48±13.6	149/51±15.8	261/22±12.25

4.6 Geomorphological map of the area

This chapter gives an overview of the area focusing on the geomorphology of deposits (Map 10).
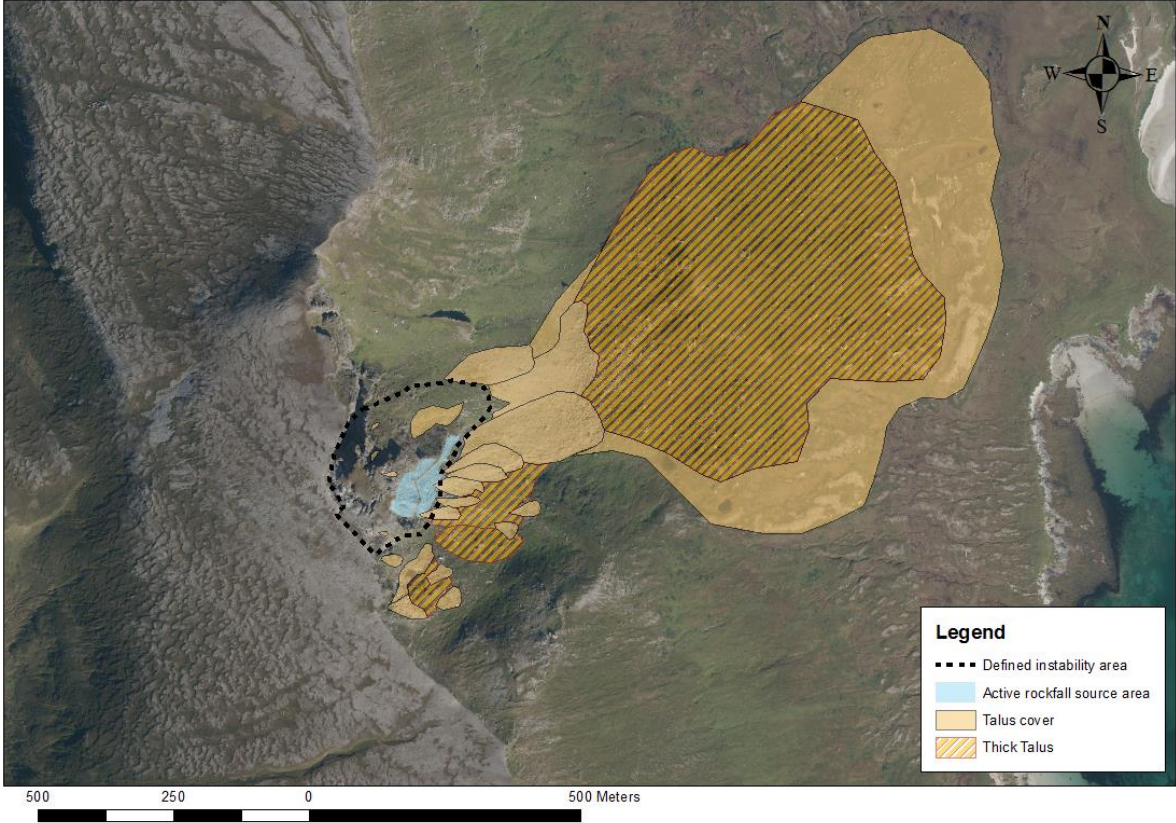
Map 10 – Geomorphology map of deposits.

The defined instability area sits between 460 and 240 m asl, and consists of vertical cliff faces on the southeastern section, whereas the northeastern section follows the gentle slope made up by talus cover or soil/vegetation. The URS does not display a distinct toe, likely because the lowermost part is masked by talus material. Multiple failure events have occurred at the site, evidenced by extensive talus cover at the foot of Skredkallen (Figure 23A). Within the talus, numerous fan shapes can be found. The talus clearly differs in age as some (e.g. under the southeastern section of the unstable area) has no vegetation cover. Older deposits form what is likely to be avalanche deposits, and thick talus can be found as far out from the base of the unstable area as 1.2 km (Figure 23B). Block sizes within the thick talus typically are c. 10 m^3, and up to a maximum of c. 1000 m^3. The fresh talus along the southeastern section of the URS is likely supplied by ongoing rockfalls from the steep cliffs above.
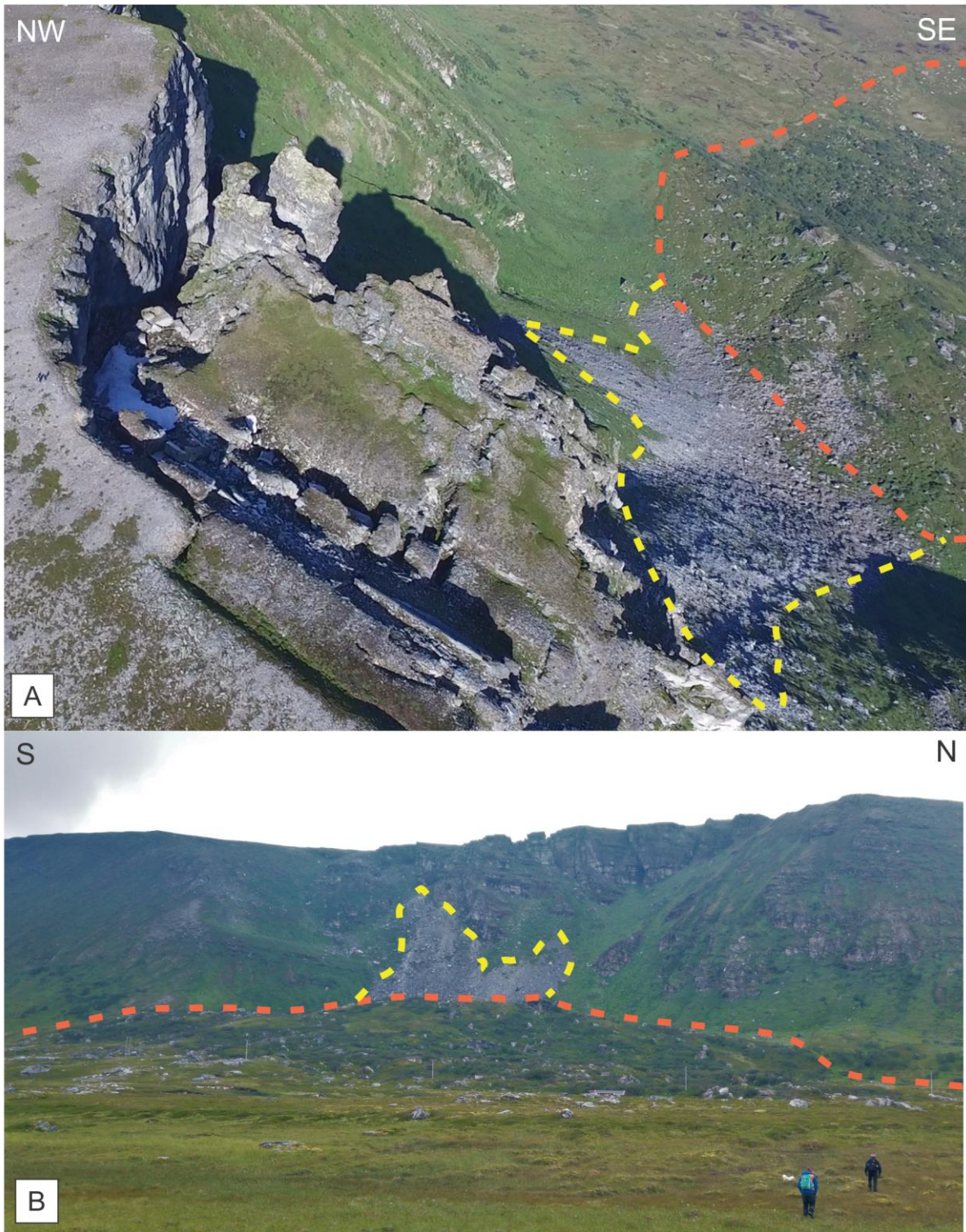
Figure 23 – A: Drone photo. Blue: Active rockfall source area. Yellow: Talus cover. Orange: Thick talus. B: Picture c. 1.2 km from the backscarp looking onto Skredkallen and 'Skrea'.

4.7 Morphostructures

This chapter presents the morphostructes within the defined instability area (Map 11).
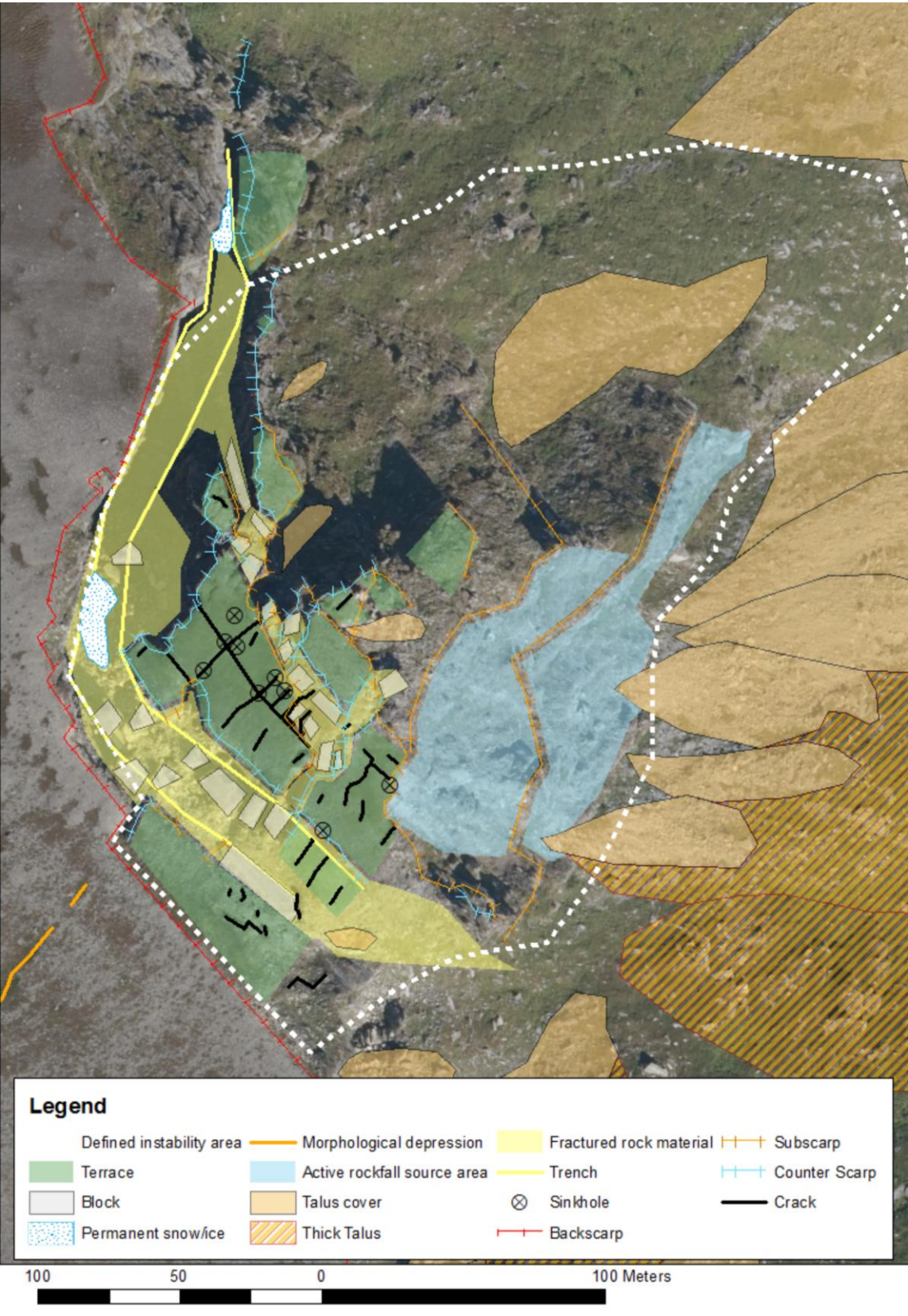
Map 11 - Morpho-structural map

The URS on Skredkallen is delimited by a main backscarp striking NW-SE and a lateral backscarp striking NNE-SSW. The backscarp is characterised by a zig-zag-shaped pattern made up of NW-SE and NE-SW-striking near vertical cliffs and subsidiary NNE-SSW striking cliffs further north (Map 12). The NW-SE striking segment follows J3 and J4, and the NE-SW to NNE-SSW striking segment follows J1 and J2.

Opening along the NNE-SSW segment of the backscarp has created a trench and exposed the backscarp vertically for c. 100 m due to the tilt downwards towards SE of the adjacent block (Figure 24A). Conversely only c. 2 m of the the NW-SE-striking section of the backscarp is exposed. However, it looks to be very steeply dipping towards NE based on field observations. Snow can be found in the trench all year round, especially at the north end, where ice was mapped in the shadows of the backscarp during the summer months.

The NE-SW striking backscarp contains a delineation at the northern end where the strike changes from NNE-SSW to NE-SW. This small section is a very distinct structure which contains smooth planes with slickenlines/slickenslides, and likely has the effect of segmenting the unstable area from the stable (see Map 11, Figure 24B).

The unstable mass is comprised of a system of moving blocks, terraces and fractured rock material. Blocks are distinguished from terraces by the lack of vegetation, small size and random orientation; whereas terraces are horizontal surfaces actively moving, but not disaggregated. The central terrace of the URS is subsided relative to the outermost terrace, forming a graben/horst complex (partly consisting of half-grabens) defined by NW-SE striking scarps and counter-scarps (Figure 24C). The graben terrace is at 454 m asl, whereas the outermost horst is 5-10 meters higher. The surfaces of terraces show signs of deformation by networks of open cracks creating morphological depressions in the vegetation cover. A morphological depression can be found in the stable part of Laukvikfjellet where it lines perfectly up with the backscarp.

The cracks are predominantly striking NE-SW or NW-SE, reflecting the same zig-zag pattern as the backscarp. Nine sinkholes were mapped in the graben, typically c. 0.5 m wide, c. 0.25 m deep and located on cross-cuts between cracks. Several large blocks can be found in between the terraces and along the backscarp. The blocks are often rectangular-shaped from orthogonal joint sets, rhombus- and trapezoid shaped from oblique sets (Figure 24D).
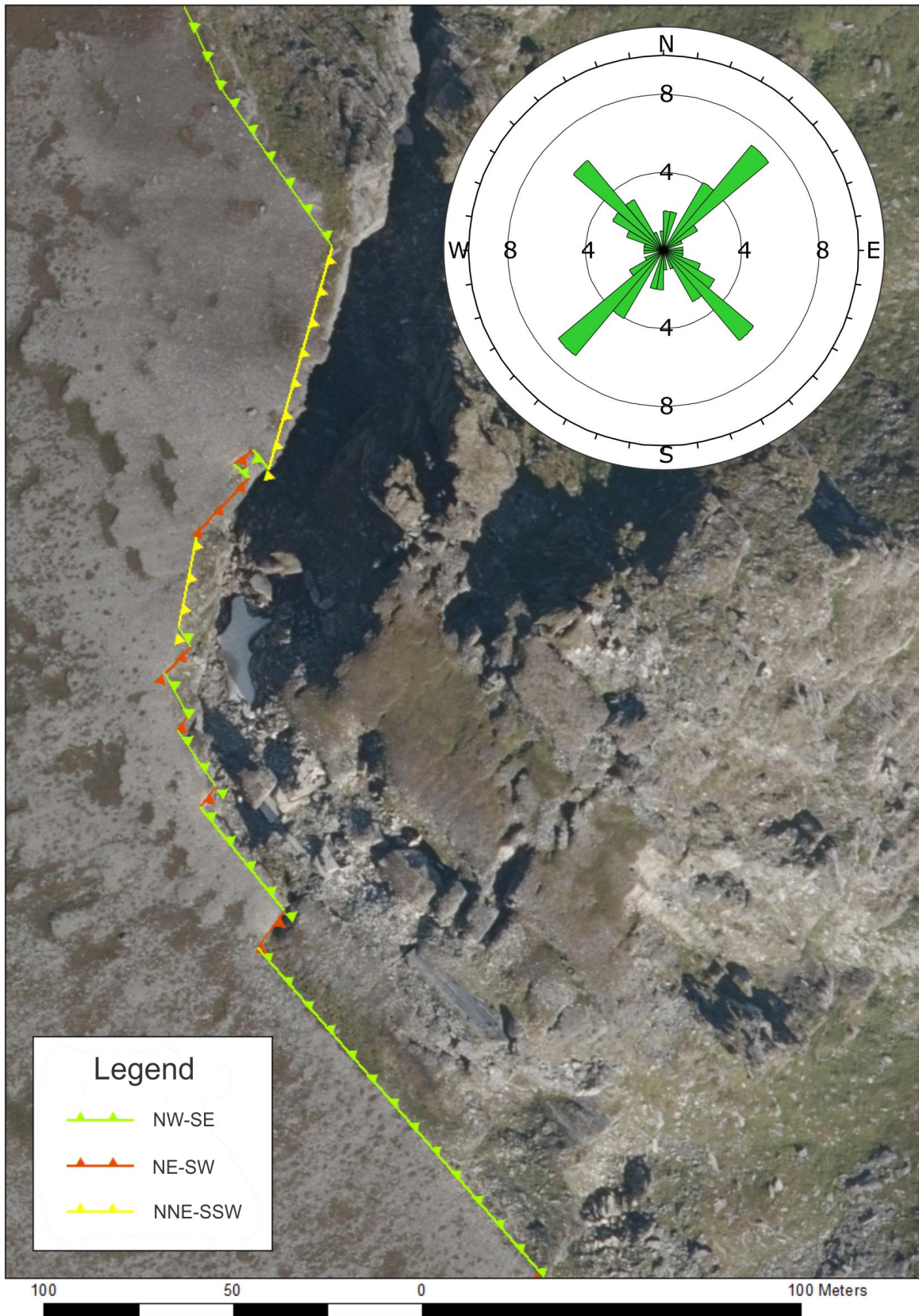
Map 12 - Orientation data on vertical cliffs along the backscarp. Note: Roseplot is based on data along the entire backscarp, c. 1 km distance.
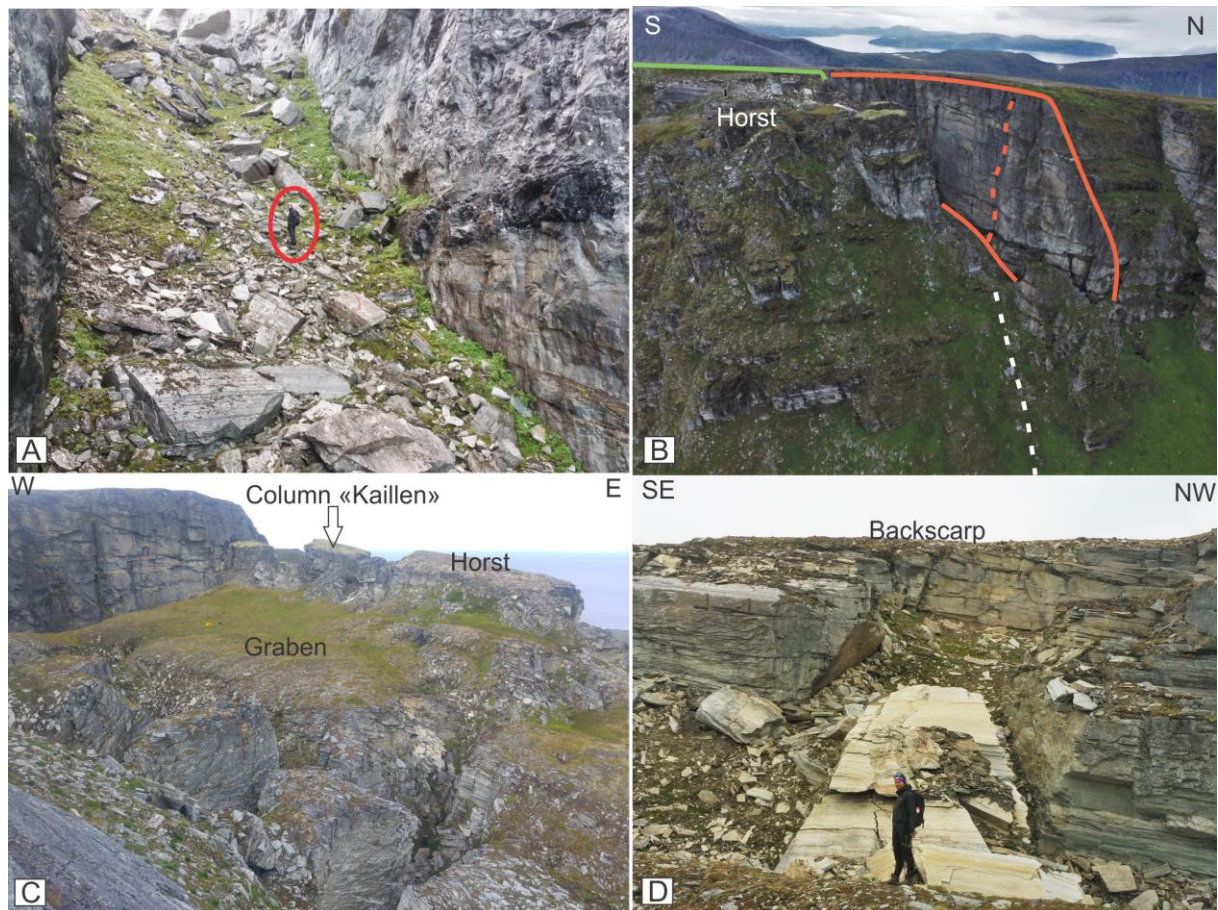
Figure 24 - A: Trench filled with fractured rock material (station 16). B: Drone photo displaying backscarp (orange/green) and delination of the backscarp / defined instability area (white). C: Graben and horst surrounded by blocks. D: Block with trapezoid shape collapsed from the main backscarp (station 22).

The URS is dominated by orthogonal subscarps, counterscarps and cracks striking NW-SE (parallel to J3 and 4) and NNE-SSW (parallel to J1 and 2) which delineates the URS into terraces and blocks (Figure 25A). The majority of these scarps are steep counter-scarps. Wide NNE-SSW-striking cracks can be traced down through the URS, as seen in Figure 25B, indicating a high persistence.

Scarps were observed to be vertical or near vertical. Those striking NW-SE generally follow a singular joint plane surface, J4. Scarps striking NNE-SSW follow a zigzag pattern alternating between a combination of mainly J1 and J4 or 3. A prominent zigzag shaped crack, parallel to the NNE-SSW striking backscarp cuts through the centre of the unstable mass (Figure 25C). This crack has effectively divided the unstable mass into two parts. Some scarps were observed to be made up of a stepwise combination of J3 and SF and formed an effective listric sliding plane for the block (Figure 25D).
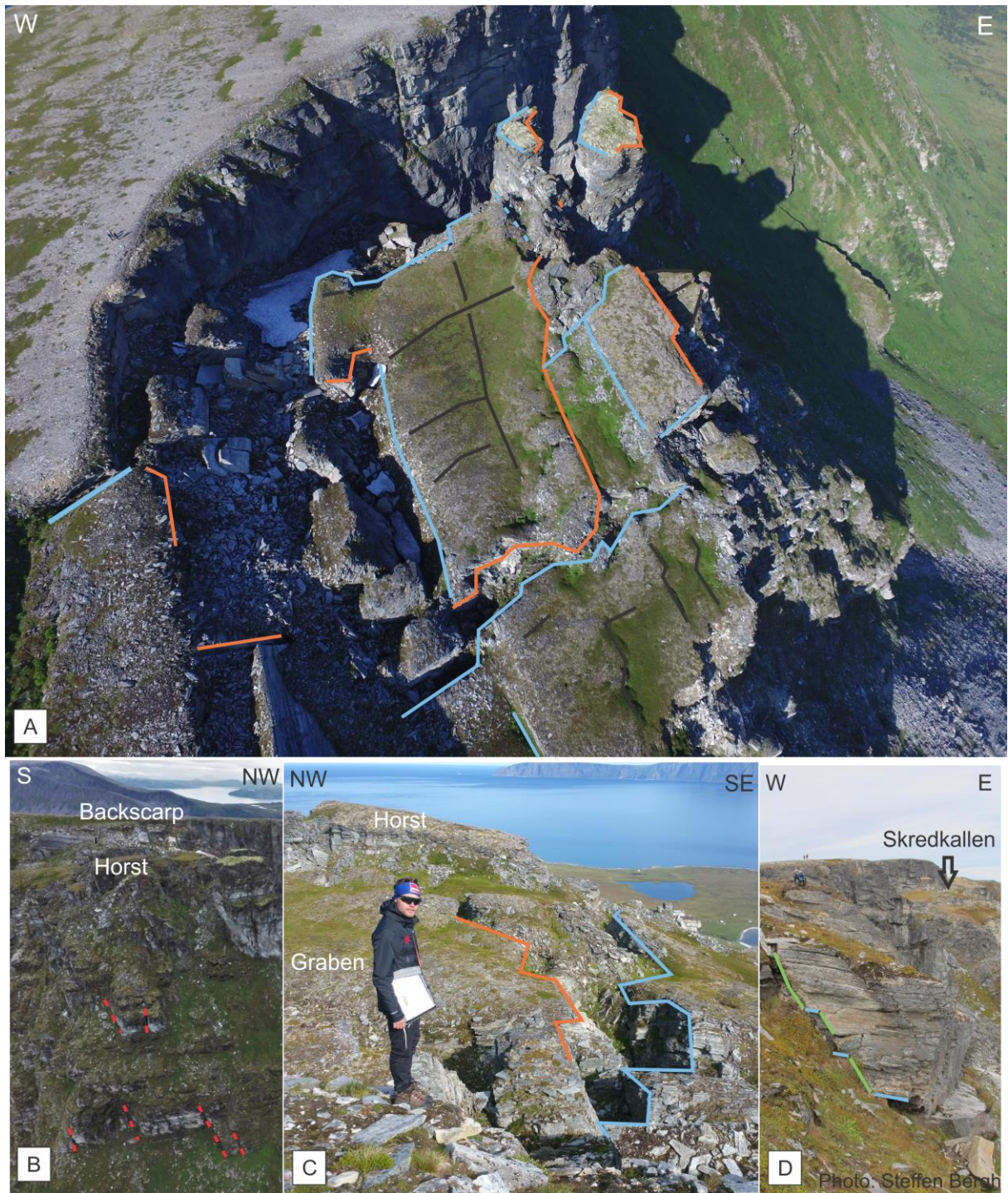
Figure 25 - A: Drone photo displaying counter-scarps (blue), sub-scarps (orange) and cracks (black). B: Drone photo displaying wide cracks. C: Major crack SE of the graben. D: Block c. 300 m SSE of Skredkallen with step path failure.

4.8 Rotational analysis

Rotational analysis was performed comparing foliation measurements from in-situ and from the lower part of the URS (station 54). The purpose of the analysis is to find out if the foliation has rotated, which gives an idea of the rockslide movement.

The rotational analysis shows that the foliation in the lower part of the URS has rotated into the slope, Trend/plunge - 222/20 (Figure 26). This assumes that the foliaton along the backscarp is continuously dipping gentle towards NNE. Conversely the foliation is folded thus leading to a false result.

The foliation measurements in the upper part of the URS, consisting of terraces and blocks, show that these parts often have tilted either towards NE or SW. Kaillen on the other hand, with a foliation dipping 23° towards NE (318/23), indicate a tilt movement more towards S.
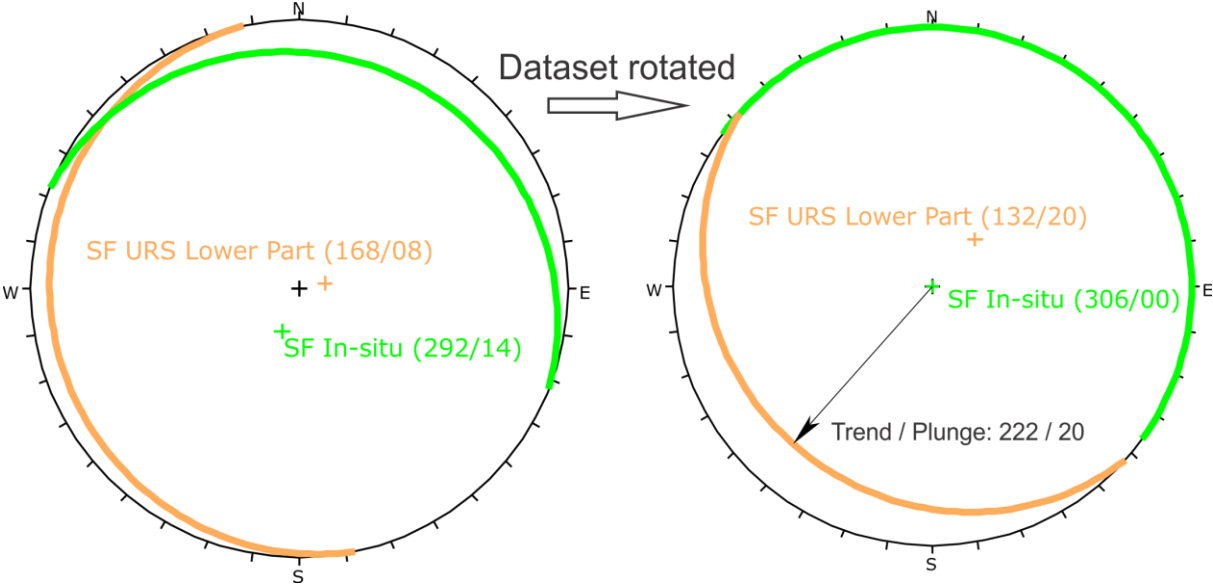
Figure 26 - Rotational analysis based on foliation data. (pole to SF In-situ rotated up to horizontal).

4.9 Kinematic analysis

This chapter presents kinematic analysis of joint sets mapped in the field. The critical area for daylighting has been defined by a slope dipping 50° towards ENE (072°), friction angle of 20°, and a lateral tolerance of 30° (after Hermanns et al, 2012;). Kinematic analysis results on the feasibility of flexural-, direct toppling, planar- and wedge-sliding failure for the Laukvikfjellet slope are given in Table 7.

Table 7 - Kinematic analysis results.

Slope aspect	Slope dip	Lateral tolerance	Friciton angle
072°	50°	30°	20°

	Critical	Total	%
Flexural Toppling (All)	25	304	8.22%
Flexural Toppling (Set 2: J2)	2	9	22.22%
Flexural Toppling (Set 4: J4)	4	49	8.16%

Flexural toppling: Total of 25 intersections critical. Flexural toppling is possible along uncertainties of J2 (22.22 %) and J4.

	Critical	Total	%
Direct Toppling (Intersection)	908	16719	5.43%
Oblique Toppling (Intersection)	1112	16719	6.65%
Base Plane (All)	46	304	15.13%
Base Plane (Set 1: SF)	44	68	64.71%

Direct toppling: Total of 908 intersections critical. Direct toppling is possible along uncertainties of SF (64.71 %), and intersections with J2 and J4. Oblique toppling is possible along uncertainties of SF, and intersections with J1, J2 and J4.

	Critical	Total	%
Planar Sliding (All)	12	304	3.95%
Planar Sliding (Set 1: SF)	10	68	14.71%

Planar sliding: Total of 12 critical. Planar sliding is possible along uncertainties of SF (14.71 %).

	Critical	Total	%
Wedge Sliding	2040	16719	12.20%

Wedge sliding: Total 2040 intersections critical (12.2 %). Wedge sliding is mainly possible at the intersection between J1 and J2, and partly between J2 and J4.

4.10 Volume estimations

The volume of the defined unstable area and the column Kaillen were obtained from the volume estimation tool in AgiSoft Photoscan. The unstable area representing a worst-case failure scenario, covers a 179,666 m^2 surface and has a volume of 1,112,200 m^3. The volume of the column Kaillen was determined to be 11,193 m^3. It should be noted that the reconstuction method of enclosing the DEM surface to make a convex hull does not take into account the

basal failure surface geometry (see apendix). Thus the volume estimation should be seen as a minimum volume estimate (Figure 27).
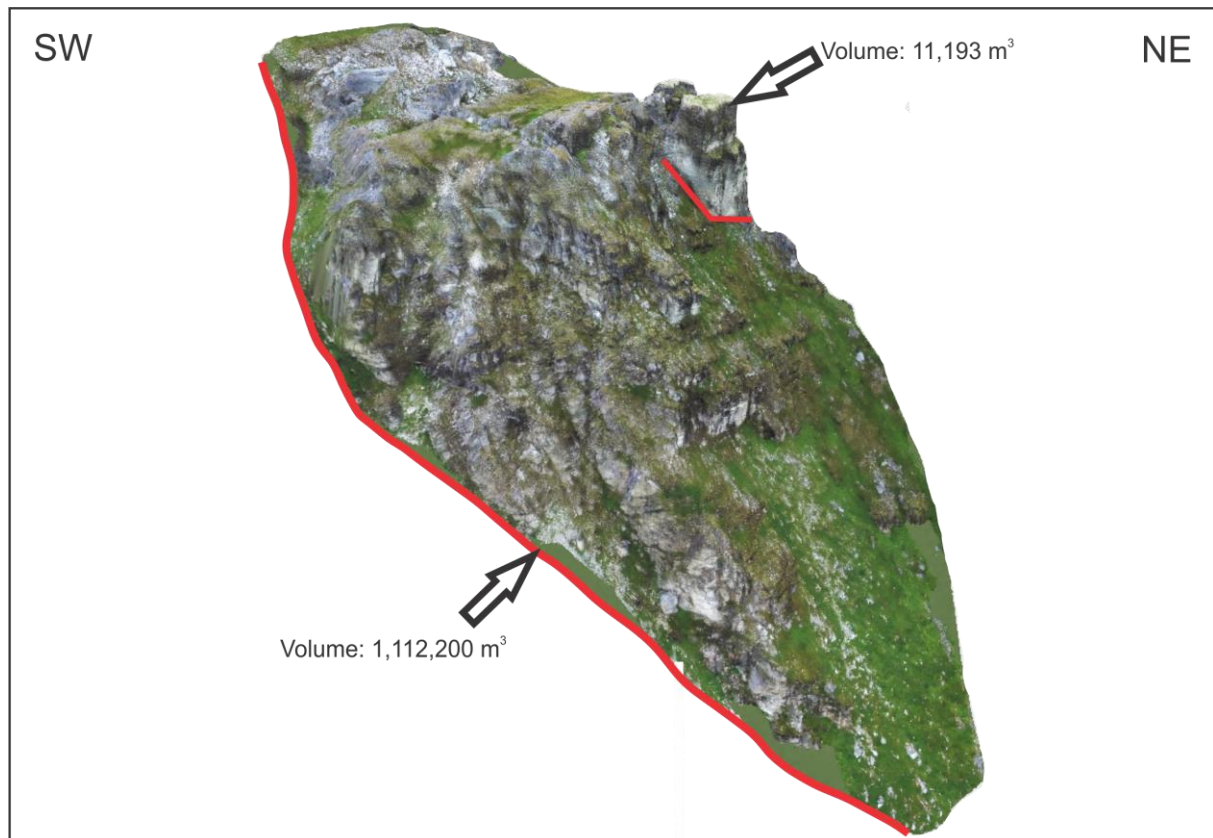
Figure 27 – Orthomosaic 3D model from AgiSoft Photoscan.

4.10.1 Run-out estimate

Volume numbers were used to estimate a possible runout length of a rock avalanche, if the defined unstable area were to fail catastrophically. The volume of the failure, 1,112,200 m^3, corresponds to an angle of reach of 25°, and c. 900 m runout length on the Scheidegger curve (Scheidegger, 1973).

The avalanche event is a worst case scenario, and the runout would not exceed the runout of the previous/prehistoric avalanche event. Since the Scheidegger curve method is a crude empirical reconstruction and does not consider topography, the run-out length might be shorter in reality. The majority of deposits from an event might not exceed the first crest in the topography (see Figure 28). The distance of the inhabited cabin would be exceeded, but not the holiday cabin furthermost down.
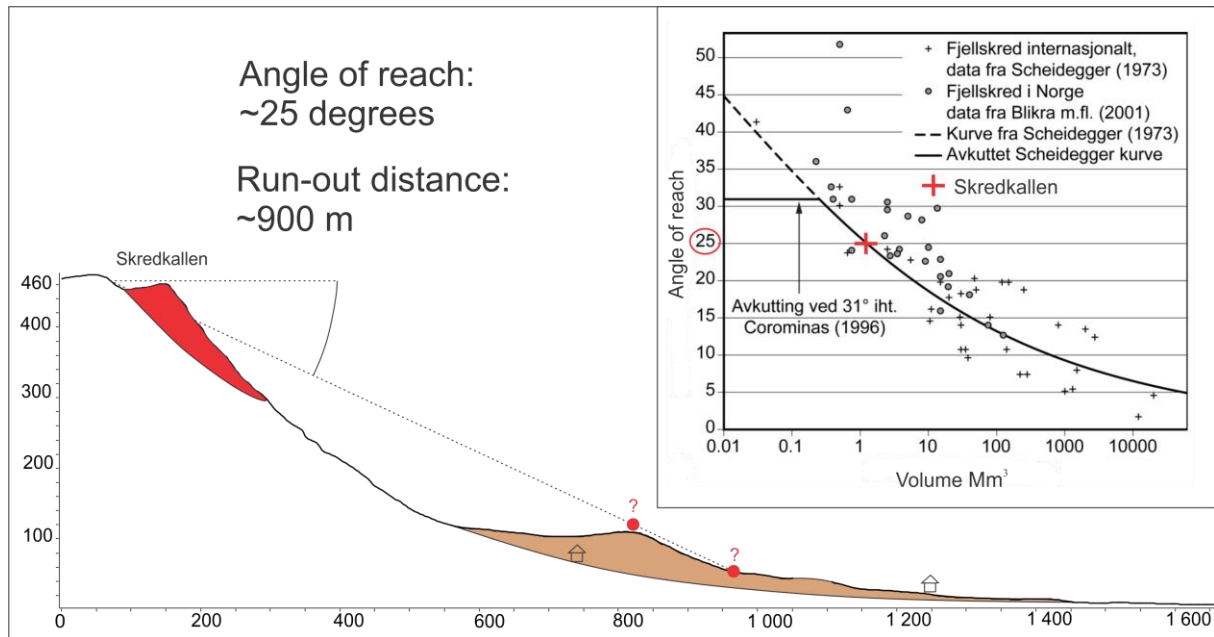
Figure 28 - Run-out distance based on the Scheidegger curve. Diagram from NGU.

4.11 InSAR data

The InSAR data show that the displacement rates are significantly different from stable parts on Laukvikfjellet (Figure 29A). Large parts of the URS is in the satellites shadow, thus data could be obtained only from the very upper part of the URS and the talus below. According to the data there is a relative difference in yearly displacement rates within the unstable area, in which the northern part (Kaillen) is more active than the central part of the URS (Figure 29B).

Dataset Ascending 1 and 2 indicate that Skredkallen in average moves between 2.73 to 12.35 mm per year in the satellite's LOS. Based on the different graphs on average displacement rates (see appendix), a rough interpretation suggests that Skredkallen moves fastest in June and September. Asc. 1 show a very similar displacement rate between Kaillen and the whole URS, whereas Asc. 2 indicate that Kaillen is moving much more than the rest of the URS (Table 8). Sporadic increase in movement in the rock talus, as seen from red dots in both datasets, indicate active rockfall processes.

Table 8 - Results from InSAR data.

Dataset	LOS (Trend/plunge)	Avg. displacement rate mm/year	
		Kaillen	**URS**
Ascending 1	076/37	3.87	2.73
Ascending 2	078/41	12.35	4.53
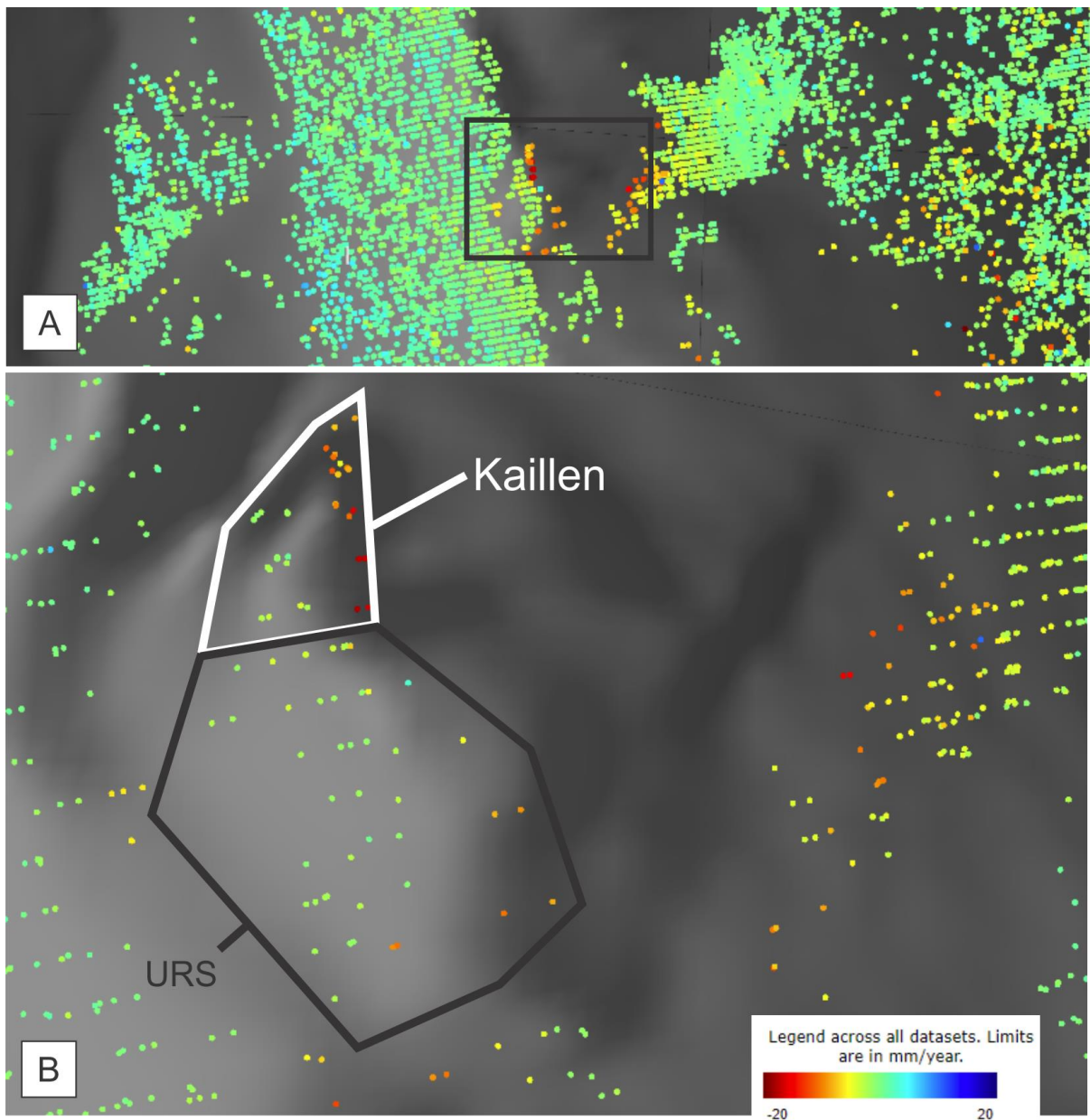
Figure 29 – A: InSAR satellite data, dataset: Ascending 1 and 2. A: Overview with inset of URS. B: URS displaying the two polygons to obtain avg. displacement rate.

5 Discussion

The main aim of this study was to structurally characterise the unstable rock slope at Skredkallen by answering the following questions:

- What are the main failure mechanisms?
- What influences does the regional geological history and inherited bedrock structure play on the failure mechanisms?
- Could the failure be described as a DSGSD?
- What are the failure scenarios?

This chapter discusses the following topics:

- Relationship between regional geological structures and location of the URS.
- Bedrock composition, geological structures and structural data validation.
- Relationship between morphostructures and bedrock structures.
- Conceptual model (with structural profiles).
- Possible failure scenarios and controlling factors.

As WTBC has undergone a much longer and complex growth history than the Caledonian rocks further inland, it is of particular interest to discuss how Pre-Caledonian regional geological history and inherited bed rock structures may define both the location and structural controls of the URS. At Skredkallen this mainly involves the thrusting of the Skipsfjord Nappe.

5.1 Relationship between regional geological structures and location of the URS

This chapter discusses how results from mapped lineaments and geophysical data could affect the location of the URS. Additionally this chapter compares Kvalkjeften and Skredkallen, and discusses their tectonic similarities, relating them to the rock avalanches that may have occurred at both sites.

5.1.1 Lineaments

Lineaments on Laukvikfjellet and Kvalkjeften show similarities to regional geological structures such as NE-SW trending faults and thrust nappes from Svecofennian deformaton. The NNW-SSE oriented lineaments are foliation-parallel, and likely represent 'thrusts' from emplacement of the nearby Skipsfjord Nappe. The 'thrust' structures can also be traced along

Kvalkjeften mountain, on the other side of Skipsfjorden, west of Laukvikfjellet (Figure 30A-B).
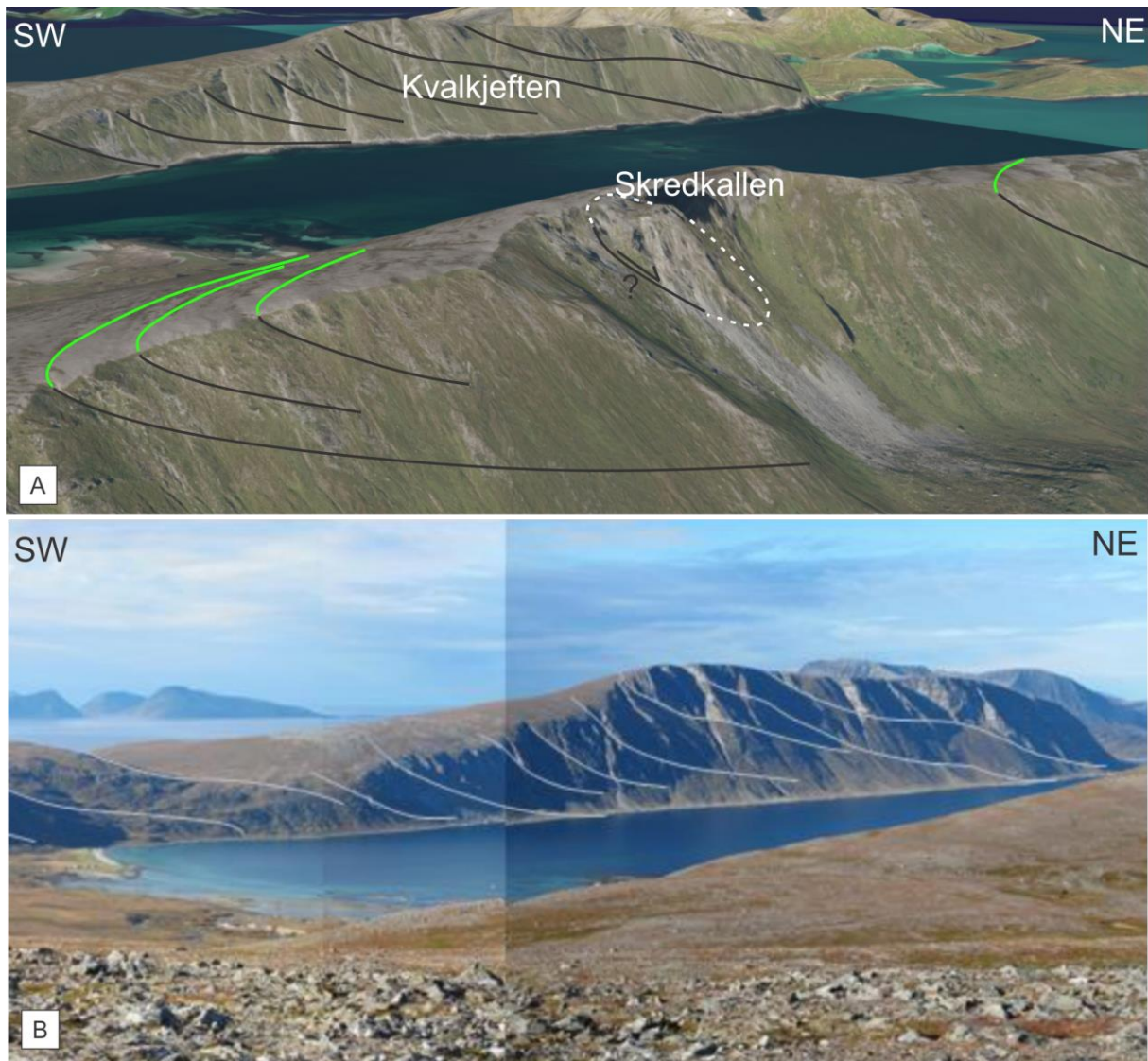
Figure 30 – A: Lineaments (green) as part of 'thrusts'. B: Photo displaying 'thrusts' along Kvalkjeften mountain. Supplied by Steffen Bergh.

According to local residents, the Kvalkjeften mountain also show signs of instability, such as cracks observed to have widened over time. Bouldery rock material on the seabed below this assumed instability, known as Skipsfjordbåan (Figure 31A) probably represent avalanche deposits from Kvalkjeften. Skredkallen and Kvalkjeften are both on a NE slope aspect, show signs of past rock avalanche events and located close to what in this thesis is called 'Upper Nappe' as mapped by Opheim and Andresen (1989).

The deformation of the surrounding rock from thrusting may have weakened the rocks, playing a role in conditioning the slope for instability and controlling the location of both sites. It might also be the case that the 'Upper Nappe' lower boundary could have formed the rupture surface of the URS (Figure 31B). However a more detailed bedrock study and subsurface information is needed to explore this idea.
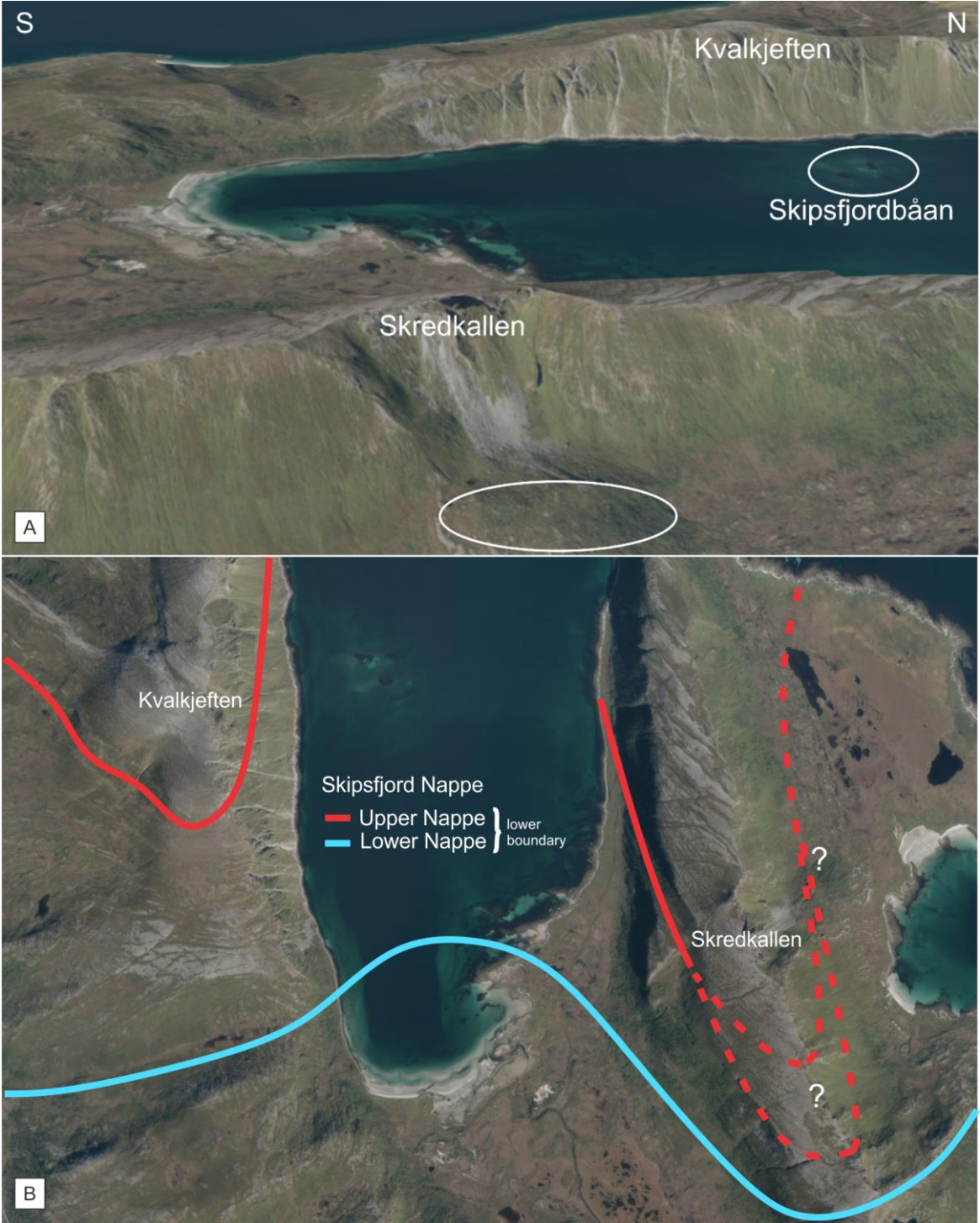
Figure 31 – A: Rock avalanche deposits beneath both Skredkallen and Kvalkjeften. B: Location of the 'Upper Nappe' and the 'Lower Nappe' lower boundaries based on (Map 3) Opheim and Andresen (1989).

5.1.2 Geophysical data

Fault related features such as slickenslides and pink staining indicating fluid flow on NE-SW striking discontinuities, may be related to a distinctive NE-SW oriented lineament in the geophysical data interpreted to be a fault, and which is traced through Skredkallen (Map 7). Although the lineament appears very similar in both length and orientation to the major Vannareid Burøysund Fault 7.5 km northwest, no wide cataclazite zones was found at Skredkallen. However, the fault morphology is convincing and can not be dismissed (Figure 32). Parts of Laukvikfjellet seem to have been down-faulted. The URS may been influenced by the occurrence of brittle faulting, in such a way that fault structures could weakened the rocks. This is supported by Abele (1974) which describes intense fracturing of the rock mass adjacent to faults as ideal conditions to slope failure.
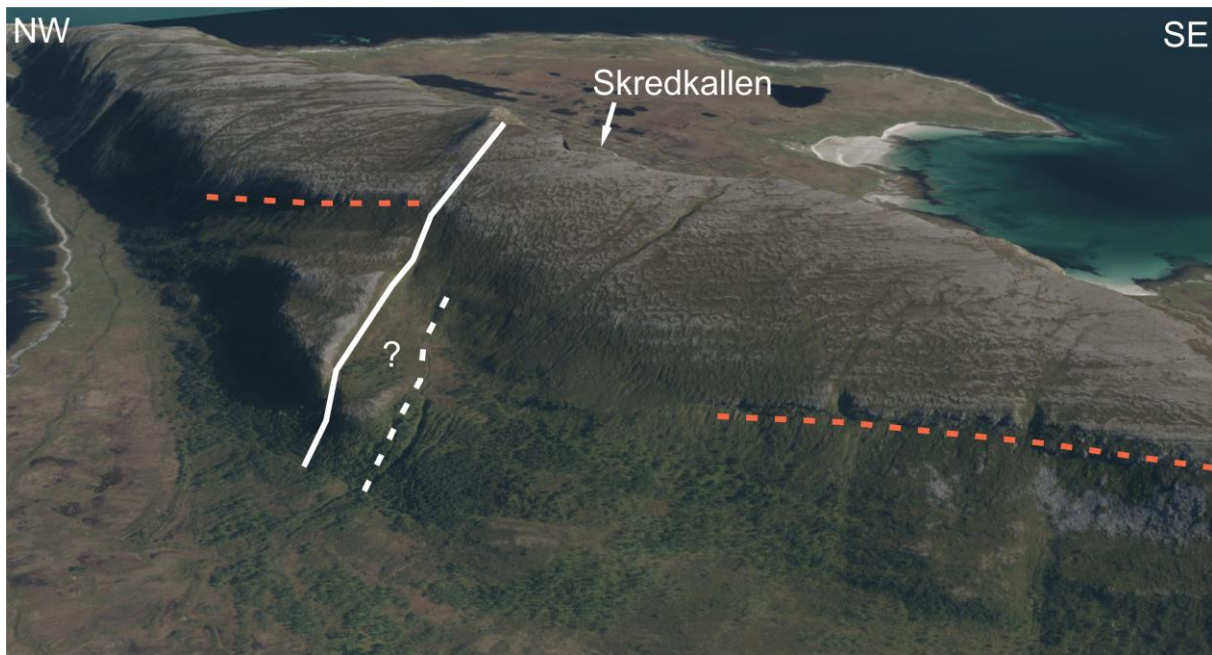
Figure 32 - 3D presentation from norgeibilder.no. Possibly faulting. Orange stippled line represents possible offset unit.

5.2 Bedrock composition and geological structures

This chapter discusses the lithology, foliation and joints, and their relevance to the URS.

5.2.1 Lithology

Skredkallen, differs from many other URS in Troms County, of which the majority are located in Caledonian Nappes (Zwaan, 1988). In terms of rock material strength properties, the gneisses at Skredkallen could only be chipped with a geological hammer, corresponding to an intact strength (unconfined compressive strength) of >250 MPa (NZGS, 2005). It would likely have a higher friction angle (as defined by Wyllie and Mah (2004)) like the commonly mica-rich schists found in Caledonian Nappes in eastern Troms (such as the instability at Jettan, Blikra et al., 2015). The weakest parts of the lithology, the phyllitic to mylonitic 'internal shear zones' appeared very weak (corresponding of 1-5 MPa in the hammer test; (NZGS, 2005)). They also weather differentially, indicating their soft nature. These zones could act as sliding surfaces based on their mechanical weakness, because:

- Low strength indicates possible low shear strength of the phyllite surfaces;
- They are mica-rich, which will weather to clay, further decreasing the shear strength of the surfaces;
- They provide a boundary for the flow of groundwater, along which pore pressures can act to decrease the shear strength of the surfaces.
- It is kinematically feasible for sliding along these surfaces, as they are parallel with the foliation dipping towards NNE.

The presence of the 'internal shear zones' can be linked to the emplacement of the Skipsfjord Nappe, as they are aligned with the foliation formed during this process. The Nappe thrusting and the proximity of the Nappe boundary indicates that larger shear zones may be present at depth.

5.2.2 Foliation

The foliation is dipping gently towards NNE (292/14±13.8) and the majority of the SF set is within the critical zone making it feasible for planar sliding. Weak zones within the lithology are foliation parallel and could define the potential failure surfaces. Foliation planes probably make up a proportion of failure surfaces forming the basal rupture surface of the unstable area.

The foliation is more or less planar without folding, however is possible that the gneisses locally show folds in some parts of the URS based on the proximity to larger folds mapped in the area. As the field data collection was mainly restricted to the upper part of the URS, the possibility of fold structures being present in the deeper parts of the URS can not be excluded.

5.2.3 Structural data validation

This section discusses the two different methods of structural analysis in this thesis and their results in comparison with each other. It is important to validate the data from both data sets since sources of error can occur.

5.2.3.1 Structural analysis of manual field measurements

Field measurements in stereonet show clear clusters, which have been assigned to four joint sets that were observed with confidence in field. However, clusters of poles are still visible outside of the 1σ variability cone, most significantly around the J1 and J4 quadrants. These concentrations could indicate great variability within/around both the J1 and 4 joint sets. Literature also indicates large variability in strike on regional geological structures, especially structures that align with J1 and 2, striking NE-SW to NNE-SSW (Indrevær et al., 2013). There is some crossover between steep foliation and gentle planes from J3, striking NW-SE, as they have very similar dip angles. This is likely because J3 was observed to refract along the foliation, so that it appears both steep and gentle.

The great variability within and outside of the cones might indicate that more than four joint sets are present. This increases the structural complexity of the URS, and means that not all failure mechanisms are accurately accounted for in the kinematic analysis.

5.2.3.2 Structural analysis based on point cloud

Semi-automatic structural recognition allows for data capture in areas of low accessibility, and increases the accuracy of structural analysis by covering areas where traditional measurements can not be obtained.

The photogrammetry point cloud only covered the NNE-SSW-striking backscarp. The structural analysis shows high concentrations of J1 and 2, striking NNE-SSW aligning with the backscarp. Ideally the NW-SE-striking backscarp would also have been mapped to capture daylighting structures that are more apparent in this orientation. The concentration of J1 and 2

in the Coltop-3D dataset may therefore be artificial, and the Coltop-3D data should be used for analytical purposes with caution. Other scarps were obscured by blocks or vegetation and therefore drone surveying was not possible.

J1 is well-developed in the model, showing smooth and highly persistent planes dipping towards SE, just as in the field. The analysis also shows J3 and J4, and displays the interaction between J3, J4 and SF seen as altered color bands on the point cloud. Foliation measurements display the lowest concentration. This is likely because foliation planes dip in the strike direction of the surveyed backscarp, so that the planes are daylighting obliquely in the face and were not very prominent.

Distortion of the point cloud caused by placing GCPs from handheld GPS measurements is the biggest uncertainty in this project. Ideally, the GCPs would have been obtained with a high-accuracy GPS. Sources of error could also be related to the mesh that is created on the basis of a point cloud. The mesh surface can average out points in the point cloud, which can lead to the structural planes appear gentler or steeper in Coltop-3D (Figure 33).
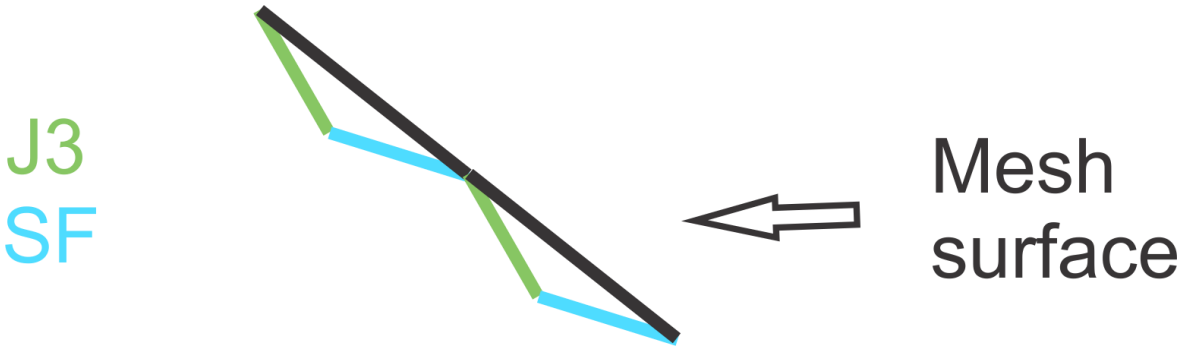
Figure 33 – Mesh surface missing structural planes (J3 and SF).

5.2.4 Comparing structural analysis based on manual field measurements and the point cloud

It is important to compare the field and Coltop-3D datasets because there are uncertainties which exist in the digital data meaning that it cannot be used as a standalone dataset. Additionally, comparison is a useful way to confirm the occurrence of the joints sets (Table 9).

Table 9 - Structural analysis results based on manual field measurements and point cloud.

Joint set	J1	J2	J3	J4	SF
Field measurements	034/82±16.9	205/68±9.0	309/68±10.5	117/83±15.5	292/14±13.8
Point Cloud	035/88±13.7	184/67±5.2	310/48±13.6	149/51±15.8	261/22±12.25

The results from the different structural analyses were quite similar in terms of joint strike orientation, with J1 and 3 only differing by 1°. The biggest differences are seen in J4 which is considerable different both in strike and dip angle. The foliation measured in the point cloud strikes more to the south, meaning that the dip is towards N rather than NNE based on manual field measurements - a significant deviation in terms of kinematic feasibility for planar sliding. J3 shows a similar strike in the two datasets, with a 20° gentler dip in the point cloud. J2 is similar in dip angle and strikes more to the south in the point cloud.

The differences in results is thought to be a combination of possible distortion of the point cloud and possible inaccuracy in the mesh surface.

5.3 Relationship between morphostructures and bedrock structures

This chapter discusses the main findings from mapping the morphostructures and their relationship to bedrock structures (Map 11). It is important to understand which joint sets the morphostructures relate to when connecting kinematic analysis results to the structural controls of the URS.

The linkage between morphostructures and bedrock structures on Skredkallen are very prominent. The orientation of cracks and scarps (NW-SE and NE-SW to NNE-SSW), is strongly related to near-vertical joints from J1 and 4, which are the most dominant bedrock structures on Skredkallen. The same applies for the trench which is oriented NW-SE and NNE-SSW. The majority of blocks are rectangular shaped from the orthogonal set made by J1 and 4. Additionally a morphological depression in the stable part of Laukvikfjellet striking NE-SW,

perfectly lines up with parts of the backscarp (Figure 34), verifying the great presence of J1 related structures (Figure 34).

Figure 34 – Station 56. Drone photo. Morphological depression lines perfectly up with the backscarp.

5.4 Conceptual model

This chapter conceptualizes the main structural features and their influence on the deformation. The interpretation on structural controls on the different parts of the URS (Map 13), will be presented within three structural profiles (Figure 35, Figure 36, Figure 37). The profiles are based on a DEM from drone photogrammetry with 7.51 cm/pixel ground resolution. This chapter also presents a schematic 3D model based on an orthomosaic from AgiSoft Photoscan, showing the main features on Skredkallen.
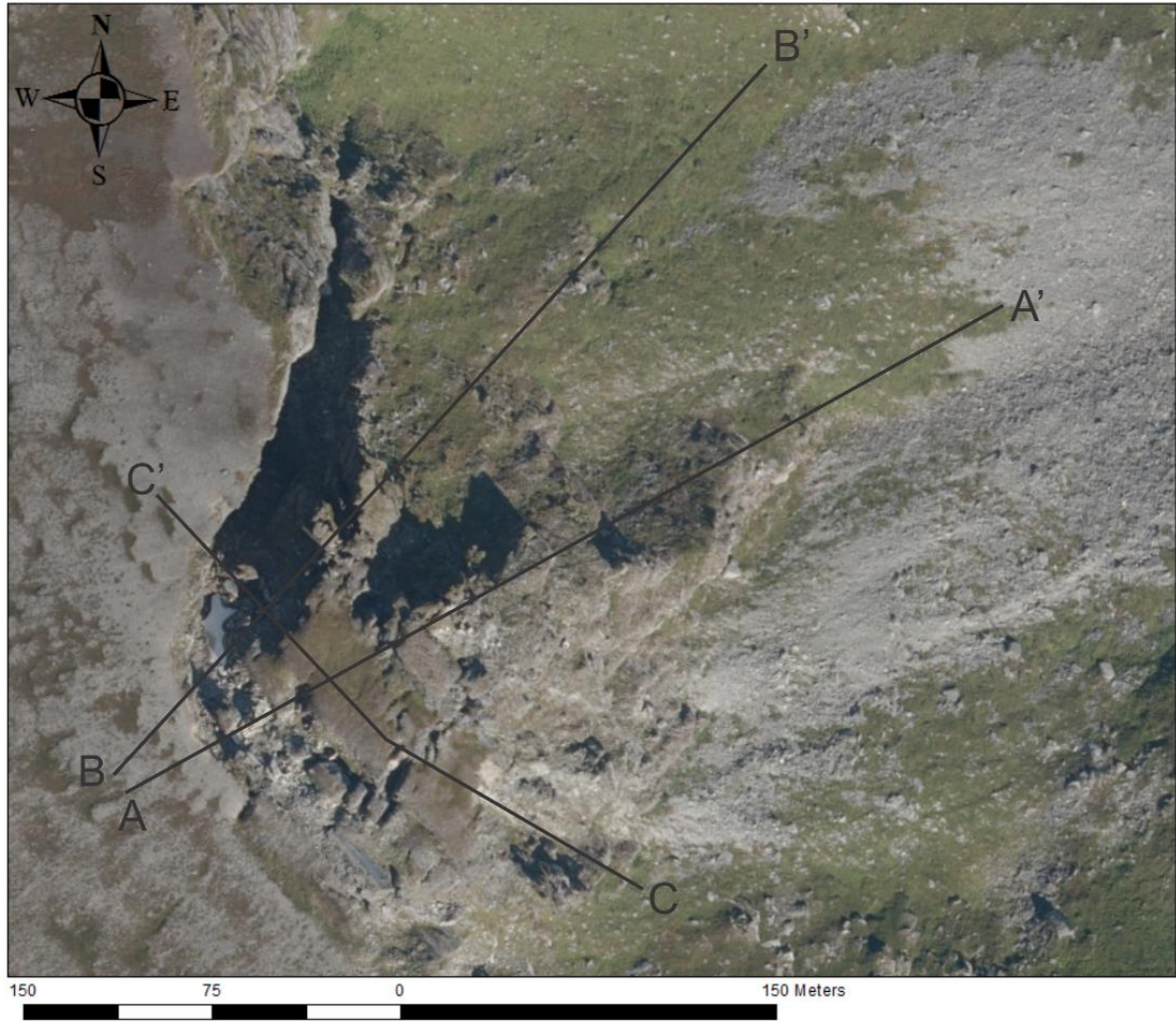
Map 13 - Location of the three structural profiles presented below.

5.4.1 URS overview
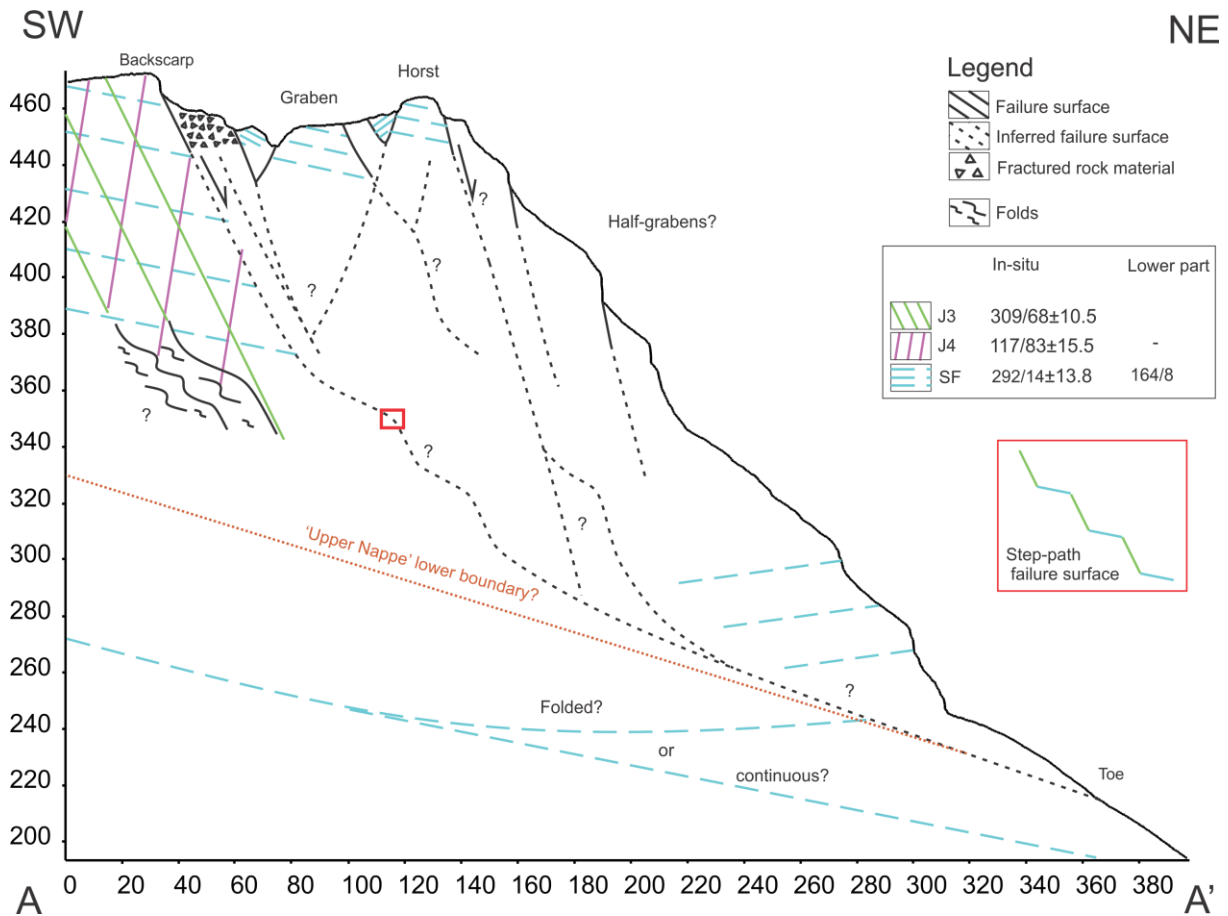
Figure 35 - Profile A-A'.

The URS is mainly controlled by J3 and SF. The failure is likely a biplanar compound slide (Hermanns and Longva, 2012, Glastonbury and Fell, 2008), made up by a combination of J3 and SF, which develop a step-path geometry. This is supported by the kinematic analysis indicating that planar sliding is feasible along steeper parts of SF. The step-path geometry leads to internal shear in parts of the URS which could have intensified the development of scarps and cracks. Interestingly the profile surface formed by previous rock slope failure(s) is also stepped. The path will follow mostly J3 at the rear (as shown by the backscarps) and following more of the foliation with depth and effectively working as a listric sliding plane. Since the foliation is gentle and the kinematics operate with 20° friction angle, the failure surface needs to be biplanar to achieve movement on such low angle surface. 'Upper Nappe' lower boundary could have formed the rupture surface of the URS.

The outermost part of the unstable mass is thought to be a complex of half-grabens. Based on observations from distance, these half-grabens looked to be controlled by J3 surfaces, however

due to the lack of information, and similar strike between J3 and 4, the bounding surfaces could also follow J4.

The foliation was mapped at the base of the unstable mass as dipping to SW. If the foliation is continuous, i.e. not folded, the URS has been subjected to a 20° tilt towards SW (Trend/plunge - 222/20 based on the rotational analysis).

5.4.2 Kaillen
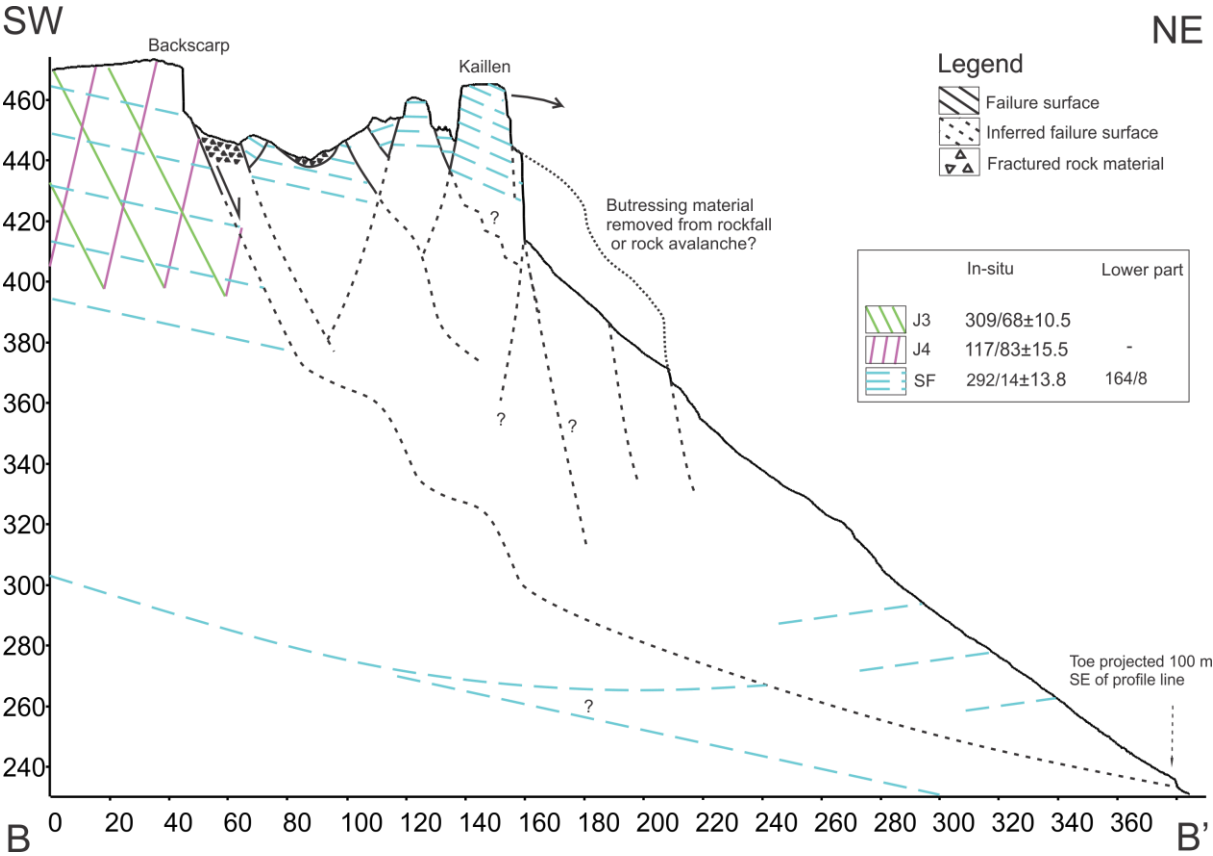
Figure 36 - Profile B-B'.

Kaillen is separated from the central part of the URS by J1 (not visible on the profile since it strikes parallel to the profile line, check scarp orientation in Map 11). Kaillen topples towards E from intersection between J1 and 4. This is supported by the kinematics, which show oblique toppling being feasible from intersection with J1 and 4. Kaillen lies at the same elevation as the horst surface, and it is likely that prior to multiple rock falls they were joined. Due to a rock avalanche event (seen by the deposits below the URS), Kaillen has been debutressed and is now metastable, tilting downwards towards E.

5.4.3 Central part of the URS
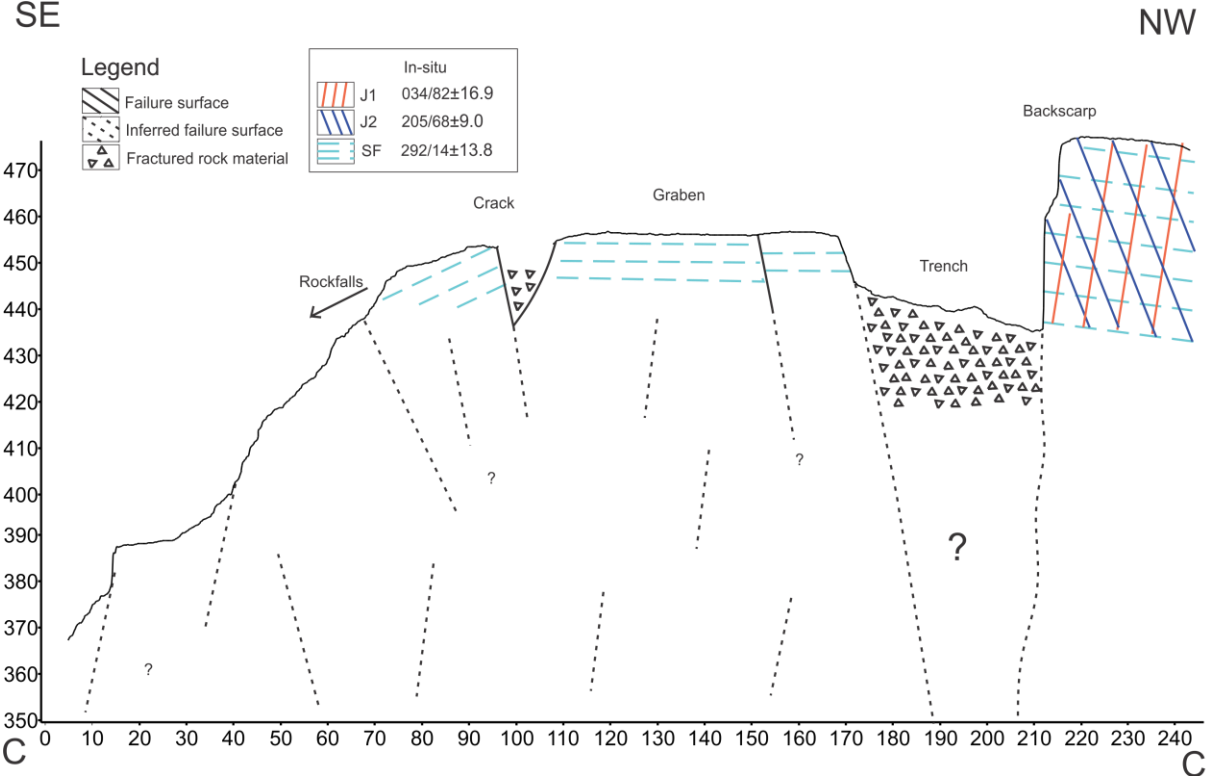
Figure 37 - Profile C-C'.

The southeastern section of the URS is separated from the rest of the unstable area by a major crack from J1 and 2 joints. The crack delineates the whole unstable area, and the material south of the crack show a toppling failure mechanism towards SE. The area is dominated by rock fall processes, probably direct toppling failure along SF and intersections with J1 and J4 (Figure 38). Stories from locals indicate that a rockfall event occurred here in the 1950s, involving the collapse of a tall column called 'Kvinnen'. The tilt movement of this terrace leading to direct toppling and the steep nature of this section, are probably the main reasons why rockfalls seem to occur frequently here.
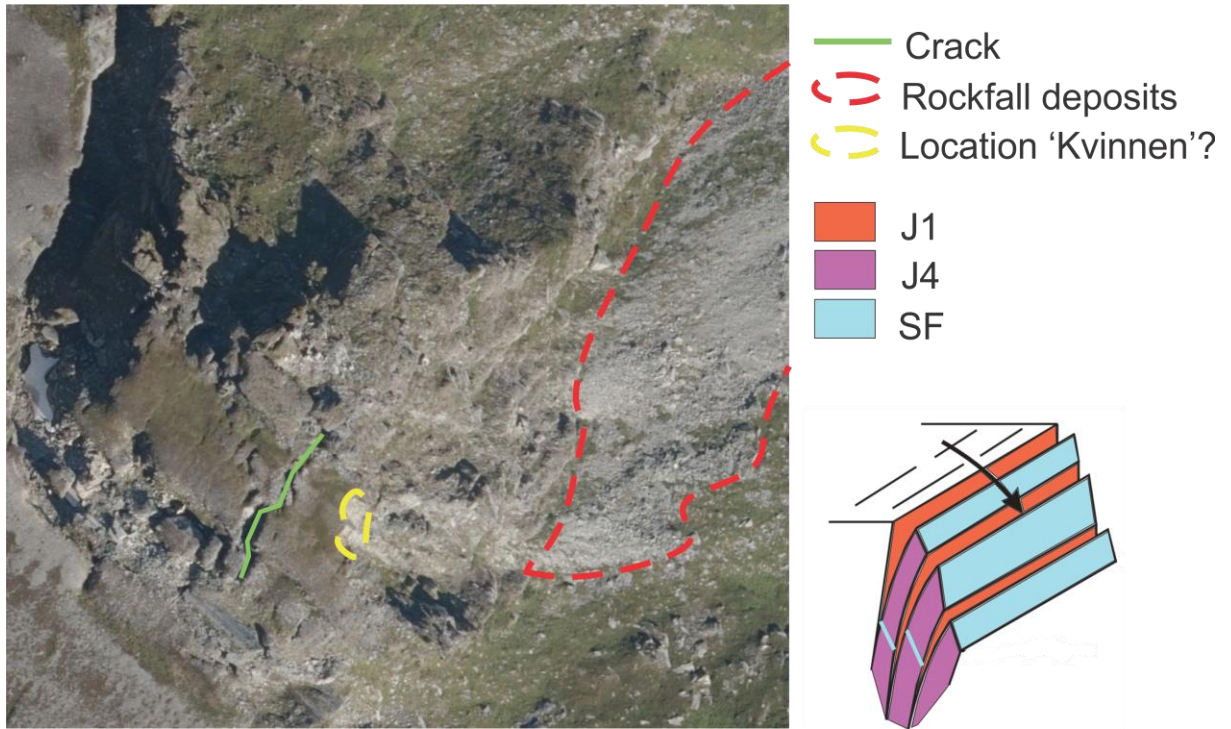
Figure 38 - Direct toppling failure. Figure to the right modified after Wyllie and Mah 2004.

5.4.4 Schematic 3D model
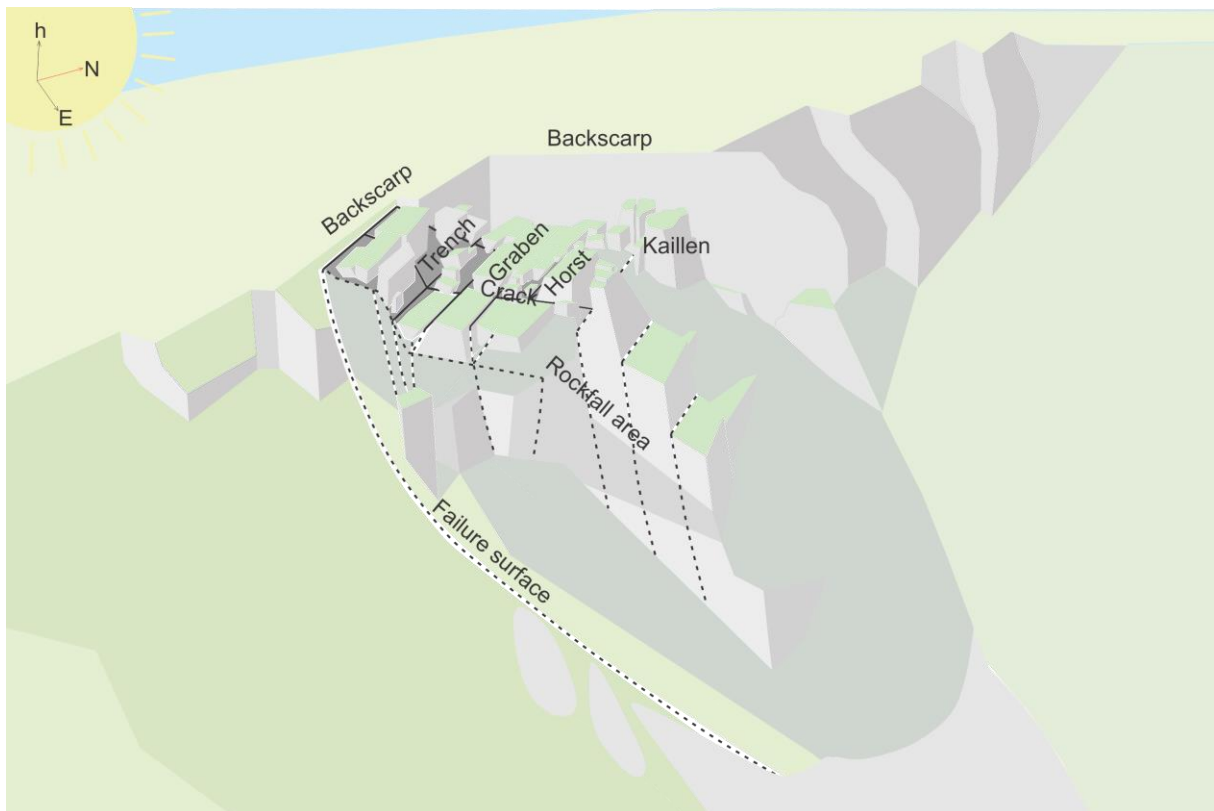
Figure 39 - Schematic 3D model presenting the main features of the URS.

5.5 The URS's similarities to a DSGSD

Morphostructural features typically related to DSGSD, as described by Agliardi et al., (2001), such as trenches, counterscarps, open tension cracks, grabens and half-grabens are present on Skredkallen (Figure 40). The most prominent features are the wide trench, the graben and the horst. Additionally the URS might be defined as a DSGSD as they commonly occur in metamorphosed foliated rock (Agliardi et al., 2012) such as in the tonalittic gneisses on Skredkallen. In addition the genesis of Skredkallen could be linked to active faults as proposed by Forcella and Orombelli (1984) and a basal sliding surface coincident to a pre-existing tectonic surface (Agliardi et al., 2001) i.e. 'Upper Nappe', which have been related to DSGSD. The glacial cycles in Scandinavia have probably played a role in developing this unstable area, as the distribution of DSGSD are commonly related to glacial debuttressing (Agliardi et al., 2001) and also post-glacial isostatic lift (Nemcok and Pasek, 1969). However the volume of Skredkallen (1.1 Mm^3) is much lower than what is common for a DSGSD (>500 Mm^3) (Agliardi et al., 2012). They also tend to show poor lateral boundaries, which is very unlike the geometry at Skredkallen.
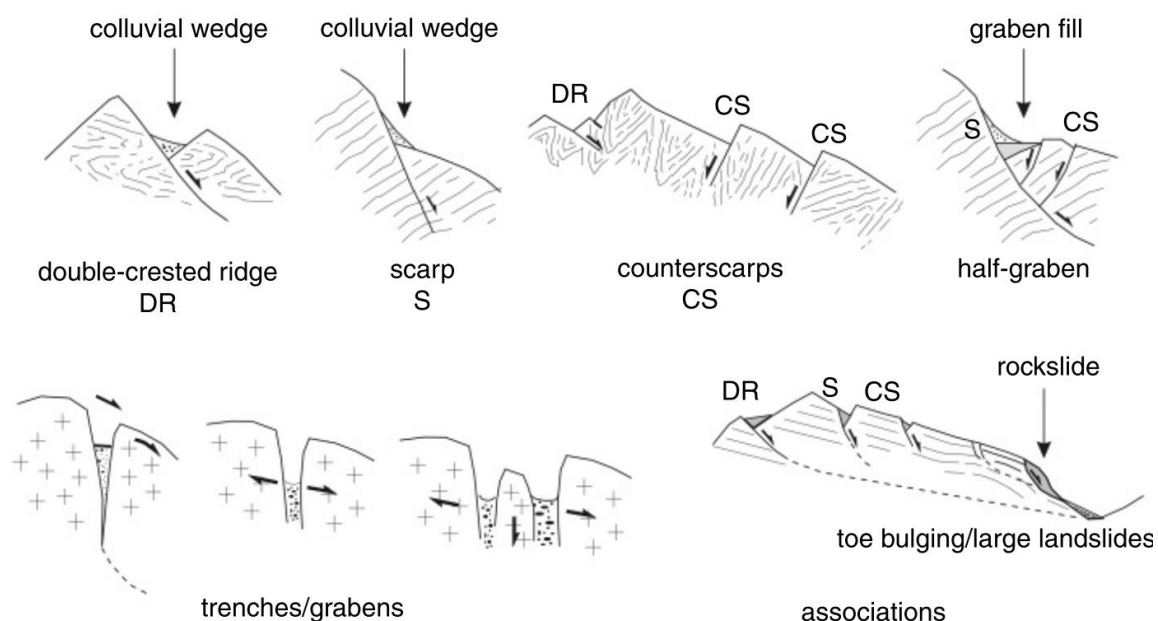
Figure 40 - Morphostructural features diagnostic of DSGSDs phenomena, related kinematic significance, and typical associations. From Clague (2012). Modified after Agliardi et al (2001).

5.6 Possible scenarios

Possible failure scenarios are presented in Figure 41.
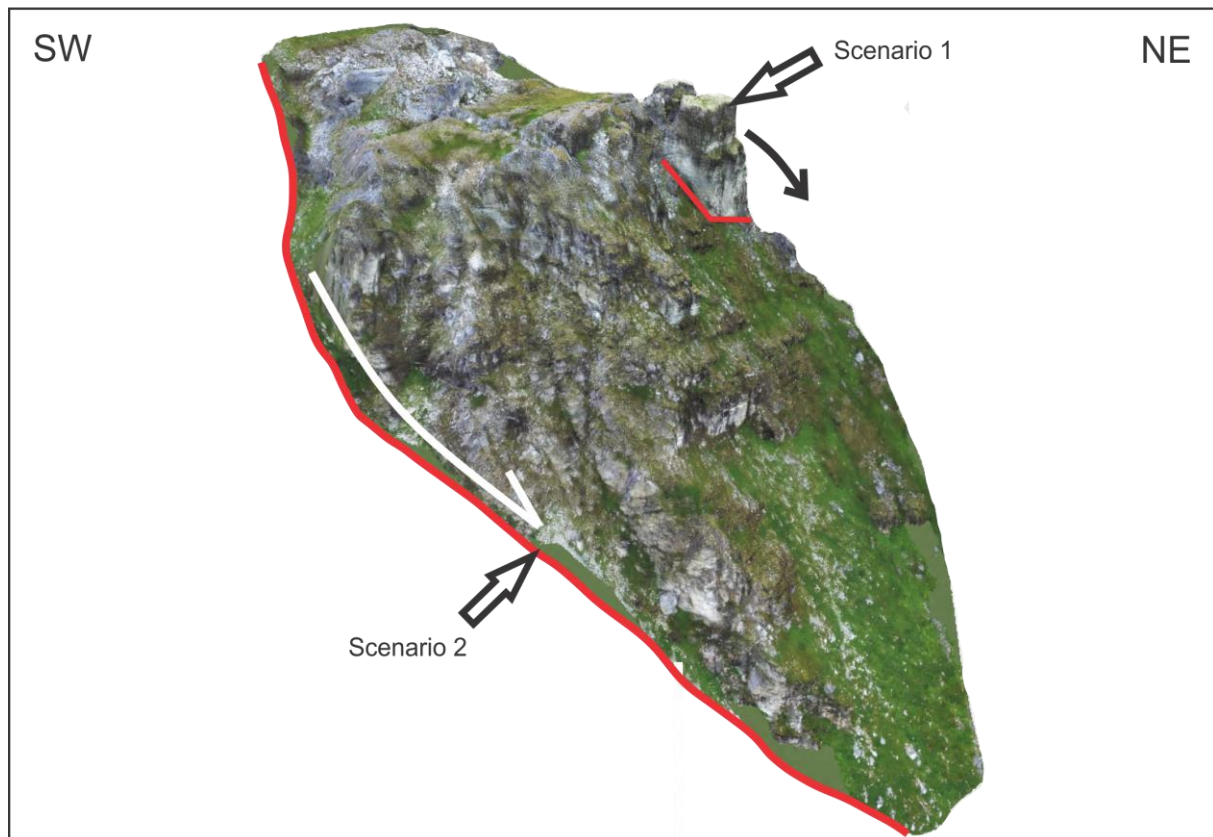
Figure 41 - Possible failure scenarios.

Based on InSAR satellite data, which shows greatest displacement rates in the northern part of the URS, the collapse of Kaillen (Scenario 1) seems most likely to occur. The column is tilting dramatically towards E (Figure 42).

Scenario 2 involves at least 1.1 Mm^3 of material failing. No run-out modelling was performed in this thesis, however based on the volume an empirical estimate on angle of reach from volume was used (Scheidegger, 1973). This suggests an angle of reach of c. 25° (Figure 43). The run-out distance then would be c. 900 m, further than the uninhabited cabin and almost reaching the holiday cabin beneath the URS. This estimate is probably not conservative, since the volume calculation in AgiSoft Photoscan misses parts of the mass, but conversely rock avalanches in Norway generally show a lower angle of reach than what is predicted using the Scheidegger method (Blikra et al., 2006).

Figure 42 - Drone picture showing the dramatic tilt of Kaillen towards E.
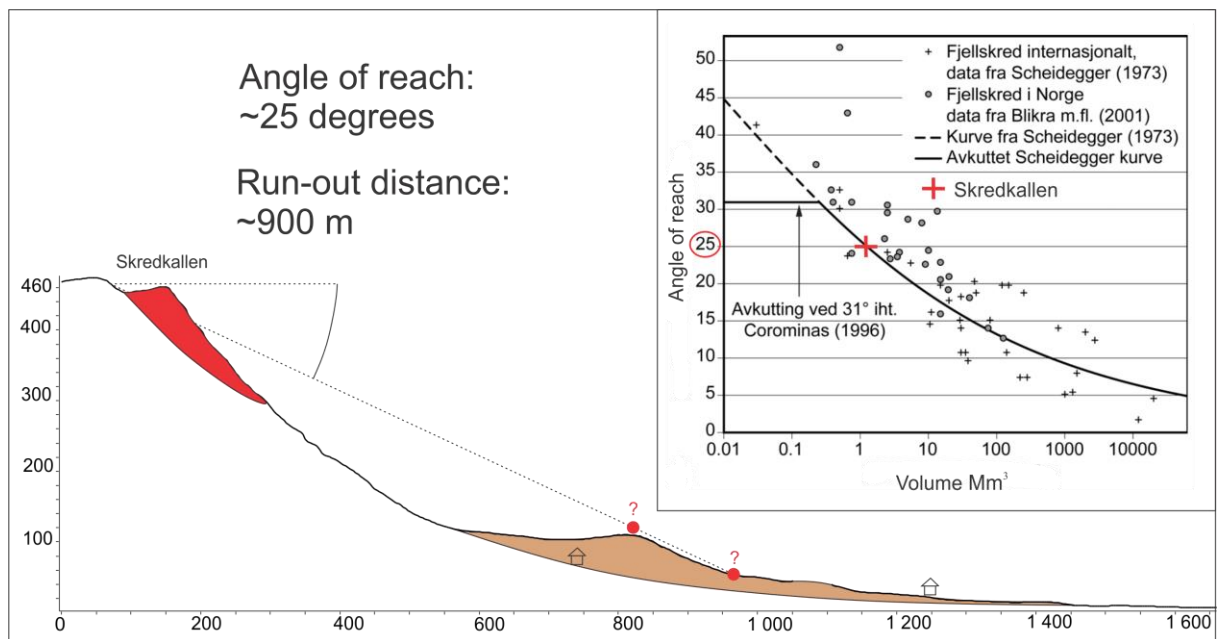
Figure 43 - Run-out distance based on the Scheidegger curve. Diagram from NGU.

5.7 Controlling factors

This chapter presents factors which may condition the rock slope for failure, and/or trigger failure in the future, as well as factors which control the ongoing displacement.

5.7.1 Permafrost and water

Factors such as downflow of dense cold air into the deep trench and very little incomingsunlight, decreases the temperature locally. Thus the local environment on Skredkallen could favour sporadic permafrost, as supported by the snow and ice found in the trench. After a short visit to the field site in March 2019 and observing the large overhanging cornices along the whole backscarp, it is thought that the collapse of snow-cornices in spring time could be a great source of ice to the trench.

Since the URS is located along the coast of Troms, precipitation rates can be very high in rainfall periods. During periods with increasing temperature and rainfall, and following increase in water pressure and melting permafrost, the URS can experience an increase in deformation. Such periods could be in late spring (June) and early autumn (September) times, based on InSAR data. Water infiltrating sliding surfaces could increase the water pressure and decrease the shear strength, and play a significant control on the URS. This also applies to mechanical weathering from freeze-thaw cycles leading to a gradual fracturing of the rock masses.

The very weak 'internal shear zones' are probably the surfaces most prone to weathering on Skredkallen, which means that these zones may play an extra role in defining main sliding surfaces.

5.7.2 Glacial processes and rebound

Debuttressing of the slopes from glacial retreat could have played a role in the past events on Skredkallen and why this is an URS today. Glacial oversteeping of the rock slope during glaciations might also be an external factor. The stress release from debuttressing may have resulted in propagation of the internal network of joints, and loss of cohesion in pre-existing discontinuities.

Isostatic adjustment following glacial retreat can lead to earthquakes triggering failures in the URS. Keefer (1984) writes that the Magnitude of an earthquake must exceed 6.0 to trigger a

rock slide. Earthquakes in Norway seldom exceed Magnitude 5.5 (Dehls et al., 2000), but this do not exclude the possibility that episodes could have occurred in pre-historic times (Braathen et al., 2004).

6 Conclusions and further investigations

Skredkallen is an actively deforming URS located on the steep eastern slope of Laukvikfjellet The main goal of this thesis has been to structurally characterise the unstable rock slope at Skredkallen to better understand past and potential future events. The structural mapping showed five different geological structures:

Geological structure	SF	J1	J2	J3	J4
Strike/dip	292/14±13.8	034/82±16.9	205/68±9.0	309/68±10.5	117/83±15.5

The main failure mechanism on Skredkallen is planar sliding, probably contributing to a biplanar compound slide made up by J3 and SF, which displays a step-path geometry and effectively working as a listric sliding plane. The rock column Kaillen is toppling towards E along the intersection between J1 and 4. J1 is the most dominant structure in the URS, and has segmented the URS into different parts along a large open crack.

The regional geological history special to this field site is the thrusting of the Skipsfjord Nappe. The deformation of the surrounding rock from thrusting weakening the rocks, may have conditioned the slope for instability. The URS location is probably influenced by Post-Caledonian brittle fault structures striking NNE-SSW, NE-SW and NW-SE, in that such structures may have developed ideal conditions to slope failure. Since the regional lineaments and faults align with the joints controlling the URS, the regional geological history plays a huge role on the failure mechanisms.

The failure on Skredkallen can be considered as a possible DSGSD based on the complexity of geometries made by the surface morphostructures, and from the inferred brittle fault and fracture geometries traced in the bedrock. The presence of a tectonic surface from the Skipsfjord Nappe thrust (i.e 'Upper Nappe') defining the rupture surface of the URS, can be compared to a DSGSD, but further studies are needed to prove this. The largest difference is the volume of Skredkallen which is only a fraction of what is common for a DSGSD.

The two proposed failure scenarios involve a worst case scenario with a minimum mass of 1.1 Mm^3 sliding down the steep eastern slope of Laukvikfjellet. A catastrophic failure will depend on the gradual accumulation of long-term damage along failure surfaces until a 'critical slope

damage threshold' is reached. Such failure surfaces prone to damage could be the 'internal thrust zones' which appeared very weak. Based on the Scheidegger curve assessment of the largest failure scenario, the 900 m run-out length would pass the uninhabited cabin and the hiking trails below the URS, but not the lowermost holiday cabin.

Because this study was done in a poorly studied area, future work will be necessary to fully understand the URS. This includes more measurements in the less studied areas of the URS, for instance in the lower part to perform a good rotational analysis including joint set data. As large parts of the URS are located in very steep and active rockfall areas which are hard to access by foot, more drone mapping would be of particular interest. A detailed bedrock study in and around the site would also be beneficial to better explain how lithological differences and regional geological structures could affect the URS, especially since there might be a regional pattern between Kvalkjeften on the other side of Skipsfjorden and Skredkallen.

7 References

ABELE, G. 1974. Bergsturze in den Alpen. Ihre Verbreitung, Morphologie und Folgeerscheinungen. *Wiss. Alpenvereinshefte,* 25.

AGISOFT.COM. *Tutorial on Volume Measurements with AgiSoft Photoscan Pro 1.1* [Online]. [Accessed].

AGLIARDI, F., CROSTA, G. & ZANCHI, A. 2001. Structural constraints on deep-seated slope deformation kinematics. *Engineering Geology,* 59**,** 83-102.

AGLIARDI, F., CROSTA, G. B. & FRATTINI, P. 2012. 18 Slow rock-slope deformation. *Landslides: Types, mechanisms and modeling***,** 207.

AGLIARDI, F., ZANCHI, A. & CROSTA, G. B. 2009. Tectonic vs. gravitational morphostructures in the central Eastern Alps (Italy): constraints on the recent evolution of the mountain range. *Tectonophysics,* 474**,** 250-270.

AMBROSI, C. & CROSTA, G. B. 2011. Valley shape influence on deformation mechanisms of rock slopes. *Geological Society, London, Special Publications,* 351**,** 215-233.

ANDRESEN, A. & FORSLUND, T. 1987. Post-Caledonian brittle faults in Troms: geometry, age and tectonic significance. *Abstract. The Caledonian and Related Geology of Scandinavia*.

BALLANTYNE, C. K. 2001. Paraglacial geomorphology.

BERGH, S. G., KULLERUD, K., ARMITAGE, P. E., BOUKE ZWAAN, K., CORFU, F., RAVNA, E. J. & INGE MYHRE, P. 2010. Neoarchaean to Svecofennian tectono-magmatic evolution of the West Troms Basement Complex, North Norway. *Norwegian Journal of Geology/Norsk Geologisk Forening,* 90.

BERGH, S. G., KULLERUD, K., CORFU, F., ARMITAGE, P. E., DAVIDSEN, B., JOHANSEN, H. W., PETTERSEN, T. & KNUDSEN, S. 2007. Low-grade sedimentary rocks on Vanna, North Norway: a new occurrence of a Palaeoproterozoic (2.4-2.2 Ga) cover succession in northern Fennoscandia. *Norwegian Journal of Geology/Norsk Geologisk Forening,* 87.

BINNS, R., CHROSTON, P. & MATHEWS, D. 1981. Low-grade sedi ments on Precambrian gneiss on Vanna. *Troms, Northern Nor*.

BLIKRA, L. H., LONGVA, O., BRAATHEN, A., DEHLS, J. F., STALSBERG, K. & ANDA, E. 2006. Rock slope failures in norwegian fjord areas: Examples, spatial distribution and temporal pattern. *Landslides,* 49**,** 475-496.

BLYSTAD, P. 1995. Structural elements of the Norwegian continental shelf. Part 2: The Norwegian Sea region. *NPD Bull.,* 8.

BRAATHEN, A., BLIKRA, L. H., BERG, S. S. & KARLSEN, F. 2004. Rock-slope failures in Norway; type, geometry, deformation mechanisms and stability. *Norwegian Journal of Geology/Norsk Geologisk Forening,* 84.

BREKKE, H., SJULSTAD, H. I., MAGNUS, C. & WILLIAMS, R. W. 2001. Sedimentary environments offshore Norway—an overview. *Norwegian Petroleum Society Special Publications.* Elsevier.

BUNKHOLT, H., OSMUNDSEN, P. T., REDFIELD, T., OPPIKOFER, T., EIKEN, T., L'HEUREUX, J.-S., HERMANNS, R. & LAUKNES, T. R. 2011. ROS Fjellskred i Troms: status og analyser etter feltarbeid 2010. NGU.

BÖHME, M. 2014. Spatial and temporal variability of rock slope instability in western Norway:: Implications for susceptibility and hazard assessment.

CHRISTIANSEN, H. H., ETZELMÜLLER, B., ISAKSEN, K., JULIUSSEN, H., FARBROT, H., HUMLUM, O., JOHANSSON, M., INGEMAN‐NIELSEN, T., KRISTENSEN, L. & HJORT, J. 2010. The thermal state of permafrost in the Nordic area during the

International Polar Year 2007–2009. *Permafrost and Periglacial Processes,* 21**,** 156-181.

CLAGUE, J. J. & STEAD, D. 2012. *Slow rock-slope deformation,* Cambridge, Cambridge: Cambridge University Press.

CORNER, G. D. & HAUGANE, E. 1993. Marine-lacustrine stratigraphy of raised coastal basins and postglacial sea-level change at Lyngen and Vanna, Troms, northern Norway. *Norsk Geologisk Tidsskrift,* 73**,** 175-197.

CROSTA, G. & ZANCHI, A. Deep seated slope deformations: huge, extraordinary, enigmatic phenomena. Landslides in Research, Theory and Practice: Proceedings of the 8th International Symposium on Landslides held in Cardiff on 26–30 June 2000, 2000. Thomas Telford publishing, 1: 351-358.

CRUDEN, D. M. & VARNES, D. J. 1996. Landslides: investigation and mitigation. Chapter 3-Landslide types and processes. *Transportation research board special report.*

DAHL, R. & SVEIAN, H. 2004. *Ka dokker mein førr stein!: geologi, landskap og ressurser i Troms*, Norges geologiske undersøkelse.

DEHLS, J. F., OLESEN, O., OLSEN, L. & BLIKRA, L. H. 2000. Neotectonic faulting in northern Norway; the Stuoragurra and Nordmannvikdalen postglacial faults. *Quaternary science reviews,* 19**,** 1447-1460.

DORÉ, A. 1991. The structural foundation and evolution of Mesozoic seaways between Europe and the Arctic. *Palaeogeography, Palaeoclimatology, Palaeoecology,* 87**,** 441-492.

DORÉ, A. & LUNDIN, E. 1996. Cenozoic compressional structures on the NE Atlantic margin; nature, origin and potential significance for hydrocarbon exploration. *Petroleum Geoscience,* 2**,** 299-311.

EBERHARDT, E. & STEAD, D. 2013. UNDERSTANDING THE MECHANICS OF LARGE LANDSLIDES. *Italian Journal of Engineering Geology and Environment.*

FALEIDE, J. I., TSIKALAS, F., BREIVIK, A. J., MJELDE, R., RITZMANN, O., ENGEN, O., WILSON, J. & ELDHOLM, O. 2008. Structure and evolution of the continental margin off Norway and the Barents Sea. *Episodes,* 31**,** 82-91.

FALEIDE, J. I., VÅGNES, E. & GUDLAUGSSON, S. T. 1993. Late Mesozoic-Cenozoic evolution of the south-western Barents Sea in a regional rift-shear tectonic setting. *Marine and Petroleum Geology,* 10**,** 186-214.

FORCELLA, F. & OROMBELLI, G. 1984. Holocene slope deformations in Valfurva, central Alps, Italy. *Geografia Fisica e Dinamica Quaternaria,* 7**,** 41-48.

FORSLUND, T. 1988. Post-Kaledonske forkastninger i Vest-Troms, med vekt på Kvaløyslettaforkastningen, Kvaløya. *Unpublished master thesis, University of Tromsø.*

GLASTONBURY, J. & FELL, R. 2008. A decision analysis framework for the assessment of likely post-failure velocity of translational and compound natural rock slope landslides. *Canadian Geotechnical Journal,* 45**,** 329-350.

HENKEL, H. 1991. Magnetic crustal structures in northern Fennoscandia. *Tectonophysics,* 192**,** 57-79.

HERMANNS, R., OPPIKOFER, T., ANDA, E., BLIKRA, L., BÖHME, M., BUNKHOLT, H., CROSTA, G., DAHLE, H., DEVOLI, G. & FISCHER, L. 2012. Recommended hazard and risk classification system for large unstable rock slopes in Norway. *NGU rapport.*

HERMANNS, R., OPPIKOFER, T., ANDA, E., BLIKRA, L., BÖHME, M., BUNKHOLT, H., CROSTA, G., DAHLE, H., DEVOLI, G. & FISCHER, L. 2013. Hazard and risk classification for large unstable rock slopes in Norway. *Italian Journal of Engineering Geology and Environment,* 2013**,** 245-254.

HERMANNS, R. L. 2016. Landslide. *Encyclopedia of Engineering Geology*, 1-3.

HERMANNS, R. L. & LONGVA, O. 2012. Rapid rock-slope failures. *Landslides: types, mechanisms and modeling*, 59-70.

HERMANNS, R. L. & STRECKER, M. R. 1999. Structural and lithological controls on large Quaternary rock avalanches (sturzstroms) in arid northwestern Argentina. *Geological Society of America Bulletin,* 111, 934-948.

HUNGR, O., LEROUEIL, S. & PICARELLI, L. 2014. The Varnes classification of landslide types, an update. *Landslides,* 11, 167-194.

INDREVÆR, K., BERGH, S. G., KOEHL, J.-B., HANSEN, J.-A., SCHERMER, E. R. & INGEBRIGTSEN, A. 2013. Post-Caledonian brittle fault zones on the hyperextended SW Barents Sea margin: New insights into onshore and offshore margin architecture. *Norwegian Journal of Geology,* 93.

INSAR.NGU.NO. *InSAR data* [Online]. [Accessed].

JABOYEDOFF, M., OPPIKOFER, T., METZGER, R. & COUTURE, R. 2007. New insight techniques to analyze rock-slope relief using DEM and 3Dimaging cloud points: COLTOP-3D software.

JOHANSEN, H. 1987. Forholdet mellom det prekambriske underlaget og overliggende sedimentære bergarter sørøst på Vanna, Troms. *Unpublished Cand. Scient thesis, University of Tromsø.*

KEEFER, D. K. 1984. Landslides caused by earthquakes. *Geological Society of America Bulletin,* 95, 406-421.

MARIOTTO, F. P. & TIBALDI, A. 2015. Inversion kinematics at deep-seated gravity slope deformations: a paleoseismological perspective. *Natural Hazards & Earth System Sciences Discussions,* 3.

MARTHINUSSEN, M. 1960. Coast and fjord area of Finnmark. *Geology of Norway.* Norges Geologiske Undersökelse.

MOSAR, J., EIDE, E. A., OSMUNDSEN, P. T., SOMMARUGA, A. & TORSVIK, T. H. Greenland–Norway separation: a geodynamic model for the North Atlantic. Norwegian Journal of Geology, 2002. 282.

NEMCOK, A. & PASEK, J. 1969. Mountain Slope Deformations, Geol. *Prace, Spravy,* 50, 5-28.

NGU. Available: ngu.no [Accessed].

NGU 2012. Helicopter-borne magnetic,electromarnetic and radiometric geophysical survey at Vanna, Karlsøy,Tromsø.

NGU. 2018. *Løsmassekart* [Online]. Available: ngu.no [Accessed].

NORGEIBILDER. 2018. Available: https://www.norgeibilder.no/ [Accessed].

NZGS 2005. Field description of soil and rock - field sheet. New Zealand Geotechnical Society.

OPHEIM, J. & ANDRESEN, A. 1989. Basement-cover relationships on northern Vanna, Troms, Norway. *Norsk geologisk tidsskrift,* 69, 67-81.

OPPIKOFER, T., NORDAHL, B., BUNKHOLT, H., NICOLAISEN, M., JARNA, A., IVERSEN, S., HERMANNS, R. L., BÖHME, M. & YUGSI MOLINA, F. X. 2015. Database and online map service on unstable rock slopes in Norway — From data perpetuation to public information. *Geomorphology,* 249, 69-81.

PETTERSEN, T. W. 2007. *Strukturell analyse av metasedimentære bergarter på Vanna, Troms.* Universitetet i Tromsø.

PGC.UMN.EDU/DATA/ARCTICDEM/. 2018. *ArcticDem* [Online]. Polar Geospatial Center. Available: pgc.umn.edu [Accessed].

RICE, A. 1990. A discussion–Basement-cover relationships on Northern Vanna, Troms, Norway. *Norsk geologisk tidsskrift,* 70, 179-184.

ROBERTS, D., OLESEN, O. & KARPUZ, M. 1997. Seismo-and neotectonics in Finnmark, Kola Peninsula and the southern Barents Sea. Part 1: Geological and neotectonic framework. *Tectonophysics,* 270**,** 1-13.

ROCSCIENCE 2018.

RØRVIK, K. L., RASMUSSEN, T. L., HALD, M. & HUSUM, K. 2013. Intermediate water ventilation in the Nordic seas during MIS 2. *Geophysical Research Letters,* 40**,** 1805-1810.

SCHEIDEGGER, A. E. 1973. On the prediction of the reach and velocity of catastrophic landslides. *Rock Mechanics and Rock Engineering,* 5**,** 231-236.

SCHLEIER, M., HERMANNS, R. L., ROHN, J. & GOSSE, J. C. 2015. Diagnostic characteristics and paleodynamics of supraglacial rock avalanches, Innerdalen, Western Norway. *Geomorphology,* 245**,** 23-39.

STEAD, D., EBERHARDT, E. & COGGAN, J. 2006. Developments in the characterization of complex rock slope deformation and failure using numerical modelling techniques. *Engineering geology,* 83**,** 217-235.

STEAD, D. & WOLTER, A. 2015. A critical review of rock slope failure mechanisms: The importance of structural geology. *Journal of Structural Geology,* 74**,** 1-23.

STOKES, C. R., CORNER, G. D., WINSBORROW, M. C., HUSUM, K. & ANDREASSEN, K. 2014. Asynchronous response of marine-terminating outlet glaciers during deglaciation of the Fennoscandian Ice Sheet. *Geology,* 42**,** 455-458.

TELFORD, W. M., TELFORD, W., GELDART, L., SHERIFF, R. E. & SHERIFF, R. 1990. *Applied geophysics*, Cambridge university press.

VALLEY, M. 2018. FieldMove Clino.

VARNES 1978. LANDSLIDES ANALYSIS AND CONTROL. *Special Report - National Research Council, Transportation Research Board*.

WYLLIE, D. & MAH, C. 2004. Rock Slope Engineering. Civil and Mining. Spon Press. *New York, NY (431pp.)*.

YR.NO. NRK og Meteorologisk institutt. Available: yr.no

 [Accessed].

ZWAAN, K. 1995. Geology of the West Troms Basement Complex, northern Norway, with emphasis on the Senja Shear Belt: a preliminary account. *Geological Survey of Norway Bulletin,* 427**,** 33-36.

ZWAAN, K. B. 1988. *Berggrunnskart Nordreisa M 1:250 000*.

8 Appendix

A: Average displacement rates on Kaillen based on InSAR satellite data from insar.ngu.no.

Dataset: InSAR Ascending 1
Point ID: Average series 1 of 1 (21 total all series)
Position: 70.169557 N 19.854392 E 448.03 m
Mean velocity: -3.87
Coherence: 0.74

Incidence angle: 36.74°
Track angle: -13.99°
Azimuth angle: 76.01°

Dataset: InSAR Ascending 2
Point ID: Average series 1 of 1 (12 total all series)
Position: 70.169636 N 19.854815 E 446.65 m
Mean velocity: -12.35
Coherence: 0.69

Incidence angle: 41.26°
Track angle: -12.07°
Azimuth angle: 77.93°

B: Average displacement rates on URS based on InSAR satellite data from insar.ngu.no.
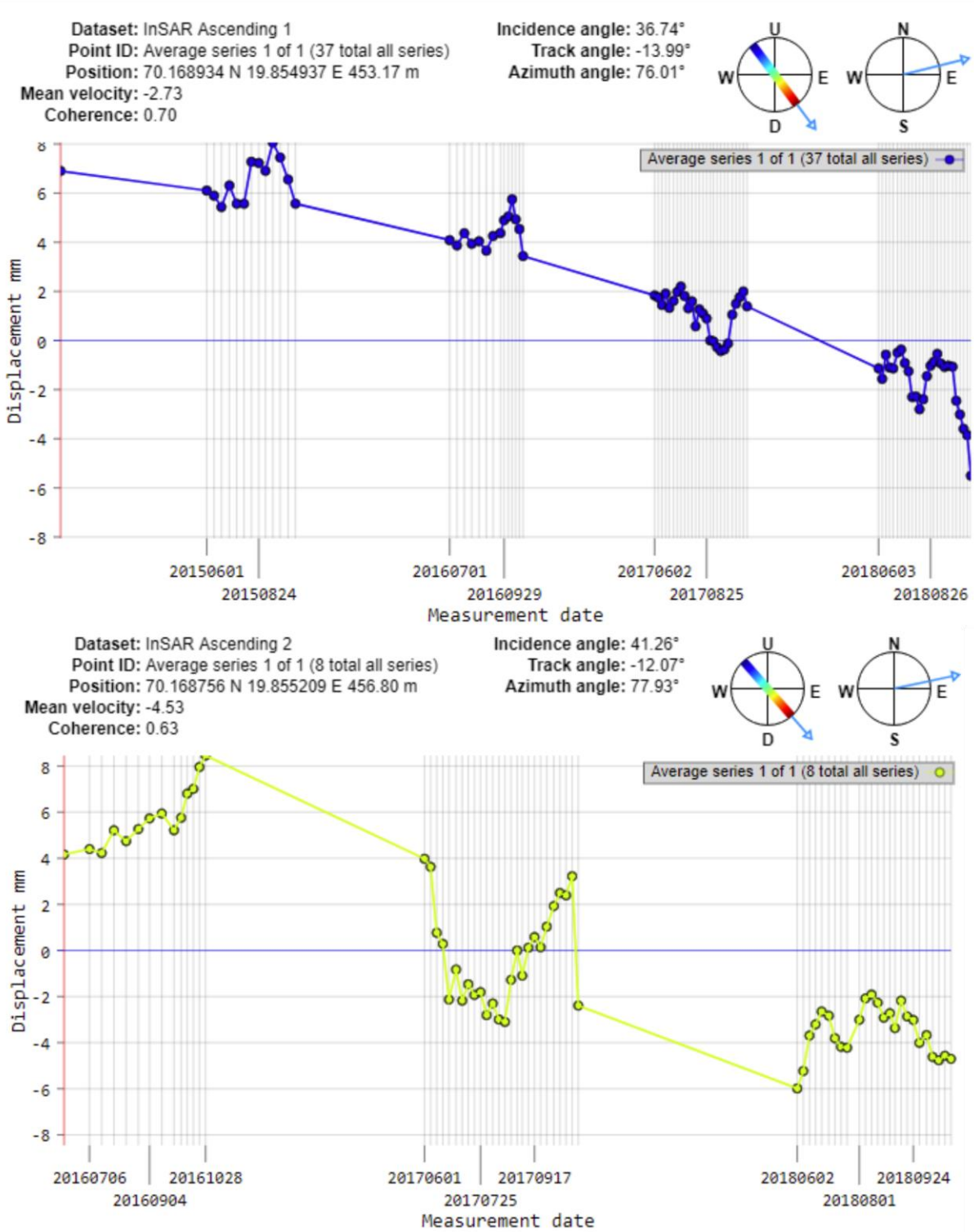
C: Best fit plane made in AgiSoft for volume calculations.

NW SE

Best fit plane (AgiSoft)

SW NE

Area: 179 666 m²

D: Agisoft Photoscan project whole URS
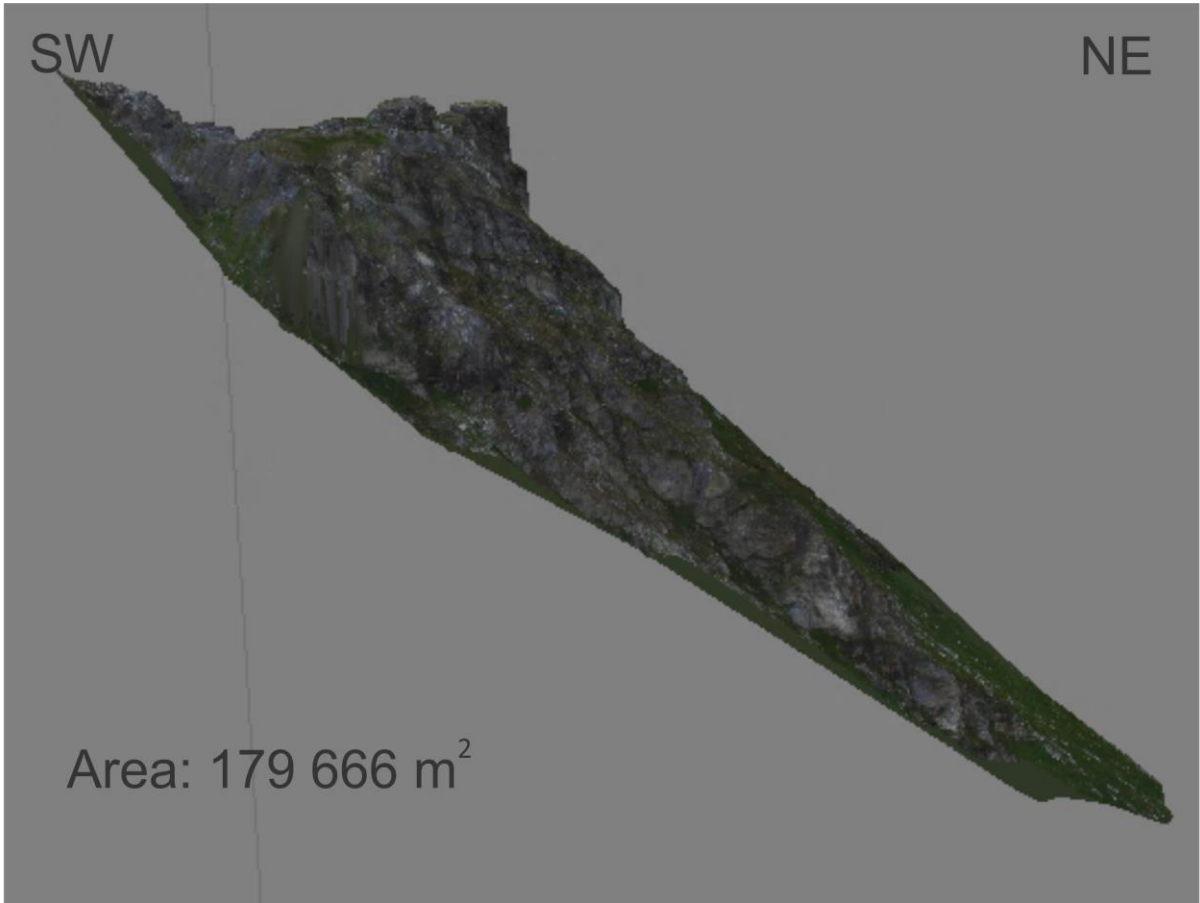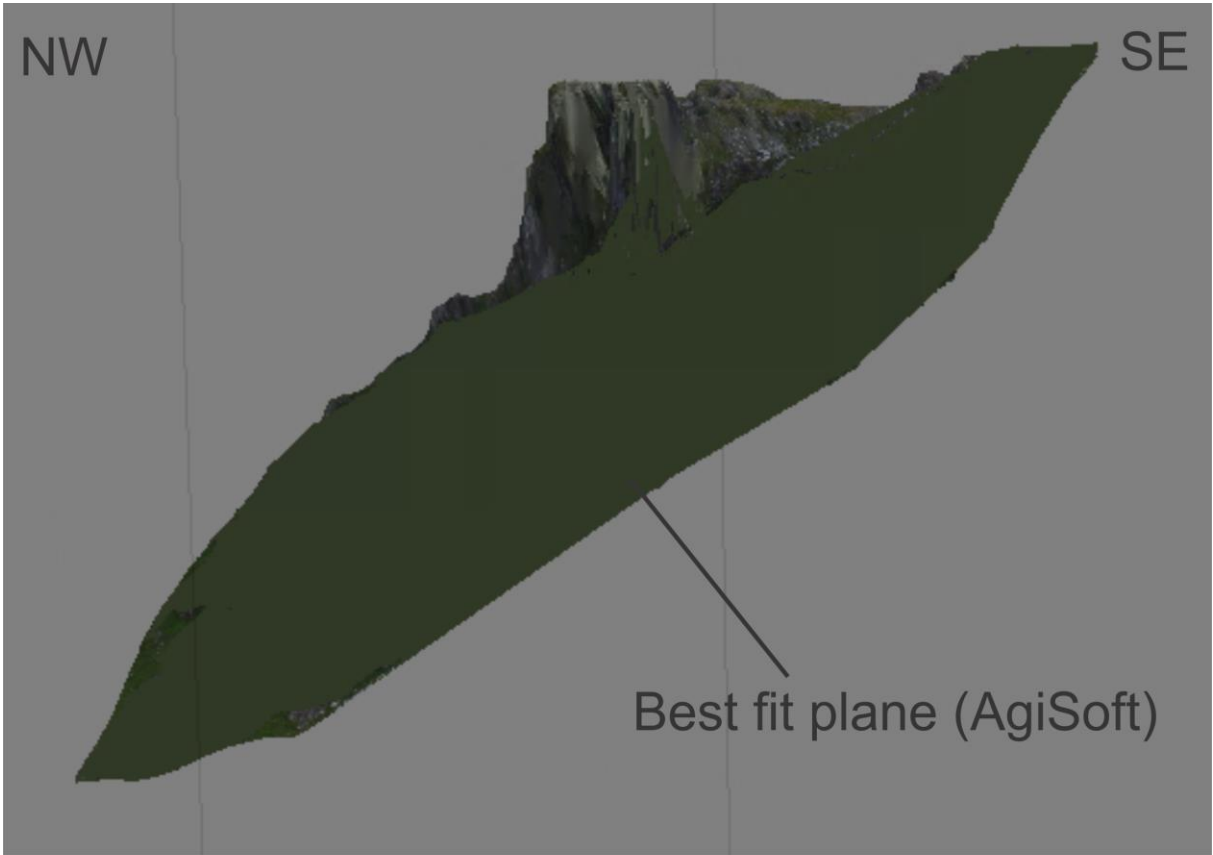
Survey Data
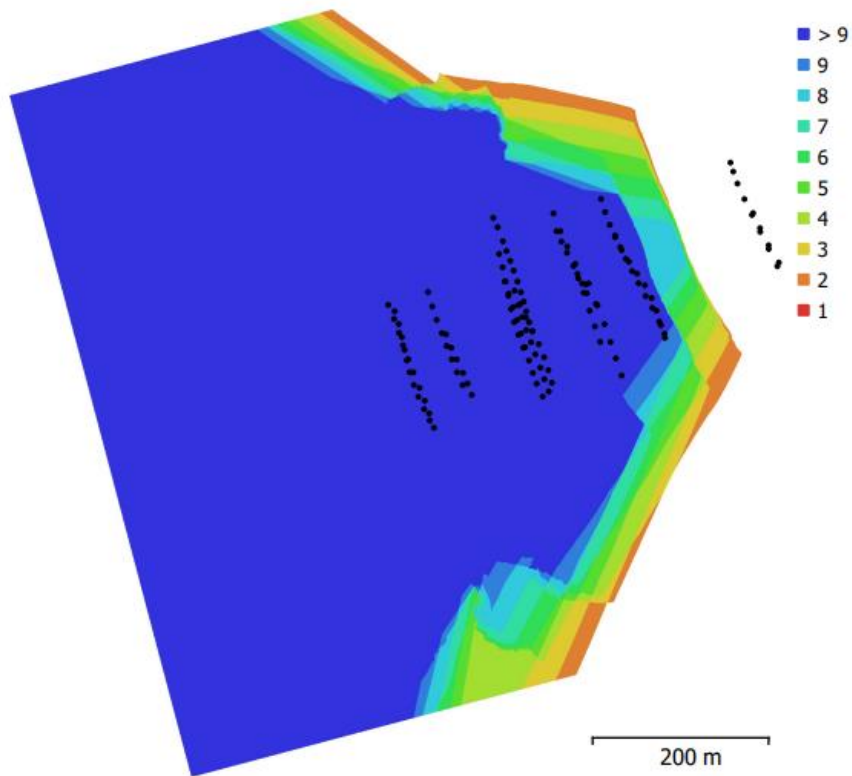
Fig. 1. Camera locations and image overlap.

Number of images:	137	Camera stations:	137
Flying altitude:	204 m	Tie points:	6,199
Ground resolution:	7.51 cm/pix	Projections:	112,533
Coverage area:	0.485 km²	Reprojection error:	5.79 pix

Camera Model	Resolution	Focal Length	Pixel Size	Precalibrated
FC350 (3.61mm)	4000 x 3000	3.61 mm	1.56 x 1.56 μm	No

Table 1. Cameras.

Camera Calibration

4 pix
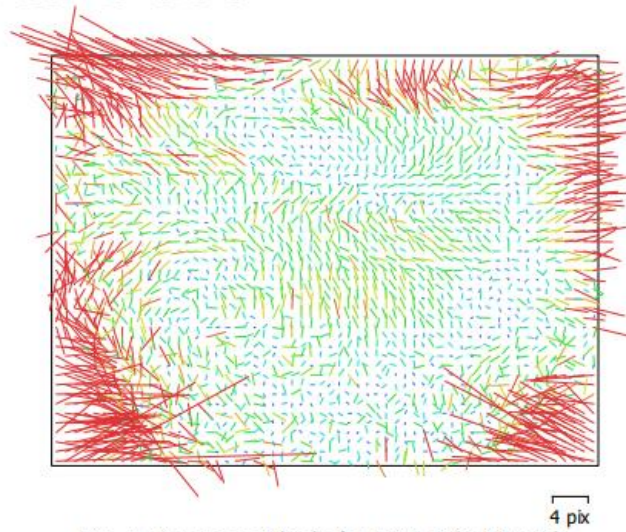
Fig. 2. Image residuals for FC350 (3.61mm).

FC350 (3.61mm)

137 images

Type
Frame

Resolution
4000 x 3000

Focal Length
3.61 mm

Pixel Size
1.56 x 1.56 μm

	Value	Error	F	Cx	Cy	B1	B2	K1	K2	K3	P1	P2
F	2335.47	0.55	1.00	0.17	0.09	-0.47	-0.12	-0.30	0.30	-0.24	0.12	0.11
Cx	14.0862	0.69		1.00	0.15	-0.10	0.05	-0.02	0.04	-0.01	0.88	0.15
Cy	30.3024	0.67			1.00	-0.32	-0.46	0.01	0.01	-0.02	0.15	0.69
B1	-11.7744	0.37				1.00	0.01	-0.05	0.02	-0.03	-0.10	-0.10
B2	10.6862	0.34					1.00	-0.05	0.05	-0.05	-0.06	-0.24
K1	-0.126707	0.00069						1.00	-0.97	0.91	-0.02	-0.04
K2	0.114205	0.0015							1.00	-0.98	0.02	0.05
K3	-0.0220427	0.00097								1.00	0.01	-0.06
P1	0.000908814	7.5e-05									1.00	0.11
P2	0.00407862	6.2e-05										1.00

Table 2. Calibration coefficients and correlation matrix.

Digital Elevation Model
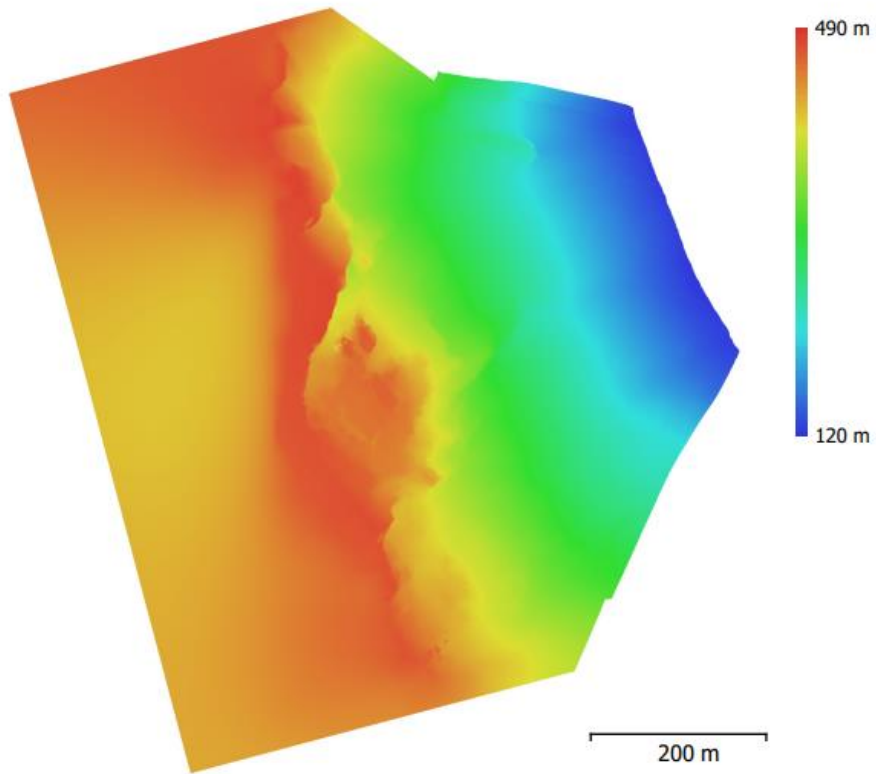
Fig. 3. Reconstructed digital elevation model.

Resolution: 15 cm/pix
Point density: 44.3 points/m²

Processing Parameters

General
  Cameras   137
  Aligned cameras   137
  Coordinate system   WGS 84 / UTM zone 34N (EPSG::32634)
  Rotation angles   Yaw, Pitch, Roll
Point Cloud
  Points   6,199 of 14,244
  RMS reprojection error   1.5439 (5.79384 pix)
  Max reprojection error   15.5779 (80.385 pix)
  Mean key point size   3.76936 pix
  Point colors   3 bands, uint8
  Key points   No
  Average tie point multiplicity   16.1803
  Alignment parameters
    Accuracy   High
    Generic preselection   Yes
    Reference preselection   Yes
    Key point limit   40,000
    Tie point limit   1,000
    Adaptive camera model fitting   No
    Matching time   22 minutes 40 seconds
    Alignment time   44 seconds
  Optimization parameters
    Parameters   f, b1, b2, cx, cy, k1-k3, p1, p2
    Adaptive camera model fitting   No
    Optimization time   3 seconds
Dense Point Cloud
  Points   22,676,718
  Point colors   3 bands, uint8
  Reconstruction parameters
    Quality   High
    Depth filtering   Aggressive
    Depth maps generation time   16 hours 46 minutes
    Dense cloud generation time   4 hours 7 minutes
Model
  Faces   841,240
  Vertices   420,624
  Vertex colors   3 bands, uint8
  Texture   4,096 x 4,096, 4 bands, uint8
  Reconstruction parameters
    Surface type   Height field
    Source data   Dense
    Interpolation   Enabled
    Quality   High
    Depth filtering   Aggressive
    Face count   4,535,343
    Processing time   56 seconds
  Texturing parameters
    Mapping mode   Generic
    Blending mode   Mosaic
    Texture size   4,096 x 4,096
    Enable hole filling   Yes
    Enable ghosting filter   Yes
    UV mapping time   1 minutes 37 seconds
    Blending time   11 minutes 54 seconds

Page 5

DEM
  Size   6,089 x 6,399
  Coordinate system   WGS 84 / UTM zone 34N (EPSG::32634)
  Reconstruction parameters
    Source data   Dense cloud
    Interpolation   Enabled
    Processing time   53 seconds
Orthomosaic
  Size   11,068 x 11,594
  Coordinate system   WGS 84 / UTM zone 34N (EPSG::32634)
  Colors   3 bands, uint8
  Reconstruction parameters
    Blending mode   Mosaic
    Surface   DEM
    Enable hole filling   Yes
    Processing time   5 minutes 30 seconds
Software
  Version   1.4.4 build 6848
  Platform   Windows 64

E: Agisoft Photoscan project backscarp

Survey Data
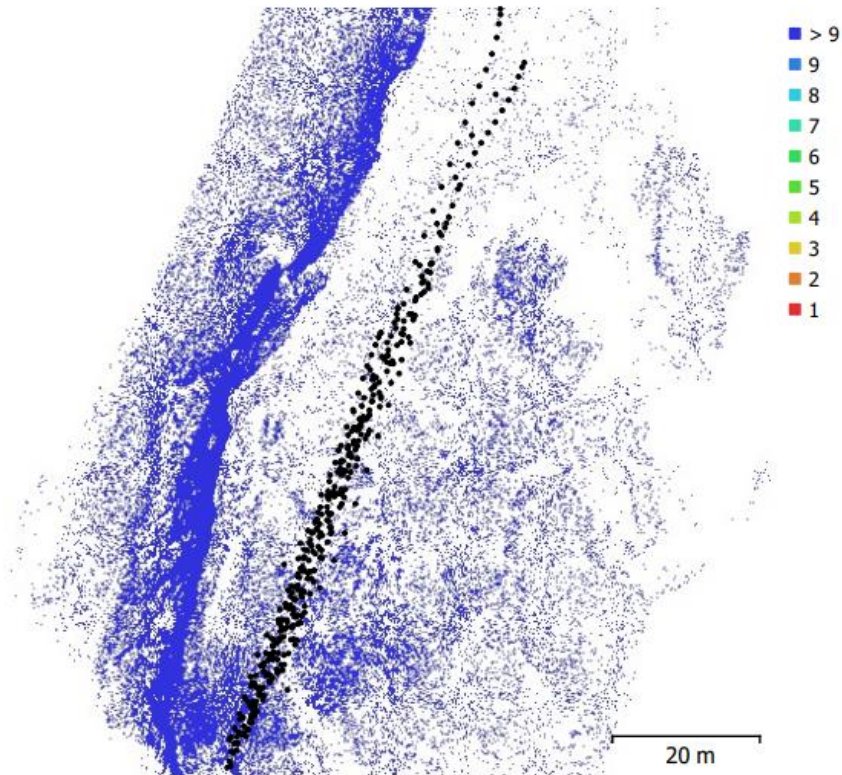
Fig. 1. Camera locations and image overlap.

Number of images:	396	Camera stations:	396
Flying altitude:	28.9 m	Tie points:	234,012
Ground resolution:	1.25 cm/pix	Projections:	1,152,975
Coverage area:	1.96e+03 m²	Reprojection error:	1.11 pix

Camera Model	Resolution	Focal Length	Pixel Size	Precalibrated
FC350 (3.61mm)	4000 x 3000	3.61 mm	1.56 x 1.56 µm	No

Table 1. Cameras.

Camera Calibration
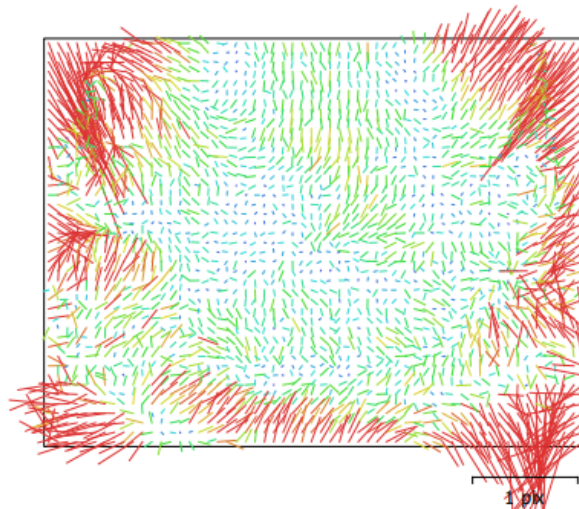
Fig. 2. Image residuals for FC350 (3.61mm).

FC350 (3.61mm)
396 images

Type	Resolution	Focal Length	Pixel Size
Frame	**4000 x 3000**	**3.61 mm**	**1.56 x 1.56 µm**

	Value	Error	F	Cx	Cy	B1	B2	K1	K2	K3	K4	P1	P2
F	**2317.33**	0.11	1.00	0.13	-0.21	-0.18	0.01	-0.24	0.24	-0.21	0.19	-0.01	-0.27
Cx	**26.5827**	0.073		1.00	0.10	-0.00	0.13	0.09	-0.09	0.09	-0.10	0.48	0.09
Cy	**-12.2658**	0.088			1.00	-0.03	-0.01	-0.01	0.02	-0.04	0.05	0.05	0.56
B1	**33.4094**	0.1				1.00	0.09	-0.04	0.01	0.01	-0.02	-0.07	-0.01
B2	**3.61777**	0.076					1.00	0.03	-0.03	0.03	-0.03	-0.17	0.15
K1	**-0.13768**	0.00014						1.00	-0.97	0.92	-0.87	0.06	-0.03
K2	**0.129561**	0.00046							1.00	-0.99	0.96	-0.07	0.04
K3	**-0.0376078**	0.00059								1.00	-0.99	0.07	-0.05
K4	**0.00914773**	0.00026									1.00	-0.08	0.05
P1	**0.000958346**	8.7e-06										1.00	-0.00
P2	**-0.00114338**	7.6e-06											1.00

Table 2. Calibration coefficients and correlation matrix.

Page 3

Ground Control Points
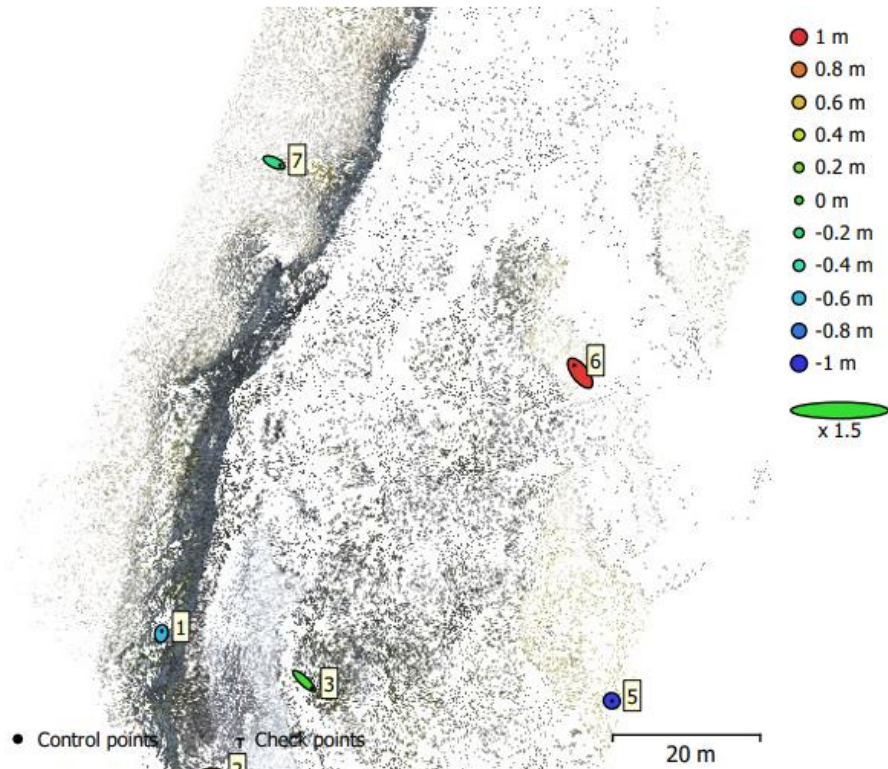
Fig. 3. GCP locations and error estimates.
Z error is represented by ellipse color. X,Y errors are represented by ellipse shape.
Estimated GCP locations are marked with a dot or crossing.

Count	X error (m)	Y error (m)	Z error (m)	XY error (m)	Total (m)
6	1.04552	0.832769	0.658782	1.33664	1.49017

Table 3. Control points RMSE.
X - Easting, Y - Northing, Z - Altitude.

Page 4

Label	X error (m)	Y error (m)	Z error (m)	Total (m)	Image (pix)
1	0.0780386	0.43984	-0.604514	0.751656	2.144 (69)
2	-1.49711	-0.139392	0.566805	1.60688	0.690 (98)
3	1.40353	-1.31173	0.0514063	1.92176	1.010 (55)
5	0.0702941	-0.0250873	-0.955854	0.958763	1.043 (15)
6	-1.06791	1.40204	0.977835	2.01552	1.629 (37)
7	1.0936	-0.511047	-0.211649	1.22553	1.001 (32)
Total	**1.04552**	**0.832769**	**0.658782**	**1.49017**	**1.361**

Table 4. Control points.
X - Easting, Y - Northing, Z - Altitude.

Processing Parameters

General
Cameras   396
Aligned cameras   396
Markers   6
Coordinate system   WGS 84 / UTM zone 34N (EPSG::32634)
Rotation angles   Yaw, Pitch, Roll
Point Cloud
Points   234,012 of 1,336,992
RMS reprojection error   0.333675 (1.1073 pix)
Max reprojection error   8.18712 (21.5185 pix)
Mean key point size   3.32581 pix
Point colors   3 bands, uint8
Key points   No
Average tie point multiplicity   5.65886
  Alignment parameters
  Accuracy   High
  Generic preselection   Yes
  Reference preselection   Yes
  Key point limit   40,000
  Tie point limit   0
  Adaptive camera model fitting   Yes
  Matching time   1 hours 0 minutes
  Alignment time   42 minutes 24 seconds
  Optimization parameters
  Parameters   f, b1, b2, cx, cy, k1-k4, p1, p2
  Adaptive camera model fitting   No
  Optimization time   16 seconds
Depth Maps
Count   291
  Reconstruction parameters
  Quality   High
  Filtering mode   Aggressive
  Processing time   11 hours 20 minutes
Software
Version   1.4.4 build 6848
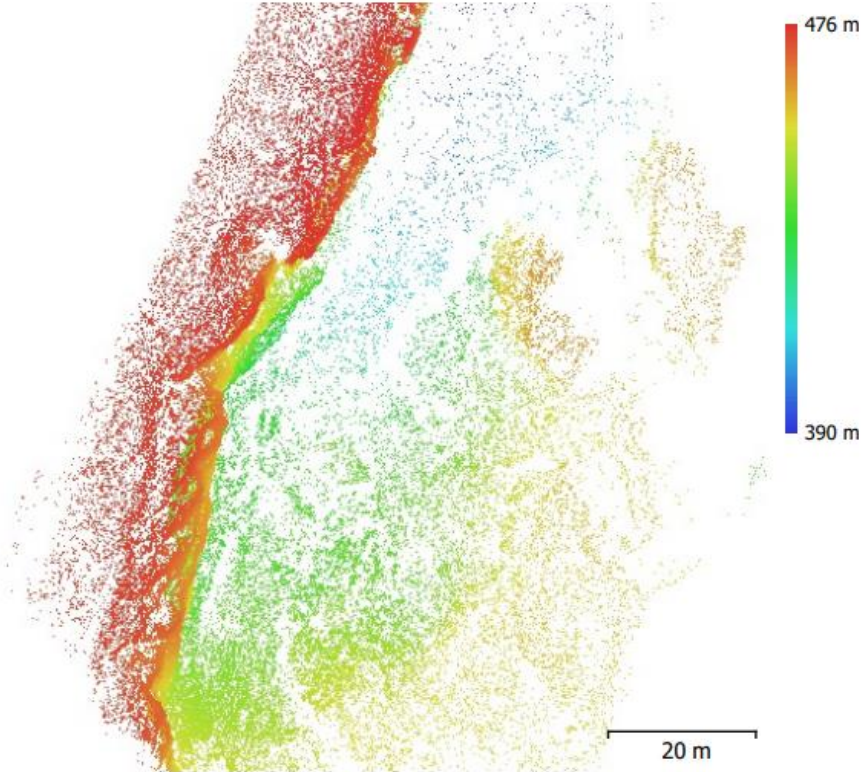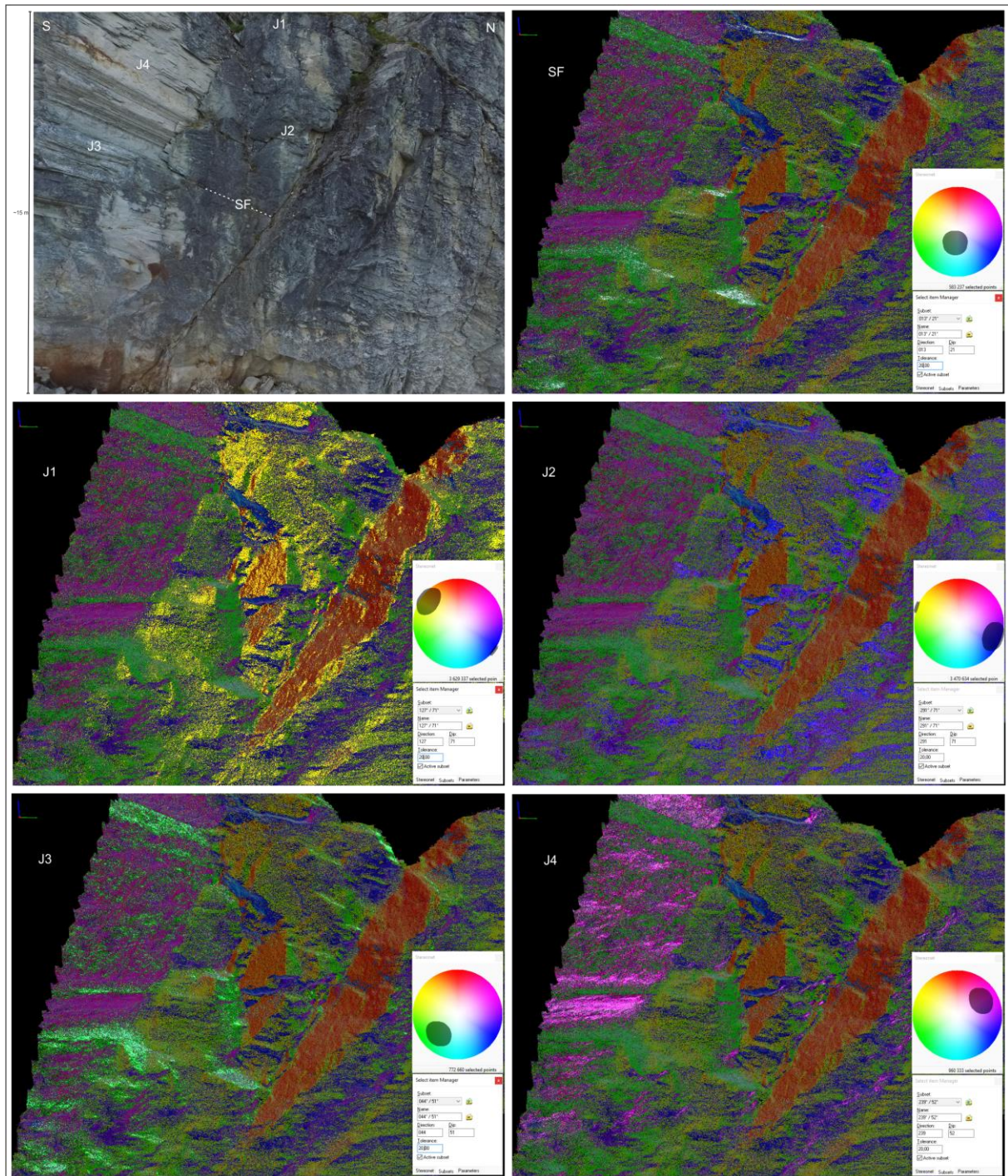Platform   Windows 64

Digital Elevation Model

Fig. 4. Reconstructed digital elevation model.

F: Coltop-3D. Location of defined polygons and respective poles for each polygon / joint set.

Appendix G: AppendixField description of soil and rock - field sheet

NZ GEOTECHNICAL SOCIETY INC
ROCK > field guide sheet
FIELD DESCRIPTION OF ROCK

SEQUENCE OF TERMS – weathering – colour – fabric – rock name – strength – discontinuities – additional

SCALE OF ROCK MASS WEATHERING

Term	Grade	Abbreviation	Description
Unweathered (fresh rock)	I	UW	Rock mass shows no loss of strength, discolouration or other effects due to weathering. There may be slight discolouration on major rock mass defect surfaces or on clasts.
Slightly Weathered	II	SW	The rock mass is not significantly weaker than when fresh. Rock may be discoloured along defects, some of which may have been opened slightly.
Moderately Weathered	III	MW	The rock mass is significantly weaker than the fresh rock and part of the rock mass may have been changed to a soil. Rock material may be discoloured and defect and clast surfaces will have a greater discolouration, which also penetrates slightly into the rock material. Increase in density of defects due to physical disintegration.
Highly Weathered	IV	HW	Most of the original rock mass strength is lost. Material is discoloured and more than half the mass is changed to a soil by chemical decomposition or disintegration (increase in density of defects/fractures). Decomposition adjacent to defects and at the surface of clasts penetrates deeply into the rock material. Lithorelicts or corestones of unweathered or slightly weathered rock may be present.
Completely Weathered	V	CW	Original rock strength is lost and the rock mass changed to a soil either by decomposition (with some rock fabric preserved) or by physical disintegration.
Residual Soil	VI	RS	Rock is completely changed to a soil with the original fabric destroyed (pedological soil).

ROCK STRENGTH TERMS

Term	Field Identification of Specimen	Unconfined uniaxial compressive strength q_u (MPa)	Point load strength $I_{s(50)}$ (MPa)
Extremely strong	Can only be chipped with geological hammer	> 250	>10
Very strong	Requires many blows of geological hammer to break it	100 – 250	5 – 10
Strong	Requires more than one blow of geological hammer to fracture it	50 – 100	2 – 5
Moderately strong	Cannot be scraped or peeled with a pocket knife. Can be fractured with single firm blow of geological hammer	20 – 50	1 – 2
Weak	Can be peeled by a pocket knife with difficulty. Shallow indentations made by firm blow with point of geological hammer	5 – 20	<1
Very weak	Crumbles under firm blows with point of geological hammer. Can be peeled by a pocket knife	1 – 5	
Extremely weak (soil description required)	Indented by thumb nail or other lesser strength terms used for soils	<1	

Note: • No correlation is implied between q_u and $I_{s(50)}$

SPACING OF DEFECTS/ DISCONTINUITIES

Term	Spacing
Very widely spaced	>2 m
Widely spaced	600 mm – 2 m
Moderately widely spaced	200 mm – 600 mm
Closely spaced	60 mm – 200 mm
Very closely spaced	20 mm – 60 mm
Extremely closely spaced	<20 mm

APERTURE OF DISCONTINUITY SURFACES

Term	Aperture (mm)	Description
Tight	Nil	Closed
Very Narrow	> 0 – 2	
Narrow	2 – 6	
Moderately Narrow	6 – 20	Gapped
Moderately Wide	20 – 60	Open
Wide	60 – 200	
Very Wide	> 200	

BEDDING THICKNESS TERMS

Term	Bed Thickness
Thinly laminated	< 2 mm
Laminated	2 mm - 6 mm
Very thin	6 mm - 20 mm
Thin	20 mm - 60 mm
Moderately thin	60 mm - 200 mm
Moderately thick	0.2 m - 0.6 m
Thick	0.6 m - 2 m
Very thick	> 2 m

BEDDING INCLINATION TERMS

Term	Inclination (from horizontal)
Sub-horizontal	0° – 5°
Gently inclined	6° – 15°
Moderately inclined	16° – 30°
Steeply inclined	31° – 60°
Very steeply inclined	61° – 80°
Sub-vertical	81° – 90°

ROUGHNESS AND APERTURE

STEPPED

UNDULATING

PLANAR

compiled by KATE WILLIAMS design KARRYN MUSCHAMP

NZ GEOTECHNICAL SOCIETY INC

This field sheet has been taken from and should be used and read with reference to the document FIELD DESCRIPTION OF SOIL AND ROCK. Guideline For the Field Classification and Description of Soil and Rock for Engineering Purposes. NZ Geotechnical Society Inc, December 2005. www.nzgeotechsoc.org.nz

NZ GEOTECHNICAL SOCIETY INC
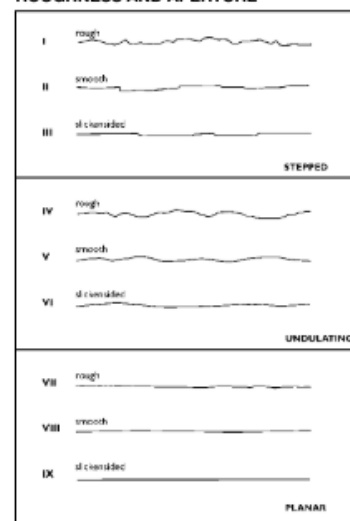
SOIL > field guide sheet
FIELD DESCRIPTION OF SOIL

SEQUENCE OF TERMS – fraction – colour – structure – strength – moisture – bedding – plasticity – sensitivity – additional

GRAIN SIZE CRITERIA

TYPE	COARSE								FINE		ORGANIC
	Boulders	Cobbles	Gravel			Sand			Silt	Clay	Organic Soil
			coarse	medium	fine	coarse	medium	fine			
Size Range (mm)	200	60	20	6	2	0.6	0.2	0.06	0.002		
Graphic Symbol											

SOIL CLASSIFICATION

MATERIAL

Fraction finer than 0.06mm

<35% → COARSE SOIL → Particle size composition → BOULDERS / COBBLES / GRAVEL / SAND

>35% → FINE SOIL → Quick/dilatant behaviour → SILT ; Plastic behaviour → CLAY

PROPORTIONAL TERMS DEFINITION (COARSE SOILS)

Fraction	Term	% of Soil Mass	Example
Major	(….) [UPPER CASE]	≥ 50 [major constituent]	GRAVEL
Subordinate	(….) y [lower case]	20 – 50	Sandy
Minor	with some … with minor …	12 – 20 5 – 12	with some sand with minor sand
	with trace of (or slightly)…	< 5	with trace of sand (slightly sandy)

DENSITY INDEX (RELATIVE DENSITY) TERMS

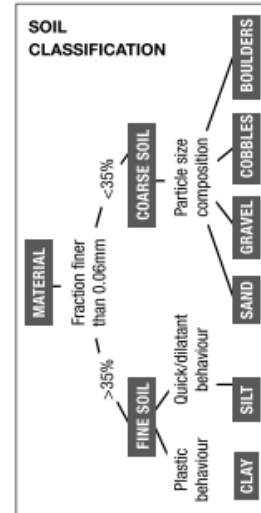| Descriptive Term	Density Index (R_D)	SPT "N" value (blows / 300 mm)	Dynamic Cone (blows / 100 mm)
Very dense	> 85	> 50	> 17
Dense	65 – 85	30 – 50	7 – 17
Medium dense	35 – 65	10 – 30	3 – 7
Loose	15 – 35	4 – 10	1 – 3
Very loose	< 15	< 4	0 – 2

Note: • No correlation is implied between Standard Penetration Test (SPT) and Dynamic Cone Test values.
• SPT "N" values are uncorrected. • Dynamic Cone Penetrometer (Scala)

CONSISTENCY TERMS FOR COHESIVE SOILS

Descriptive Term	Undrained Shear Strength (kPa)	Diagnostic Features
Very soft	< 12	Easily exudes between fingers when squeezed
Soft	12 – 25	Easily indented by fingers
Firm	25 – 50	Indented by strong finger pressure and can be indented by thumb pressure
Stiff	50 – 100	Cannot be indented by thumb pressure
Very stiff	100 – 200	Can be indented by thumb nail
Hard	200 – 500	Difficult to indent by thumb nail

ORGANIC SOILS/ DESCRIPTORS

Term	Description
Topsoil	Surficial organic soil layer that may contain living matter. However topsoil may occur at greater depth, having been buried by geological processes or man-made fill, and should then be termed a buried topsoil.
Organic clay, silt or sand	Contains finely divided organic matter; may have distinctive smell; may stain; may oxidise rapidly. Describe as for inorganic soils.
Peat	Consists predominantly of plant remains. *Firm*: Fibres already compressed together *Spongy*: Very compressible and open stucture *Plastic*: Can be moulded in hand and smears in fingers *Fibrous*: Plant remains recognisable and retain some strength *Amorphous*: No recognisable plant remains
Roolets	Fine, partly decomposed roots, normally found in the upper part of a soil profile or in a redeposited soil (e.g. colluvium or fill)
Carbonaceous	Discrete particles of hardened (carbonised) plant material.

MOISTURE CONDITION

Condition	Description	Granular Soils	Cohesive Soils
Dry	Looks and feels dry	Run freely through hands	Hard, powdery or friable
Moist	Feels cool, darkened in colour	Tend to cohere	Weakened by moisture, but no free water on hands when remoulding
Wet			Weakened by moisture, free water forms on hands when handling
Saturated	Feels cool, darkened in colour and free water is present on the sample		

GRADING (GRAVELS & SANDS)

Term	Description	
Well graded	Good representation of all particle sizes from largest to smallest	
Poorly graded	Limited representation of grain sizes - further divided into:	
	Uniformly graded	Most particles about the same size
	Gap graded	Absence of one or more intermediate sizes

PLASTICITY (CLAYS & SILTS)

Term	Description
High plasticity	Can be moulded or deformed over a wide range of moisture contents without cracking or showing any tendency to volume change
Low plasticity	When moulded can be crumbled in the fingers; may show quick or dilatant behaviour

NZ GEOTECHNICAL SOCIETY INC

This field sheet has been taken from and should be used and read with reference to the document FIELD DESCRIPTION OF SOIL AND ROCK. Guideline For the Field Classification and Description of Soil and Rock for Engineering Purposes. NZ Geotechnical Society Inc, December 2005. **www.nzgeotechsoc.org.nz**

compiled by KATE WILLIAMS design KARRYN MUSCHAMP